Electronic Thesis and Dissertation Repository

2-18-2022 10:30 AM

Kinetic and structural influences of acetylation on ubiquitin processing

Rachel E. Lacoursiere, *The University of Western Ontario*

Supervisor: Shaw, Gary S., *The University of Western Ontario*
A thesis submitted in partial fulfillment of the requirements for the Doctor of Philosophy degree in Biochemistry
© Rachel E. Lacoursiere 2022

Follow this and additional works at: https://ir.lib.uwo.ca/etd

Part of the Biochemistry Commons

Recommended Citation

Abstract

Ubiquitin (Ub) is a small modifying protein abundant in cells where it serves numerous regulatory roles including immune signaling, transcriptional regulation, and proteostasis. To exert its function, Ub covalently interacts with a series of E1, E2, and E3 enzymes before final substrate modification. Dysregulation of Ub signaling has implications in human maladies such as cancer, autoimmune disorders, and neurodegenerative diseases. In these diseases and associated in cellulo models, modifications to Ub serve an additional role in Ub regulation. Post-translational modifications like acetylation or phosphorylation modulate protein-protein interactions and Ub signaling. To understand how acetylation of Ub alters the central E2 step in the Ub cascade, we used orthogonal translation to synthesize seven unique versions (K6, K11, K27, K29, K33, K48, or K63) of acetylated Ub (acUb) and showed them to be competent in RING and HECT-type ubiquitination experiments. We then created a library of acUb proteins labeled with the CyPet fluorophore, and in conjunction with the YPet-labeled E2 proteins UBE2D1 and UBE2L3, we optimized a Förster Resonance Energy Transfer (FRET) experiment that highlighted how Ub acetylation modulates the catalytic activity of the E1 protein UBA1. We found that Ub acetylation at most sites significantly altered the formation of both the UBE2D1~Ub and UBE2L3~Ub conjugates. The unloading of the UBE2D1~Ub and UBE2L3~Ub conjugates was then evaluated with the acUb proteins in the presence of small nucleophiles. Our findings that both E2 proteins were sensitive to nucleophilic cysteine prompted the use of cysteine-dependent E3 proteins IPAH3 and HUWE1 to study how acUb alters transthiolation from the E2 protein to an E3 ligase. We used Nuclear Magnetic Resonance (NMR) spectroscopy to study conformation of the UBE2L3~Ub and acUb conjugates. Together, these sets of experiments demonstrated that a subset of the acUb proteins were ineffective in supporting E3 function likely through E2~Ub conformational changes and E3-chain building preference. Overall, we provide the first analysis of the complete set of acUb proteins and how they modulate E2-dependent steps in ubiquitination. We expect our data will guide future experiments to understand the full involvement of Ub acetylation in regulating cellular processes.

Keywords

Summary for Lay Audience

Our bodies are made of tiny compartments called cells. These cells are controlled by a variety of factors, one of which are protein molecules. One protein called ubiquitin is responsible for the maintenance of our cells. Similar to how a handyman is called upon to build, fix, or destroy, ubiquitin helps guide the body to make new proteins, repair damaged structures, and remove unneeded components. An incapacitated handyman is detrimental to your life, as is an incapacitated ubiquitin. When this protein cannot exert its handyman function, the chance of diseases like cancer, Parkinson's, or Alzheimer's increases.

The job of a handyman depends on the function of their vision and their hands: wearing sunglasses or thick gloves might alter how quickly their work is done. Ubiquitin is the same way: changing certain physical aspects has an impact on function. In my thesis, I have optimized a method to make physical changes to ubiquitin, and I created an experiment to examine how fast or slow ubiquitin can function with these changes. I found that most physical changes to ubiquitin mimic what might be expected of a handyman wearing thick gloves: slower overall, but still capable of getting the job done.

The impairment in function caused by the physical changes is expected to cause a problem within cells, but the full effects are still unknown. Can ubiquitin compensate for physical changes to still get the job done? What exactly happens in cells when physical changes incapacitate ubiquitin? There are still many questions that remain to be answered, but my thesis provides an excellent foundation to continue studying physical changes to ubiquitin. It provides information on how the changes alter specific functions that might have unknown roles in various human diseases.

Co-Authorship Statement

Chapter 4

Crystallization screens for acUbK48 were set up under the guidance of Dr. Roya Tadayon. All crystal fishing, data collection, and structure refinement was conducted by Dr. Roya Tadayon.

Dedication

For all the little girls dreaming of a career in STEM: Embrace it.

Acknowledgements

First and foremost, to my supervisor Dr. Gary Shaw, thank you for everything these past few years. Thank you for taking the chance on me and recruiting me to join your lab. Thank you for letting me choose where my project went as much as I did, but always being there to provide guidance. Your teaching and leadership style will impact me for the rest of my career.

To my lab mates Tara, Yuning, Karen, Aisha, Anne, Richard, and Beth: Thank you for countless trips to the Grad Club for lunch, lab events, and dinners out. Most importantly, thank you for always being around to bounce ideas off and providing detailed feedback on my experiments. Thank you to the undergraduate students I have helped over the years – Ghadeir, Emily, Winnie, Sina – you have all taught me a lot more than I could have ever taught you, and for that, I am appreciative. Thank you to Kathy Barber for keeping the lab running smoothly for much of my time here (and for forcing me to wear a lab coat).

Thank you to my advisory committee, Dr. Murray Junop and Dr. Patrick O'Donoghue, for always providing me with good feedback on my experiments and new directions for my project. To Lee-Ann Briere, Paula Pittock, Victoria Clarke, and Yinyin (Heidi) Liao, thank you for your hard work maintaining our facilities so I could always get my experiments done with proper training and functional equipment.

A big thank you to Folawiyo Laditi and Connor Virtue for really having no idea what I talk about but always wanting to hear more. You guys are the best! To Roya Tadayon– Baba, I am SO LUCKY that you joined the lab shortly after I did. You shaped my grad school experience more than anyone else. From weekends in the lab to pizza dinner parties, I have countless memories of us.

Finally, a huge shout out to my parents Kevin and Judy and my sister Lauren for their support in everything that I do. I can't wait to show you what I do next!

Table of Contents

List of Tables

List of Figures

List of Abbreviations and Nomenclature

AAD	Active adenylation [domain]
acK	Acetyl-lysine
acUb	Acetylated ubiquitin
acUbKx	Acetylated ubiquitin at lysine x
Ches	2-(Cyclohexylamino)ethanesulfonic acid
$Cys_{cat(X)}$	Catalytic cysteine of protein X
DNA	Deoxyribonucleic acid
DSS	2,2-Dimethyl-2-silapentane-5-sulfonic acid
DTT	Dithiothreitol
E1	Ubiquitin activating enzyme
E2	Ubiquitin conjugating enzyme
E3	Ubiquitin ligase
EDTA	Ethylenediaminetetraacetic acid
FCCH	First catalytic cysteine half [domain]
FRET	Förster resonance energy transfer
GST	Glutathione S-transferase
HAT	Histone acetyltransferase
HECT	Homologous to E6AP C-terminus
Hepes	4-(2-hydroxyethyl)-1-piperazineethanesulfonic acid
HSQC	heteronuclear single quantum coherence
HUWE1	HECT, UBA, and WWE domain containing protein 1
IAD	Inactive adenylation [domain]
IPAH3	Invasion plasmid antigen H3
IPTG	Isopropyl β-D-1-thiogalactopyranoside
KAT	Lysine acetyltransferase
k_{cat}	Turnover number
k_{cat}/K_M	Catalytic efficiency
kDa	Kilodalton
K_M	Michaelis constant
LB	Luria broth

LC-MS	Liquid chromatography-mass spectrometry
MES	2-(N-morpholino)ethanesulfonic acid
MgATP	Magnesium adenosine triphosphate
NaCl	Sodium chloride
Ni^{2+}-NTA	Nickel-nitrilotriacetic acid
NMR	Nuclear magnetic resonance
PCR	Polymerase chain reaction
PDB	Protein data bank
polyUb	Poly-ubiquitin [chains]
ppm	Parts per million
PTM	Post-translational modification
pUb	Phosphorylated ubiquitin
QToF	Quadrupole time of flight [mass spectrometry]
RBR	Ring-in-between-ring
RING	Really interesting new gene
RNA	Ribonucleic acid
RNF8	Ring finger protein 8
RP-HPLC	Reverse phase-high performance liquid chromatography
SCCH	Second catalytic cysteine half [domain]
SDS	Sodium dodecyl sulfate
SDS-PAGE	Sodium dodecyl sulfate-polyacrylamide gel electrophoresis
SEM	Standard error of the mean
SEC-MALS	Size exclusion chromatography-multi angle light scattering
TCEP	Tris(2-carboxyethyl)phosphine
TEV	Tobacco etch virus
Tris	Trisaminomethane (2-Amino-2-hydroxymethyl-propane-1,3-diol)
$tRNA^{Pyl-opt}$	Pyrrolysine-optimized transfer RNA
tRNA	Transfer RNA
Ub	Ubiquitin
Ub(a)	Ubiquitin adenylate
UBA1	E1 activating enzyme
Ub^{CyPet}	Ubiquitin with a CyPet fluorophore

UBE2D1	E2 conjugating enzyme 2D1 (ubcH5a)
UBE2L3	E2 conjugating enzyme 2L3 (ubcH7)
Ub(t)	Ubiquitin thioester
UFD	Ubiquitin fold domain
^{YPet}E2	E2 conjugating enzyme with a YPet fluorophore
4HB	Four helix bundle
A	Alanine (Ala)
C	Cysteine (Cys)
D	Aspartic acid (Asp)
E	Glutamic acid (Glu)
F	Phenylalanine (Phe)
G	Glycine (Gly)
H	Histidine (His)
I	Isoleucine (Ile)
K	Lysine (Lys)
L	Leucine (Leu)
M	Methionine (Met)
N	Asparagine (Asn)
P	Proline (Pro)
Q	Glutamine (Gln)
R	Arginine (Arg)
S	Serine (Ser)
T	Threonine (Thr)
V	Valine (Val)
W	Tryptophan (Trp)
Y	Tyrosine (Tyr)
~	Denotes a high energy thioester linkage between two proteins
–	Denotes a stable isopeptide linkage between two proteins
X:Y interactions	Non-covalent interactions between species X and Y

List of Appendices

1
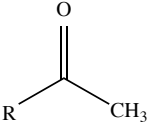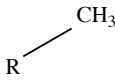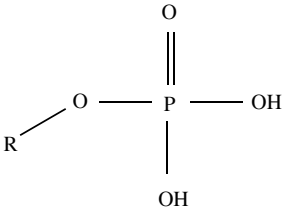
Introduction

1.1 Post-translational modifications

Decoding of the messenger RNA transcript at the ribosome produces a linear protein structure that is capable of folding into tertiary and quaternary structures. After complete folding, most proteins are in their active state (ie. The state required for various roles in cells); but sometimes, other modifications to the structure of a protein are required. Most commonly, these extra modifications occur in the form of post-translational modifications (PTMs) and require the catalytic activity of a variety of other classes of proteins.

Compared to the total size of a protein, PTMs are small modifications that occur at a specific site and contribute to overall protein charge, change protein conformation, or modulate interactions with other cellular components. PTMs such as acetylation, methylation, or phosphorylation occur on various polar residues. In addition to these smaller modifications, some PTM pathways covalently modify substrates with smaller proteins such as in ubiquitination, sumoylation, and neddylation. Table 1.1 highlights these common PTMs found on proteins.

Table 1.1. Common post-translational modifications.

Modification	Modifier	Structure	Amino Acid(s)	Mass Addition (Da)	Cellular Roles
Acetylation	Acetyl		Lysine	42.01	Gene transcription, metabolic regulation
Methylation	Methyl		Arginine, Lysine, Histidine	14.03	Gene transcription, signal transduction
Neddylation	Neural precursor cell expressed developmentally down-regulated protein 8 (NEDD8)		Lysine	8559.97	Metabolism, immunity
Phosphorylation	Phosphate		Serine, Threonine, Tyrosine	79.99	Signal transduction, protein activation
Sumoylation	Small ubiquitin-like modifier (SUMO) 1/2/3		Lysine	11132.53 10608.91 10524.83	Metabolism, trafficking
Ubiquitination	Ubiquitin		Lysine, Serine, Threonine	8564.84	Proteostasis, signal transduction

PTM pathways are typically circular, consisting of three main classes of proteins: writers, readers, and erasers. Accordingly, "writer" proteins are responsible for modifying the substrate with a PTM, "reader" proteins contain domains that recognize and bind a PTM to amplify signaling, and "eraser" proteins undo the modification to leave behind an unmodified substrate. Part of the complexity of PTM signaling networks arises in the

thousands of proteins known to write, read, or erase certain PTMs, and not all pathways are equally as complicated. For example, some PTM pathways are straightforward; that is, only one writer is required to modify a substrate protein. This is the case with PTMs like methylation and acetylation, where the writers require only a cofactor and the protein substrate. Other PTM pathways like ubiquitination, sumoylation, and neddylation require a hierarchy of enzymes that function cooperatively to modify substrate proteins. Finally, phosphorylation pathways are often a combination of these two extremes: sometimes a single phosphorylation event is necessary, but other times kinase activation cascades are required to amplify the necessary signal.

To modify substrate function and the associated signaling, one-writer PTM systems frequently act to alter amino acid charge by either introducing (as in phosphorylation) or neutralizing charge (as in methylation or acetylation). Numerous proteins in cells have been observed to be post-translationally modified at one or more points in their natural lifecycle; and frequently, protein PTMs are dysregulated in various diseases. For example, phosphorylation has been implicated in several diseases including breast cancer [1–3], Parkinson's [4,5], and Alzheimer's [6–8]. Dysregulation of the acetylation pathways has ties to prostate and lung cancers [9,10] and Alzheimer's disease [11,12]. For ubiquitination, modulated expression of numerous "writer" proteins has been observed to play roles in prostate, colorectal, and pancreatic cancers [13,14]. Additionally, ubiquitination is involved in immune [15], developmental [16], and neurological disorders [17,18].

1.1.1   Acetylation

Among methylation and phosphorylation, acetylation is one of the most prevalent forms of single-writer modifications to occur post translation. It is a small covalent modification of the amine in the lysine side chain that was first characterized on histone proteins, where it was thought to play a role in RNA synthesis [19]. Years later, it is known that histones are highly acetylated proteins and various acetylation sites including Histone H3 Lys56 [20,21] and Histone H4 Lys16 [22] influence chromatin remodeling events necessary for transcriptional regulation. As a result of this early discovery, the writer enzymes discovered were named histone acetyltransferases (HATs). Years later, the finding that non-histone

proteins could also be substrates of these writers prompted their renaming to lysine acetyltransferases (KATs) [23]. Today, both terms are used interchangeably for protein lysine acetylation.

KAT proteins simultaneously interact with a protein substrate and the cofactor acetyl-coenzyme A to achieve its catalytic function, and the process of acetylation results in the release of coenzyme A, a hydrogen ion, and the protein substrate with an N_ε-acetyl lysine. In addition to the domains required for acetylation, various KAT proteins contain other domains crucial for signaling and various protein interactions. Based on compartmentalization, KATs can be separated into nuclear or cytoplasmic families. Nuclear KATs are currently the best understood and are implicated in several human cancers [24]; however, the cytoplasmic KATs are still largely uncharacterized. This is exacerbated by several challenges: 1) many substrates localize to both the nucleus and the cytoplasm, 2) acetylation sites are identified but frequently unmatched to specific KAT activity, and 3) multiple KAT proteins could target the same substrate lysine. As studies into cytoplasmic KAT activity become more abundant in the literature, development of specific KAT inhibitors and the advancement of mass spectrometry techniques will provide a better correlation between enzyme and substrate acetylation.

To regenerate the natural substrate protein, deacetylase enzymes function to remove the acetylation signal. For simplicity, deacetylases can be separated into two groups based on their mechanism of function, but these groups can be further subdivided based on domain architecture and evolution [25]. The histone deacetylases (HDACs 1-11) are zinc-dependent, while the Sirtuin proteins (SIRTs 1-7) are regulated by nicotinamide adenine dinucleotide (NAD^+). These distinct mechanisms allow the development of inhibitors to selectively target a subgroup of deacetylases for the treatment of various diseases.

In addition to chromatin remodeling and gene transcription, protein lysine acetylation has roles in metabolism and stress response, and it can modulate a variety of protein interactions. For example, acetylation of α-synuclein has an anti-aggregative effect [26], of Beclin-1 inhibits autophagy [27], and acetylation of p53 stabilizes its protein levels and promotes nuclear localization [28]. The multitude of outcomes associated with protein

acetylation demonstrates the importance of fully characterizing each acetyl protein, as one blanket outcome does not apply.

1.1.2   Ubiquitination

To ubiquitinate substrates, cells adhere to a linear pathway involving the E1, E2, and E3 enzymes, which cooperate as a cascade of "writer" proteins. The abundance of the modifier ubiquitin (Ub) in cells allows for these enzymes to exist primed for ubiquitination. The initial step in ubiquitination requires the E1 activating enzyme and adenosine triphosphate (ATP) to sequentially adenylate the C-terminus of Ub and form a thioester linkage at the catalytic cysteine of the E1 protein ($Cys_{cat(E1)}$) (Fig. 1.1). From here, recruitment of an E2 conjugating protein permits a transthiolation reaction where the C-terminus of Ub is ligated onto the catalytic cysteine of the E2 protein ($Cys_{cat(E2)}$). The E2~Ub conjugate then gets recruited by an E3 ligase. E3 proteins make up the largest number of ubiquitination proteins and can be divided into two major mechanistic classes. The first and largest class of E3 proteins are the cysteine-independent Really Interesting New Gene (RING) family of proteins [29]. RING E3 proteins act as scaffolds that bring the E2~Ub and the substrate into proximity to enable ubiquitination. The second mechanistic class of E3 ligases are the cysteine-dependent ligases. This class includes the Homologous to E6-associated protein C-terminus (HECT) [30] and RING-inBetween-RING (RBR) [31] classes of proteins, which utilize a catalytic cysteine ($Cys_{cat(E3)}$). The ubiquitination mechanism used by HECT and RBR E3 proteins is similar to the transthiolation reaction that occurs between the E1 and E2 proteins, where these E3 proteins form a covalent E3~Ub prior to covalent substrate modification. Uniquely, in addition to the catalytic domain, RBR ligases contain a RING domain that is required for E2~Ub binding. For this reason, RBR E3 proteins are commonly referred to as having a hybrid RING/HECT mechanism but can ultimately be classified as cysteine-dependent ligases. Regardless of the family of E3 protein, other regions of the ligase bind and position a substrate so the target residue lies in proximity to the active thioester bond. Ubiquitination conventionally occurs on lysine residues of substrates where the formed bond (termed isopeptide bond) mimics a peptide linkage found naturally in proteins, though other linkages are becoming evident [32]. Substrate ubiquitination can be reversed with "eraser" proteins called deubiquitinating enzymes

(DUBs) that recognize and cleave the C-terminal isopeptide linkage to replenish the Ub pool in cells. The steps involved in the forward ubiquitination pathway (involving the E1, E2, and E3 enzymes) are discussed in more detail below in sections 1.2-1.4.
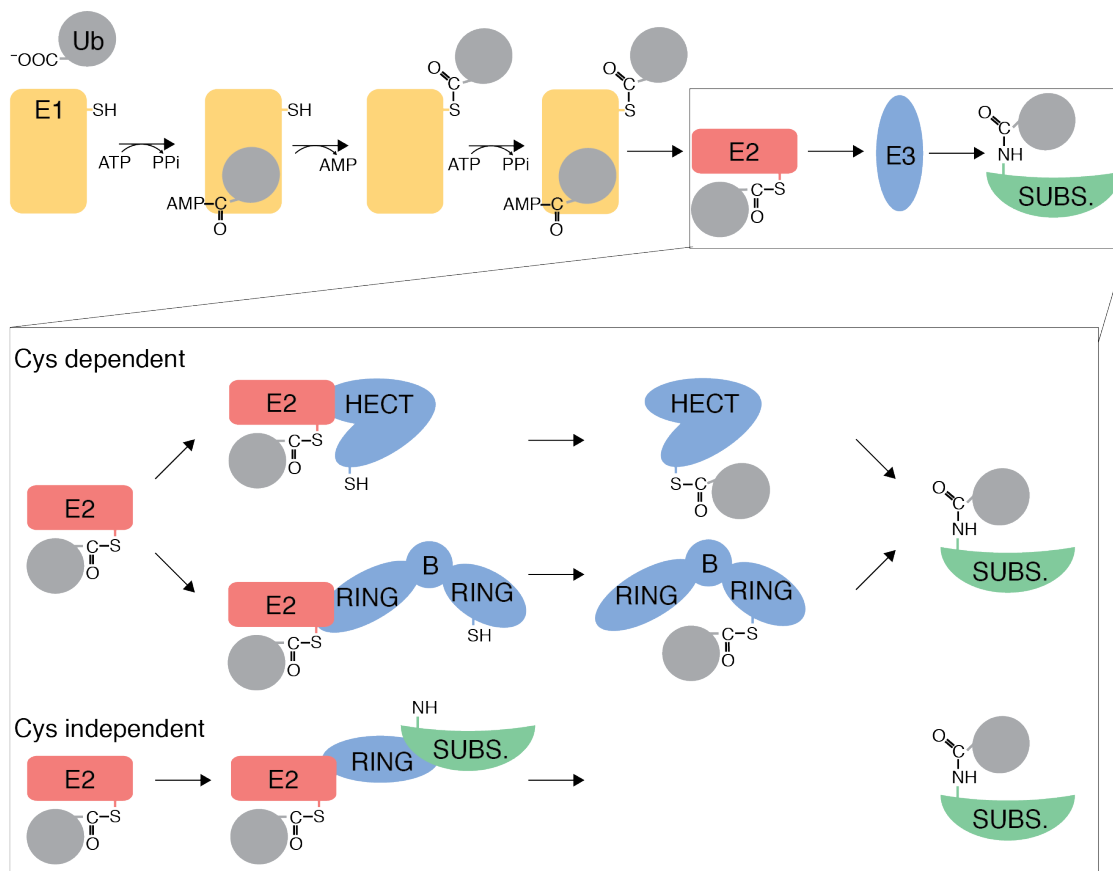
Figure 1.1. Mechanisms of ubiquitination.
The activity of the ubiquitination cascade results in substrate post-translational modification with ubiquitin. Two common mechanisms (cysteine dependent and cysteine independent) are highlighted, where the enzymes in the Ub cascade are labeled E1, E2, E3, and the substrate is labeled SUBS. The expanded box describes specific mechanisms involved in HECT (top), RBR (middle), and RING (bottom) pathways.

1.2 Ubiquitin activation

1.2.1   Ubiquitin

Ubiquitin (Ub), an 8.5 kDa protein, lies at the center of the ubiquitination PTM pathway. This 76-amino acid polypeptide is evolutionarily conserved and contains only three residue modifications from *Saccharomyces cerevisiae* to human (Ser vs. Pro 19, Glu vs. Asp 24, and Ser vs. Ala 28) [33]. Ub contains surfaces that enable its interaction with other macromolecules. The hydrophobic patch consisting of L8, I44, H68, and V70 (herein termed the I44 hydrophobic patch) (Fig. 1.2A) and the smaller I36 patch comprised of I36, L71, and L73 (Fig. 1.2B) mediate protein-protein interactions involving Ub [34]. Towards the N-terminus of Ub, there lies a TEK box motif comprised of K6, L8, T9, K11, E34, and I36 that enables DNA interaction (Fig. 1.2C) [35,36]. Further, there are seven lysine residues (K6, K11, K27, K29, K33, K48, and K63) (Fig 1.2D) and eleven serine, threonine, or tyrosine residues (T7, T9, T12, T14, S20, T22, T55, S57, Y59, S65, T66) (Fig. 1.2E) in Ub that can be sites for modification with the appropriate PTMs.
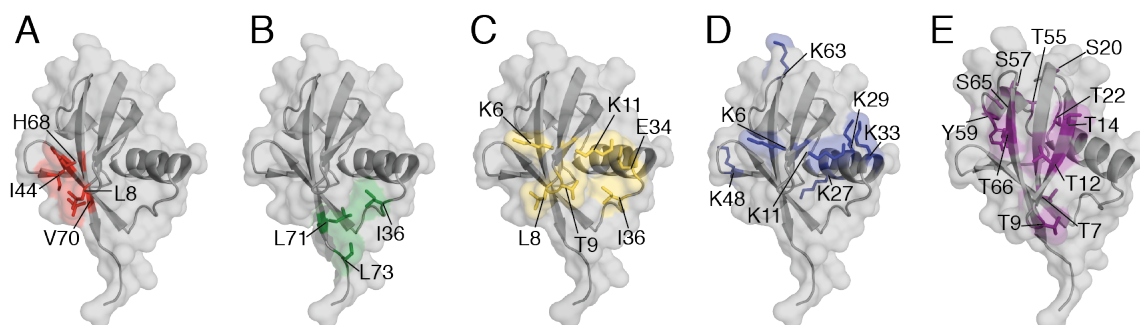
Figure 1.2. Interacting regions of ubiquitin.
The structure of ubiquitin is shown as a cartoon and a semi-transparent surface representation is shown (PDB: 1UBQ). Regions of importance are highlighted as (A) the I44 hydrophobic patch, (B) the I36 hydrophobic patch, (C) the TEK box, and residues of post-translational modification: (D) lysines, and (E) serines, threonines, and tyrosine.

1.2.2   Ub-activating enzyme 1 (UBA1)

The most abundant E1 protein specific to Ub is a large 117 kDa protein called Ub activating enzyme 1 (UBA1). It is arranged into five structural domains (First and Second Catalytic

Cysteine Half (FCCH, SCCH) domains, Inactive Adenylation (IAD) domain, Active Adenylation (AAD) domain, and the Ub-fold domain (UFD)) and contains a four Helix Bundle (4HB) connecting the IAD and FCCH domains [37] (Fig. 1.3, Left). UBA1 contains dual catalytic functions. First, Ub activation with ATP occurs by the AAD domain in the adenylation site. The sidechains of various residues in UBA1 (D463, D465, N471, R474, D537, and N538; *Schizosaccharomyces pombe* (*S. pombe*) numbering) position MgATP in its binding pocket while other residues (T561, N567, Q569, Y579, S582, D584, and E587; *S. pombe*) [38] guide the C-terminal tail of Ub into proximity (Fig. 1.3, Middle). The globular fold of Ub is positioned non-covalently on the anterior of the E1 protein forming
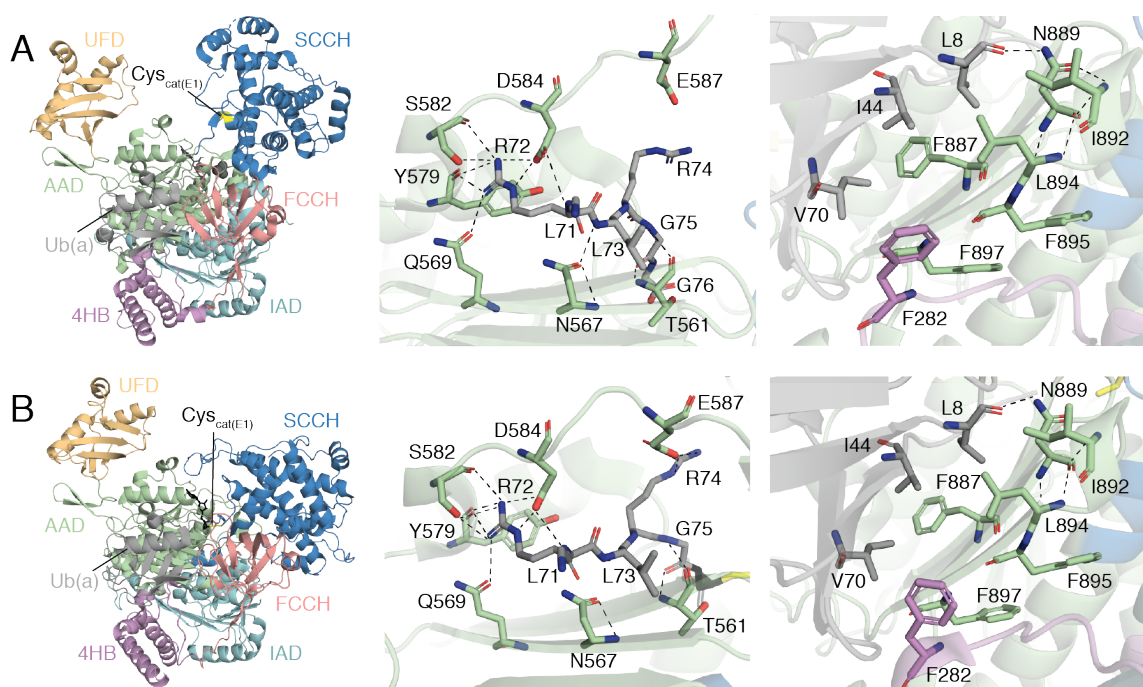
Figure 1.3. UBA1 domain organization and interactions with the Ub-adenylate.
Left: The structure of UBA1 with a non-covalently bound Ub-adenylate [Ub(a)]. The SCCH domain can adopt an (A) open (PDB: 4II3) or (B) closed (PDB: 6O83) conformation. Middle: Residues involved in guiding the C-terminal tail of Ub (shown as grey sticks) are highlighted and coloured according to domain. Right: Residues involved in the non-covalent positioning of Ub(a) against the AAD domain. Polar interactions between residues are indicated with a dashed line.

contacts between the Ub I44 hydrophobic patch and residues in the AAD domain (Fig. 1.3, Right). Activation of the C-terminus of Ub requires the UBA1 protein to be in an open

conformation [39], where the SCCH domain extends upwards parallel to the UFD, and the Cys$_{cat(E1)}$ lies over 30 Å away from the C-terminus of Ub.

Ub activation forms the Ub-adenylate species (herein termed Ub(a)) that is non-covalently bound to UBA1. To form the reactive Ub-thioester (referred to as Ub(t)) species, the SCCH domain of UBA1 rotates posteriorly to a downward facing orientation to position the SCCH into a closed conformation, increasing contacts between the FCCH and SCCH domains [39,40]. In the closed conformation, the Cys$_{cat(E1)}$ folds towards the adenylation pocket to bring the activated C-terminal tail and the cysteine side chain into proximity. The reactivity of the cysteine side chain displaces the adenylate from the Ub C-terminus to form the thioester-linked E1~Ub(t) species. Once the thioester has formed, the Ub releases from the non-covalent binding surface on the IAD and FCCH domains and remains covalently
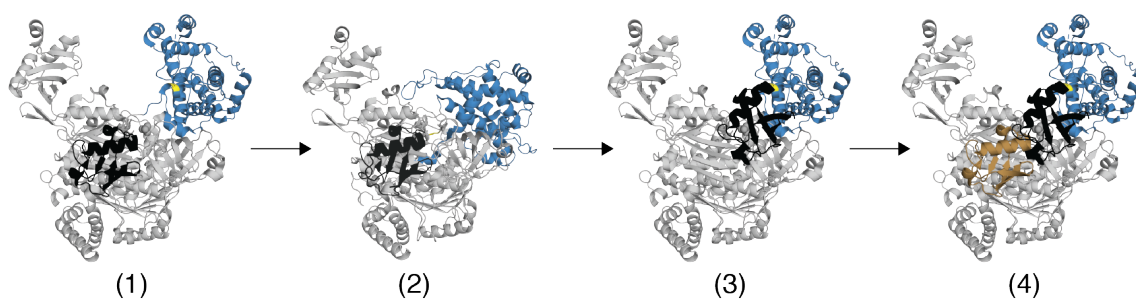
Figure 1.4. The catalytic activity of UBA1 results in a doubly-loaded active complex. The SCCH domain is shown in blue, and the Cys$_{cat(E1)}$ is shown in yellow in all structures. (1) Activation of the C-terminus of Ub (black) forms the Ub-adenylate [Ub(a)] structure bound non-covalently to the open UBA1 conformation. (2) Rotation of the SCCH domain posteriorly to the closed conformation positions the Cys$_{cat(E1)}$ in proximity to the C-terminus of Ub(a) to enable thioesterfication to form UBA1~Ub(t). (3) SCCH domain rotation back into the open conformation pulls Ub(t) upwards, away from the non-covalent binding surface. (4) Recruitment of another molecule of Ub (brown) to the adenylation site re-establishes the Ub(a) species bound non-covalently on the UBA1~Ub(t) complex to form the active UBA1~Ub(t):Ub(a) complex.

tethered to the Cys$_{cat(E1)}$ in the SCCH domain. The SCCH domain then rotates upwards, back into an open conformation. The liberation of the Ub(a) non-covalent binding surface enables the recruitment of a second molecule of Ub(a) to form a fully loaded (active) UBA1 species that contains both Ub(t) and Ub(a) [41]. This active complex (referred to as

UBA1~Ub(t):Ub(a) or UBA1 active complex) is primed for E2 recruitment. Figure 1.4 shows a catalytic flow with structures describing the formation of the UBA1 active complex. Discharge of the Ub(t) onto an E2 protein (described in section 1.3.2) enables the re-formation of the UBA1 active complex through repetition of the adenylation and thioesterfication steps.

1.3 The E2~Ub conjugate

1.3.1   Ub-conjugating E2 enzymes

The human family of E2 conjugating enzymes contains ~35 members that function with Ub. Each E2 protein contains a core catalytic domain (UBC domain) around 150 amino acids in length, and some proteins contain N- or C-terminal extensions that aid in their activity. For example, UBE2D1 and UBE2L3 both contain the UBC domain only, while UBE2K contains a C-terminal extension required for polyUb chain extension [42,43]. The UBC domain of E2 proteins is comprised of four α-helices, a four-stranded anti-parallel β-sheet, and a 3_{10}-helix [44,45], and the catalytic cysteine residue lies in a small, conserved loop between β4 and helix α2 (Fig. 1.5). Protein-protein interactions can be mediated through multiple regions on an E2 protein including the N- and C-termini and the posterior helix α2 (crossover helix) [45].

1.3.2   Formation of E2~Ub

An E2 protein gets recruited to the top portion of the E1 active complex, binding the cleft between the UFD and SCCH domain when the UBA1 is in an open conformation. The binding of an E2 enzyme to the UBA1 complex occurs through charge-charge interactions where acidic residues in the UFD extend towards basic residues in helix α1 at the N-terminus of the E2 [46,47]. Although these basic residues are well conserved among E2 proteins, not every E1:E2 complex will utilize these interactions. In the case of ubc4, for example, the basis of the UFD:E2 interaction occurs through a series of non-polar residues that interact with the loop C-terminal to helix α1 [38]. On the opposite side of the cleft, the interaction is mostly non-polar, involving key phenylalanine residues (F598, F689, and F701; *S. pombe* numbering) in the SCCH domain and helix α3 towards the C-terminus of
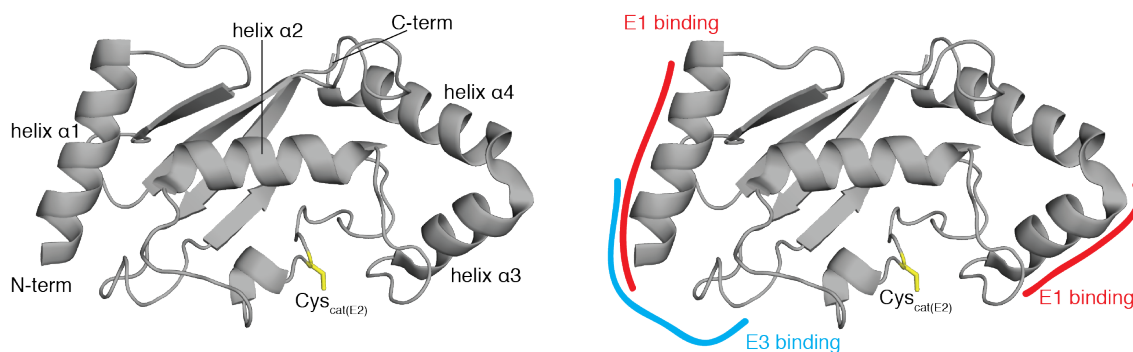
Figure 1.5. The UBC domain of E2 enzymes has a conserved fold.
The catalytic core of E2 proteins is shown in cartoon representation and important secondary structures are labeled. The catalytic cysteine ($Cys_{cat(E2)}$) lies in a loop between β4 and helix α2 (yellow). Non-covalent binding surfaces for the E1 protein and E3 ligases are indicated on the right by red and blue lines, respectively.

the E2 protein. Interestingly, the crystal structures of the non-covalent E1:E2 binding surface show that the positioning of the E2 differs based on identity, as the structures for cdc34, ubc4, and ubc15 do not overlay perfectly. Instead, minor rotation in the UFD or SCCH domain modify the positioning of helix α1 or α3, respectively [38,46,47].

After E2 binding and the transthiolation from $Cys_{cat(E1)}$ to $Cys_{cat(E2)}$, the newly formed E2~Ub species dissociates from the UBA1:Ub(a) complex and exists until recruited by an E3 protein. The E1 and E3 binding sites on an E2 protein (Fig. 1.5, Right) contain overlapping regions, indicating that non-covalent interactions with these two different classes of ubiquitination proteins must be mutually exclusive: it is unlikely that an active E1, E2, E3 complex exists in solution. In cells, the majority of the E2 enzyme pool exists pre-conjugated to a Ub molecule enabling a significant proportion of the E2 population to be primed for E3 ligase interaction [48].

1.3.3   E2~Ub conformations

The E2~Ub intermediate, joined together by a single intermolecular covalent bond, allows the two proteins to adopt a globular structure (closed conformation), or a dumbbell-shaped structure (open conformation). In the closed conformation, the conjugated Ub folds back onto the E2 and has significant non-covalent interaction with the crossover helix α2 of the

E2 protein. The closed conformation of E2~Ub has been observed for multiple E2 proteins including UBE2D2 [49,50], UBE2N [51], and *S. cerevisiae* ubc1 [52]. Despite lacking an appropriate three-dimensional structure, in-solution data for UBE2L3~Ub indicates this enzyme can also adopt a closed conformation [53]. The available structures of UBE2L3~Ub conjugates were solved in complex with various E3 proteins and occupy the open conformation [54–56]. The open conformation lacks non-covalent interaction between the E2 protein and the Ub. While there is only one way to form the closed species, the open conformation is less stringent and the Ub can adopt a wide array of positions along the x-, y-, and z-axes (Fig. 1.6). The distinction between open and closed conformations has downstream implications in ubiquitination, where certain E3 proteins require the E2~Ub species to adopt a specific conformation for binding and catalysis. Various biophysical and structural experiments such as Nuclear Magnetic Resonance (NMR) spectroscopy [53], X-ray crystallography [57–59], or fluorescence-based experiments such as Förster Resonance Energy Transfer (FRET) [60] have been elegantly used to provide insight on the conformation of E2~Ub conjugates in the presence and absence of an E3 ligase.
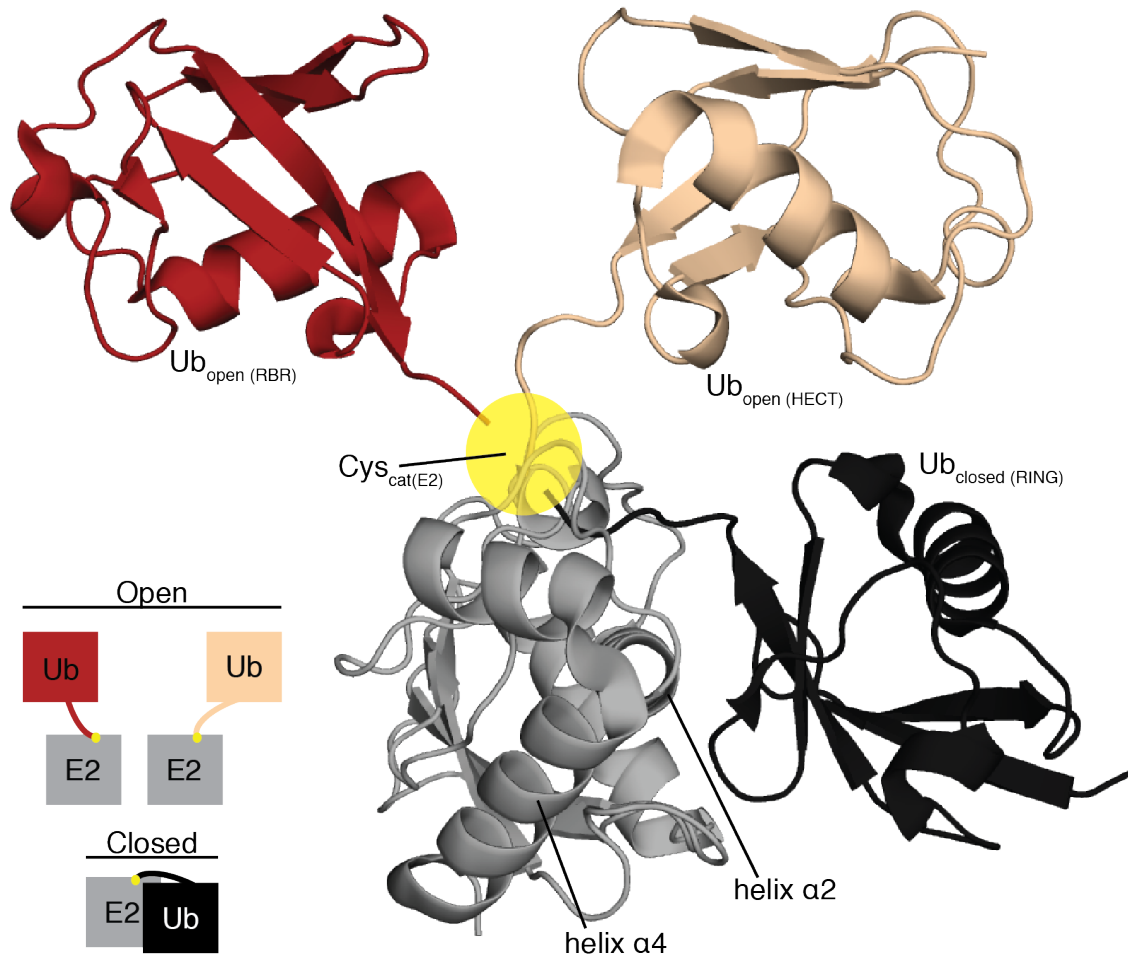
Figure 1.6. E2~Ub conjugates adopt an array of conformations.
Shown are three representative structures of E2~Ub conjugates demonstrating the closed (black) and open (beige and maroon) conformations preferred by RING, HECT, and RBR E3 ligases, respectively. Structures were sampled from the Protein Data Bank (PDB) and contain coordinates 4AP4, 3JVZ, and 5EDV, respectively. The schematic in the bottom left shows the non-covalent interaction between the E2 and Ub in the closed conformation, which is not present in open conformations. The $Cys_{cat(E2)}$ is depicted in yellow and the E2 protein is in grey.

1.4 E2~Ub interactions with E3 ligases

1.4.1 Cysteine-dependent mechanisms

Around 30 of the human E3 proteins are of the HECT type, and these proteins can be further subdivided based on domain architecture [30]. Consistent across all HECT ligases,

the catalytic HECT domain is situated at the C-terminus of the protein and can be divided into two regions. Named based on their sequential order, the N-lobe of the HECT domain recruits and binds the E2~Ub conjugate, while the C-lobe contains the catalytic cysteine. Various HECT proteins have been implicated in signaling pathways such as sodium transport [61–63], the DNA damage response [64,65], and the inflammatory response [66]. When recruiting an E2~Ub conjugate, HECT proteins require the conjugate to adopt an open conformation with little non-covalent interaction between the E2 and the Ub [56]. A transthiolation reaction between the E2 and the HECT domain permits the formation of the E3~Ub intermediate, where the Ub is covalently bound to the $Cys_{cat(E3)}$. As the last enzyme to handle the Ub, HECT proteins play a role in discriminating polyubiquitin linkage type (discussed in section 1.5). HECT proteins have been shown to function with E2 proteins such as UBE2L3 [67–69] and the UBE2D family [70].

Although the HECT domain is conserved between members of the family, there exist other proteins that lack a HECT domain, but use mechanisms of cysteine-dependent ubiquitination. Many of these proteins are found in bacteria [71] and can be referred to as HECT-like. Additional classes of human E3 proteins that lack a HECT domain but have roles in cysteine-dependent ubiquitination include the RING-inBetween-RING (RBR) [31] and the newly characterized RING-Cys-Relay (RCR) proteins [72]. By forming the RBR~Ub or RCR~Ub intermediates, these classes of E3 proteins also hold the key to polyubiquitin specificity.

1.4.2   Cysteine-independent mechanisms

The second and largest class of E3 ligases utilize a cysteine-independent catalytic mechanism to support auto- or substrate ubiquitination. These families include the well-studied RING and Cullin proteins [73,74]. These E3 proteins do not form an E3~Ub intermediate; rather, they co-bind a substrate and an E2~Ub conjugate in the closed conformation to facilitate transfer directly to a substrate lysine. Cysteine-independent E3 proteins can use a larger subset of the E2 conjugating enzymes including the UBE2D family and UBE2N:UBE2V2, and sometimes use multiple to modify a single substrate [35]. The lack of a distinct E3~Ub intermediate therefore puts the chain specificity on the

E2 protein. Among other involvements, cysteine-independent E3 proteins have been implicated in DNA damage repair, transcriptional regulation, and immune signaling [75–77].

1.5 Polyubiquitination

Consecutive rounds of the E1, E2, E3 cascade enable the repeated ubiquitination of a substrate. Multiple rounds of ubiquitination results in a protein species that is polyubiquitinated, where sequential ubiquitin molecules can be covalently attached at different target residues or the original target residue. The former, termed mono-ubiquitination, often acts as a signaling event in cells [78]. Sequential additions of Ub at the original target residue occurs through the formation of polyubiquitin (polyUb) chains. During polyUb formation, the C-terminus of the initial Ub modifies the substrate residue, while the succeeding Ub molecules modify a residue within the initial Ub. The seven lysine residues (K6, K11, K27, K29, K33, K48, and K63) as well as methionine1 (M1) act as Ub acceptor sites in chain formation. The outcome of polyubiquitination, whether it be a signaling event such as endocytosis or DNA damage repair, or protein degradation via the 26S proteasome or lysosome, depends on the topology of polyUb [79]. In addition to substrate and auto-ubiquitination, some chain-driving proteins can synthesize free (unanchored) polyUb chains. Here, the substrate protein is a monomer of Ub acting as an acceptor for ubiquitination. For example, UBE2K can synthesize free polyUb connected through K48 without the requirement for an E3 protein [80], while the RING system containing UBE2N:UEV2V2:RNF8 can synthesize K63 linkages [81].
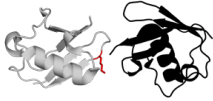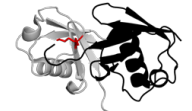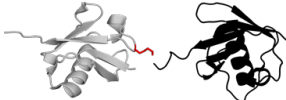
The eight polyUb chain attachment sites on Ub are contained within different secondary elements of Ub; therefore, it would be expected that different linkages would be structurally distinct. The Protein Data Bank (PDB) contains structures for all eight di-Ub molecules (Ub_2) that contain a range of conformations both with and without accessory proteins like E3 ligases. Most of the structures available depict a single conformation captured in X-ray crystallography experiments, but similar to E2~Ub conformations discussed above in section 1.3.3, polyUb chains can adopt an array of conformations in solution. In chains longer than two Ub molecules, regions of the chain might adopt more

compact conformations while others could be more open, significantly complicating the analysis of available structures. Table 1.2 summarizes the current knowledge of polyubiquitination outcomes and depicts some of the Ub_2 structures available.

Table 1.2. Summary of homotypic polyUb chains[a].
In the diUb structures, the donor Ub is in black in the same orientation throughout, and the acceptor Ub is shown in grey with the linked Lys in red.

Chain Type	diUb Structure	PDB code	E2/E3 proteins[†]	Cellular involvement
Met 1		3AXC	HOIP (LUBAC)	Inflammation and immunity (NFkB, TNF signalling), kinase recruitment and signalling
Lys 6		2XK5	NleL*, BRCA1-BARD1, HUWE1	Autophagy, DNA damage response
Lys 11		2MBQ	NEDD4, UBE2S, RNF8	Proteasomal degradation, cell cycle progression
Lys 27		6ISU	ITCH, RNF168, HACE1	DNA damage response, protein secretion
Lys 29		4S22	UBE3C, SMURF1, TRIM13	Epigenetic regulation, WNT/β-catenin signalling
Lys 33		4XYZ	AREL1, CBL-B	Post golgi trafficking
Lys 48		3M3J	IPAH3*, UBE2K, E6AP	Proteasomal degradation
Lys 63		2JF5	Parkin, RNF8, TRAF6, UBE2N/UBE2V2	Immunity (NFkB), DNA damage response, kinase recruitment and signalling

[a] References corresponding to this table are [34,79,82–90]
[†] Exemplary E2 and E3 enzymes are included. Many other enzymes have been identified for specific polyUb chains
* Bacterial effector proteins with E3 ligase activity

1.6 Quantitative ubiquitination

The nature of the current literature surrounding ubiquitination is mostly qualitative, often identifying functional E2:E3 pairs, linkage preference/specificity, or examining various activation states in a relative manner. Endpoint ubiquitination experiments are common practice and give excellent visual insight on longer time-frame reaction progression. Typically, these experiments show minute or hour timepoints of a full ubiquitination assay when a lot of the transient covalent intermediates of the system have reached equilibrium and cannot be measured. One major benefit to using gel-based experiments is that scientists can visually conclude which systems might be better or worse than others; however, a substantial drawback of these assays is the fact that the initial stages in the reaction (namely Ub activation and E2~Ub formation) are hidden.

The methods used to study ubiquitination often rely on immunoblotting with a Ub-specific antibody or visualizing ubiquitinated species with a small fluorescently- or radio-labeled molecule. Therefore, the detection of ubiquitinated species relies heavily on the amount of a given species in the reaction. These gel-based time course experiments containing both fast timepoints and endpoints that can be used in band densitometry analyses to quantify ubiquitination reactions. Full ubiquitination patterns can be observed within minutes of starting a reaction, demonstrating that with all the right components, ubiquitination occurs rapidly. Unfortunately, each individual step in the mechanism remains poorly quantified. Early efforts focused on understanding the mechanism by which UBA1 activates and transfers the Ub onto an E2 protein. UBA1 saturation occurs rapidly with excess ATP and Ub [91,92], and it is generally accepted that the transthiolation from UBA1 to an E2 protein represents the rate-limiting step in E2~Ub formation [48]. Toward the end of the pathway, the initial Ub transfer step is the limiting factor for substrate ubiquitination by the SCF E3 ligase [93]. Other examples show that substrate ubiquitination can be limited by the choice of E2 enzyme that can have different rates for priming and elongating Ub chains. For example, the anaphase promoting complex (APC/C) E3 ligase can use UBE2C or UBE2D1 and UBE2S to prime and elongate Ub chains, respectively. In the absence of a priming E2, UBE2S cannot modify the APC/C substrate securin, but the extent of securin modification with long polyUb chains increases with either priming E2 present [94]. These studies have

elegantly provided details for the kinetics and time scales for the formation of the UBA1~Ub(t) species, various E2~Ub conjugates, and substrate–Ub complexes, and have highlighted the importance in choosing functional E2:E3 pairs.

1.7 Ubiquitin modifications

The abundance of PTM activity in cells requires both distinct and converging pathways. In addition to convergence due to targeting the same substrate residues, unique PTMs often work in cooperativity to complement or oppose actions. One of the best understood pairs of PTMs acting as opposite functional signals are acetylation and phosphorylation [95,96]. The same is true for methylation and phosphorylation, where it has been established that both PTMs can regulate processes like the cell cycle [97]. Further, many methylation enzymes contain kinase recognition signals themselves, indicating their function may be regulated by phosphorylation [98]. Phosphorylation also has roles in ubiquitination pathways where the PTM regulates the function of certain E3 proteins. Among the best understood connections between E3 ligase activity and phosphorylation are phospho-parkin and phospho-ITCH. Parkin phosphorylation at S65 by kinase PINK1 is required for complete activation of ligase activity [99,100], and ITCH phosphorylation at S257 by kinase AKT1 causes ITCH nuclear translocation and subsequent ubiquitination of histone H1.2 [64]. Finally, ubiquitination, sumoylation, and neddylation might be required for enzyme activation. The best example of these larger modifications increasing function are the Cullin-RING E3 ligases, which must be neddylated prior to their ubiquitination activity [101].

A more recently emerging PTM convergence between the smaller one-writer systems and ubiquitination occurs with modified Ub. Essentially, the convergence of two PTMs can take the form of a "PTM of a PTM", where a modifier protein like Ub acts as the substrate for various other PTM pathways. PTM sites on Ub have been discovered in recent years due to the advancement in mass spectrometry techniques to detect and isolate modified peptides. At the center of post-translationally modified Ub, phosphorylation of S65 has been extremely well studied due to its involvement in parkin-mediated mitophagy [102–104]. Other phosphorylation sites such as T12 or S57 have also been shown to be important

for the DNA damage response or parkin activation, respectively [105,106], but the full extent to which these modifications influence ubiquitination remains unknown. The identification of the requisite kinases for these phosphorylation sites has accelerated the study of phosphorylated Ub (pUb) when compared to some other modifications.

More interestingly, the discovery of Ub peptides containing acetyl-lysine from proteomics datasets implies coordination of multiple lysine PTMs during ubiquitination. In deacetylase knock-out or knock-down experiments, an increase in acetylated Ub peptides is observed, which indicates that Ub acetylation is a tightly regulated process [107–110]. An increase in acetylated Ub (acUb) peptides was also detected in whole cell lysates from experiments studying cell stress. For example, autophagy induced by treatment with rapamycin [111] and DNA damage response due to ultraviolet or ionizing radiation [112] led to the detection of acUb peptides. In these datasets, acetylation sites covered six out of the seven lysine residues in Ub; only acetylation at K29 has yet to be observed. However, early experiments studying the chemical acetylation of Ub showed that all lysine residues, including K29, are susceptible to chemical acetylation [113,114], implying that either the correct cellular conditions for enzymatic acetylation of K29 have yet to be discovered, or the peptides containing acK29 are too small to be detected using mass spectrometry.

The detection of different forms of acUb indicates there are specific KATs, yet to be characterized, that control these events. These unidentified enzymes pose a significant barrier to understanding the role acetylation might have in ubiquitination. To avoid this barrier, one approach is to substitute glutamine at the acetyl-lysine position of interest [115,116]. Glutamine contains both non-polar and polar regions similar to the structure of acetyl-lysine. However, the acetyl-lysine side chain is longer and less polar and has the potential to form more extensive hydrophobic contacts than glutamine, suggesting glutamine substitution may not be indicative of the full effects of acetylation. Recently, many acetylated proteins [117,118], including Ub [119], have been produced in *Escherichia coli* using genetic code expansion. Reassignment of the amber stop codon (UAG) and the use of tRNA$^{Pyl-opt}$ enable a fast and accurate way to produce homogeneous acetylated proteins *in vitro* and has been applied *in vivo*.

1.8 Scope of thesis

The field of post-translationally modified Ub has been dominated by studies of phosphorylation at S65. Recent studies have ventured into studying the effects of other phosphorylated residues such as T12 and S57. With the discovery that events of cell stress up-regulate signaling, trafficking, and proteostasis mechanisms, newer and more sensitive mass spectrometry techniques have enabled the detection of acetylation sites that might otherwise occur too infrequently. These identified acetylation sites include six out of the seven lysine residues in Ub: a proportion that covers 80% of possible polyubiquitin chain building loci. At the start of this thesis, there had been only one study that included Ub acetylation. However, this study had two major drawbacks: 1) only two of the lysine residues (K6 and K48) were examined, and 2) the conclusion that acetylation inhibits polyubiquitin formation was almost too intuitive. There were no examinations into how the acetylated Ub proteins were processed differently than unmodified Ub or how acUb quantitatively modulates the steps in ubiquitination. This thesis sought to provide a more complete characterization of all the different acUb proteins and addresses the following specific questions:

1)   How can acetylated ubiquitin proteins be homogeneously expressed and purified?
2)   How does acetylation alter Ub charging by the E2 proteins UBE2D1 and UBE2L3?
3)   How does acetylation modify E2 discharge in the presence of an E3 ligase?
4)   What influences does an acUb protein have on E2~Ub conjugate conformation?

To address these questions, an optimized expression and purification protocol was evolved from a standard Ub protocol. Chemical biology methods to use an orthogonal translation technique enabled the site-specific incorporation of acetyl-lysine at the position of interest. These methods proved crucial to produce large quantities of specifically acetylated Ub proteins that could not be reached with enzymatic or chemical methods alone. The competency of these acUb proteins in cysteine-dependent and independent ubiquitination pathways was then evaluated using qualitative gel-based experiments.

Next, the same orthogonal translation technique was used to create a series of acUb proteins containing an N-terminal CyPet fluorophore. These proteins, with constructs of UBE2D1 or UBE2L3 that contained an N-terminal YPet fluorophore, enabled a highly sensitive and robust Förster Resonance Energy Transfer (FRET) assay to be developed and optimized to examine the kinetics of E2~Ub conjugate formation with these E2 conjugating enzymes. To understand how acetylation alters transfer from UBE2D1 or UBE2L3, gel-based experiments monitoring the density of the E2~Ub band over time in the presence of the cysteine-dependent E3 proteins IPAH3 or HUWE1 were used. These experiments allowed both qualitative and quantitative conclusions to be drawn about how Ub acetylation modifies E2~Ub behaviour.

Finally, to provide insight on how acetylation alters Ub structure, NMR spectroscopy was used. Similar methods were applied to determine what effect acetylated Ub has on E2~Ub conjugate conformation when covalently attached to the E2 UBE2L3.

Overall, this thesis provides the first comprehensive experiments for all possible acUb variant proteins. As Reviewer #2 once said:

> *"This study is significant because recent studies have highlighted the importance of a variety of posttranslational modifications of Ub, including acetylation, in regulating its ability to regulate a variety of cellular processes and this study is the first to systematically and thoroughly analyze functional consequences of ubiquitin acetylation on its ability to progress through the Ub conjugation system."*

-Reviewer #2, 2021

2

Programmed ubiquitin acetylation reveals altered ubiquitination patterns[†]

2.1 Introduction

The use of archaically derived tRNAs and aminoacyl tRNA synthetases has rapidly expanded the field of protein biochemistry and the study of post-translational modifications. In particular, the tRNA$^{\text{Pyl-opt}}$ and acetyl-lysine tRNA synthetase (acKRS) pair that is orthogonal to *E. coli* has proved instrumental in producing and studying various acetylated proteins [117,120,121]. In terms of ubiquitination, Ohtake and colleagues used this system to study Ub acetylated at K6 or K48 [119], while work from the lab of Stefan Muller examined acetylated SUMO1 (K37) and SUMO2 (K11, or K33) [116,122].

Acetylation has been observed at over 85% of lysine residues in Ub in situations of cell stress. While the work on acetylation at K6 or K48 serves as an excellent initial study, acetylation of the other five lysine residues remains to be characterized. To address gaps in the field of ubiquitin acetylation, we developed and optimized a strategy for homogenous incorporation of acetyl-lysine at single loci in Ub to yield all possible acetylated Ub (acUb)

variants in their purified forms. The utility of these acUb variants was validated in preliminary ubiquitination studies with both HECT- and RING-type E3 ligase proteins.

2.2 Materials and methods

2.2.1 Plasmids and cloning

A wild-type Ub gene from *Saccharomyces cerevisiae (S. cerevisiae)* containing an N-terminal His-tag (His-TEV-Ub) was used as a template for all mutagenesis. Acetyl-lysine (acK) substitutions were introduced at positions K6, K11, K27, K29, K33, K48, or K63 of Ub using site-directed mutagenesis at the corresponding lysine codon to insert the amber stop codon (UAG). Successful PCR products for seven unique plasmids were confirmed with DNA sequencing and transformed into *E. coli* MM294 for plasmid maintenance. Acetylated Ub constructs were in an ampicillin-resistant pMCSG7 vector (herein referred to as His-TEV-acUbKx, where x denotes the acetylated residue), and the orthogonal acetyl-lysine tRNA synthetase (acKRS) and tRNA[Pyl-opt] were coded for on a chloramphenicol-resistant pTech-acKRS-tRNA[Pyl-opt] vector (referred to as 'pTech').

2.2.2 Protein expression and purification

2.2.2.1 *Cotransformations.* After fresh purifications of the His-TEV-acUbKx and pTech plasmids, DNA was diluted to 100 ng/µL and stored for 3-4 months at -20 °C. Competent BL21(DE3) cells were mixed with 100-200 ng of each plasmid in a 1:1 ratio and plasmid uptake was stimulated using either the heat shock method or electroporation. For heat shock transformations, the cell/DNA mixtures were incubated on ice for 30 min followed by 45 s at 42 °C. For transformations by electroporation, cell/DNA mixtures were transferred into electroporation cuvettes and air bubbles were removed by tapping the cuvette against the lab bench. The electrodes were dried, and electroporation was conducted using a BioRad gene pulser set at 2.5 kV, 200 Ω, 25 µfd. After the heat shock or electroporation, 400 µL of Super Optimal broth with Catabolite repression (SOC) media was added, and cells grew at 37 °C for 60 min. The cells were then pelleted and resuspended in 100 µL SOC for plating on selective Luria broth (LB) agar and incubated overnight at 37 °C.

2.2.2.2 *acUb optimization.* A single cotransformant was selected and used to inoculate 5 mL of selective Luria broth (LB) (50 µg/mL ampicillin and 34 µg/mL chloramphenicol) overnight at 37 °C. Following, 1 mL of the starter culture was transferred into 100 mL of fresh LB and grown to $OD_{600}= 0.4$. During these test expressions, media were supplemented with 3–100 mM acetyl-lysine as indicated (acK; Bachem) and 10 mM nicotinamide to inhibit endogenous deacetylases. Cells were then grown to $OD_{600}= 0.8$, induced with 1 mM isopropyl β-D-1-thiogalactopyranoside (IPTG), and incubated with shaking overnight at 16 °C. Cells were harvested and resuspended in 30 mL of wash buffer (50 mM Tris pH 8.0, 500 mM NaCl, 10 mM imidazole, 15 mM nicotinamide, 250 µM Tris(2-carboxyethyl)phosphine (TCEP)). One third of a tablet of ethylenediaminetetraacetic acid (EDTA)-free mini protease inhibitor cocktail and 0.7 mM phenylmethylsulfonyl fluoride were added to the cells. Cells were lysed via an EmulsiFlex-C5 homogenizer (Avestin), and the soluble fraction from a highspeed ultracentrifugation was purified on Ni^{2+}-NTA resin. The resin was washed with wash buffer, and His-TEV-acUb proteins were eluted using 50 mM Tris pH 8.0, 500 mM NaCl, 250 mM imidazole, and 250 µM TCEP. The His-tag from each acUb was removed by overnight incubation with tobacco etch virus (TEV) protease (2.5 mg TEV/ 1 L growth). Cleaved acUb proteins were further purified on Ni^{2+}-NTA resin by washing with 50 mM Tris pH 8.0, 250 mM NaCl, and 250 µM TCEP and collecting the flowthrough fractions.

After collecting the flowthrough from the second Ni^{2+}-NTA affinity column, anion exchange chromatography was used to attempt to separate the multiple species of full-length Ub expressed in growths with low concentrations (3-10 mM) of acK. The protein solution was injected onto a HiTrap Q XL column in wash buffer containing 50 mM Tris pH 9.0, 250 µM TCEP. An elution gradient from 0-1 M NaCl was used to remove bound proteins. Protein species were visualized by SDS-PAGE and masses were identified using full-length mass spectrometry.

For growths with low concentrations (3-10 mM) of acK, reverse phase-high performance liquid chromatography (RP-HPLC) was also used to try to separate mistranslated protein from acUb protein. After the initial two Ni^{2+}-NTA purifications, the protein solution was injected onto Phenomenex C18 peptide column (300 Å, 4.6 x 250 mm, 5 µm). Protein

species were separated using a water/acetonitrile gradient with 0.1% trifluoroacetic acid between 28-43% acetonitrile over 45 minutes and identified by full-length mass spectrometry.

2.2.2.3 *acUb expression and purification.* Following acUb optimization, subsequent expressions used 10 mM nicotinamide and 75 mM acK supplemented in the medium. Cells were grown, protein expression was induced, and cells were harvested as indicated in section 2.2.2.2. After harvesting, one EDTA-free mini protease inhibitor cocktail tablet and 0.7 mM phenylmethylsulfonyl fluoride was added to the pellets. Cells were lysed, the soluble fraction was obtained, and protein was purified using two step Ni^{2+}-NTA affinity chromatography as indicated in section 2.2.2.2. Subsequent purification of the flowthrough fractions was done using Superdex75 gel filtration pre-equilibrated in 25 mM Tris pH 8.0, 250 mM NaCl, and 250 µM TCEP. Protein purity and homogeneity was confirmed via SDS-PAGE, western blotting, and liquid chromatography–mass spectrometry (LC-MS). Western blots were performed after transferring proteins to a PVDF membrane using an iBlot Gel Transfer Device (Invitrogen) and the preset P0 cycle. The membrane was blocked with 5% w/v skim milk powder in TBST. Acetylated Ub proteins were detected with a rabbit anti-acetyl-lysine primary antibody (Immunechem; ICP-0380, 1:2000) and probed with IRDye 680RD goat anti-rabbit secondary antibody (LI-COR; 926- 68071, 1:20 000). Membranes were visualized using a LI-COR Odyssey Imaging System.

2.2.2.4 *Purification of ubiquitination enzymes.* Human UBA1 (E1), UBE2D1, UBE2L3, and UBE2N:UBE2V2 (E2), and the RING domain (residues 345-485) of RNF8 (herein termed RNF8) and the C-terminal domain of invasion plasmid antigen H3 (residues 270-571; herein termed IPAH3) (E3) enzymes used in ubiquitination assays were produced and purified to homogeneity as described previously [123–126]. Briefly, all proteins were overexpressed in *E. coli* BL21(DE3) cells, and most constructs except UBE2V2 and RNF8 contained a His-tag that enabled Ni^{2+}-NTA affinity purification. His-tagged proteins were purified in buffers containing 50 mM Tris pH 7.5, 500 mM NaCl, 10% glycerol with either 10 mM (wash) or 250 mM (elution) imidazole. UBE2V2 and RNF8 constructs contained an N-terminal Glutathione S-Transferase (GST) tag to enable GSTrap FF affinity purification. These proteins were purified in buffers containing 10 mM Na_2HPO_4, 1.8 mM

KH$_2$PO$_4$ pH 7.4, 137 mM NaCl, 2.7 mM KCl (1x PBS; wash), and 50 mM Tris pH 8.0, 20 mM reduced glutathione (elution). For both proteins, the GST-tag was removed with PreScission (PreSc) protease and the proteins underwent a 72-hour dialysis period to remove excess glutathione prior to subsequent purification on the GSTrap FF column. UBE2V2 was further purified using a HiLoad 16/60 Superdex75 column equilibrated in 25 mM Tris pH 8.0, 100 mM NaCl, 250 µM TCEP.

To form the UBE2N:UBE2V2 heterodimer (active E2 complex), equimolar parts UBE2N and UBE2V2 purified individually were mixed at room temperature for 10 minutes and the dimeric complex was purified using a HiLoad 16/60 Superdex75 equilibrated in 50 mM Hepes pH 7.5, 75 mM NaCl, 1 mM EDTA, 1 mM DTT. The dimer eluted with a retention volume of 72 mL and was validated by SDS-PAGE.

2.2.3   Mass spectrometry

All mass spectrometry was performed at the Biological Mass Spectrometry Laboratory at the University of Western Ontario. Full-length mass determination was performed using a QToF Ultima mass spectrometer (Waters Corporation) equipped with a Z-spray source and run in positive ion mode. An Agilent 1100 HPLC was used for liquid chromatography (LC) gradient delivery. Data were surveyed from 600 to 3000 m/z, and the instrument was calibrated with myoglobin with a mass error of 0.5 Da. A Phenomenex Luna C4 (300 Å, 1.0 x 150 mm, 5 µm) column was used for separation using a water/acetonitrile with 0.1% formic acid gradient at 0.2 mL/min. Data were acquired and processed using MassLynx 4.1 (Waters Corporation).

All acUb samples were prepared for LC-ESI-MS/MS by digestion with trypsin. Proteins were reduced with dithiothreitol (DTT) and alkylated with iodoacetamide using standard protocols. Trypsin was used to digest acUb proteins at a ratio of 1:50 for 18 h at 37 °C. A second aliquot of trypsin (1:100) was then added and the reaction continued for another 4 h. Samples were acidified and injected into an ACQUITY UPLC M-Class System fitted with an ACQUITY UPLC M-Class Symmetry C18 Trap Column (Waters Corporation). After trapping, peptides were passed through an ACQUITY UPLC M-Class Peptide BEH C18 Analytical Column (15K psi, 130 Å, 1.7 µm x 25 mm) for separation, using a 120-min

run time. The LC system was directly connected to a NanoFlex (Thermo Electron Corp.) nanospray ionization source with a source voltage of 2.4 kV and interfaced to an Orbitrap Elite mass spectrometer (Thermo Electron Corp.) controlled by XCALIBUR software and operated in the data-dependent mode using an FT/IT/CID Top 10 scheme. The 10 most abundant multiply charged ions were automatically selected for subsequent collision-induced dissociation in the ion trap (IT/CID). Collected data were processed using PEAKS X software (Bioinformatics Solutions) to identify peptides.

2.2.4   Ubiquitination assays

Ubiquitination assays were conducted using 0.2 µM UBA1, 1 µM E2, 2 µM E3, 8 µM Ub, or acUb, 5 mM MgATP, and 50 mM Hepes at pH 7.4. Reactions were conducted at 37 °C for 10 min and were subsequently quenched with SDS sample buffer containing 20 mM DTT. Ubiquitination products were resolved on gradient gels (4–12 % BisTris Plus; Thermo Fisher Scientific) with MES running buffer [50 mM MES, 50 mM Tris, 0.1% SDS, and 1 mM EDTA at pH 7.4]. Silver staining was used to visualize protein species.

2.3 Results

2.3.1   Optimization of acUb purification using orthogonal translation

The production of site-specific acetylated protein requires exogenous acetyl-lysine (acK) to be added to the growth medium prior to induction of expression. Various other proteins such as myoglobin [117], histone H3 [120], and thioredoxin reductase [118] have been successfully translated in *E. coli* with low amounts of acK. Thus, the initial attempts at producing site specific acUb proteins were done using 5 mM acK. All initial expressions were completed with DNA constructs to make acUbK48 (where the acetylation is at Lys48) because this acUb protein had previously been observed to be expressed and soluble. Figure 2.1 shows an initial purification of acUbK48 on Ni^{2+}-NTA resin. To purify acUbK48, the soluble fraction (S) from a highspeed centrifugation was batch bound to Ni^{2+}-NTA resin, and the flowthrough (FT) containing bacterial, non-His-tagged proteins was collected. The FT fraction contained low to trace amounts of acUbK48 as demonstrated by the lack of thicker bands around ~11 kDa. The final protein fractions (FP)

demonstrated that the acUbK48 protein could be purified from most other contaminants using two sequential nickel columns. Of note, a high molecular weight protein (around 75 kDa) and minor contamination with medium molecular weight protein (labeled †, ~48 kDa) can be observed in this preparation. In subsequent preparations of acUb proteins, the higher molecular weight contaminant was removed using more stringent washing conditions in affinity chromatography steps. In terms of the induced expression of the acUbK48 protein, much of the protein was full length product and only 5-10% was truncated at residue 48 to form Ub_{1-47}, evidenced by the faint band that migrated farther than acUbK48 in SDS-PAGE.

To confirm the incorporation of acK into Ub, we chose to use mass spectrometry to identify the full mass of protein species. A peak corresponding to a mass of 8859.9 Da (Fig. 2.1B) confirmed the presence of acUbK48 (MW_{exp}= 8860.11 Da). However, also detected was a mass of 8817.9 Da, a –42 Da mass difference from acUbK48. Based on this molecular weight difference, this smaller species could correspond to either wild-type or a glutamine/glutamate substitution at the acK position. As wild-type Ub could be the result of mistranslation or deacetylation, we attempted to inhibit deacetylation by adding nicotinamide, as demonstrated previously [117]. We found that the lower molecular weight species was insensitive to nicotinamide addition, suggesting this product is a mistranslated glutamine, lysine, or glutamate substitution rather than a deacetylation product. Each of these amino acids is coded for by codons only differing at the first base compared to the amber stop UAG codon (Gln: CAG, Lys: AAG, Glu: GAG), and they each cause similar mass shifts (Gln: 8818.03 Da, Lys: 8818.07 Da, Glu: 8819.02 Da). We therefore concluded that the expression of acUbK48 with 5 mM acK was significantly contaminated by mistranslated protein product.
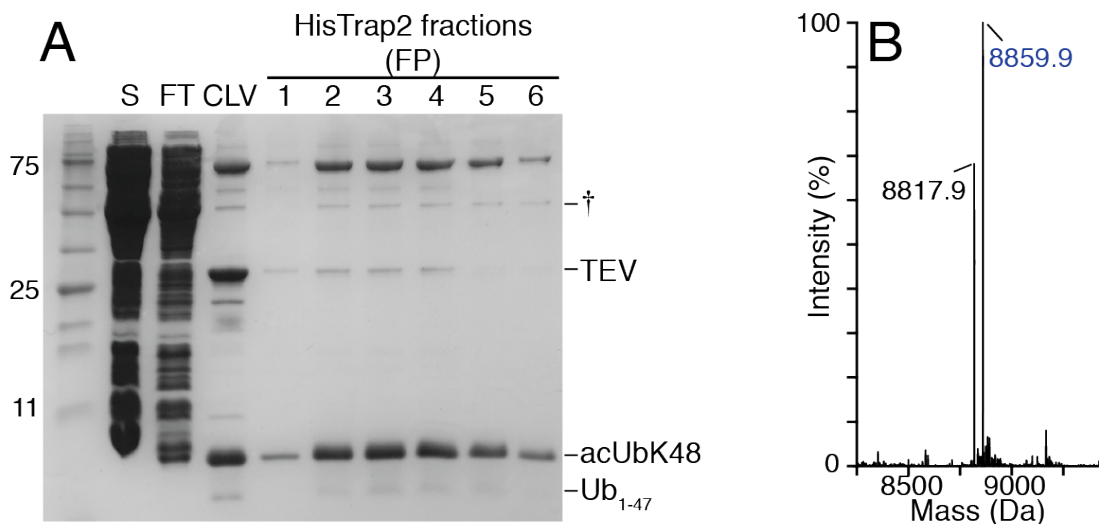
Figure 2.1. 5 mM supplemented acetyl-lysine yields heterogeneous acUbK48.
(A) acUbK48 was prepared as indicated in the Materials and methods and the purification process was monitored by SDS-PAGE. Lanes are as follows: S- highspeed supernatant, FT- flowthrough from initial Ni^{2+}-NTA affinity purification, CLV- TEV-cleaved protein, 1-6- fractions collected after second Ni^{2+}-NTA column (FP-final protein). Proteins are identified to the right of the gel, and the band marked † corresponds to a contaminant protein commonly observed in Ni^{2+}-NTA affinity purification. (B) The final protein was sent for mass identification specifically between 8-9 kDa. The major species are identified.

To obtain pure acUbK48, we first tried keeping the expression conditions the same (5 mM acK) and changed the purification protocol. Because acetylation neutralizes the positive lysine side chain, the calculated pI of acUbK48 is 1.5 pH units lower than that of Ub. For this reason, anion exchange chromatography was used at pH 9.0 with a 0 to 1 M NaCl gradient to try to separate acUbK48 from the mistranslated protein. A single peak in the chromatogram (Fig. 2.2A) eluted from the anion exchange column in buffer containing 260 mM NaCl. The fractions collected over the peak were observed on SDS-PAGE and sent for full length mass determination using mass spectrometry. Analytical liquid chromatography-mass spectrometry (LC-MS) was used to separate protein components from buffer. Two species with retention times of 20.3 and 20.4 min eluted from the LC column (Fig. 2.2B) and were automatically subjected to Quadrupole Time-of-Flight (QToF) full length mass spectrometry. The most abundant mass from the peaks at 20.3 and 20.4 min were 8817.8 Da and 8859.7 Da, respectively (Fig. 2.2C, D). Together, these

results indicated that anion exchange chromatography was not a sufficient final step in separating acUbK48 from mistranslated Ub.
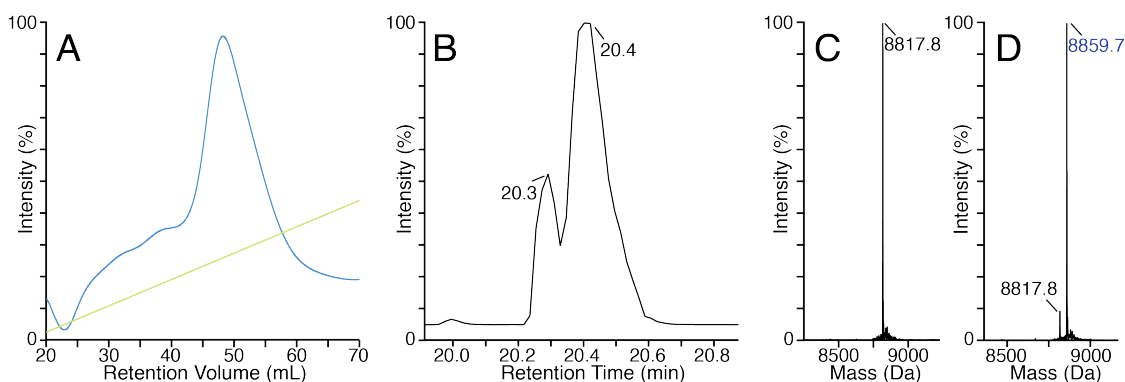
Figure 2.2. Anion exchange chromatography does not separate acUbK48 and Ub.
(A) Protein prepped from a 5 mM acK expression of acUbK48 was injected onto a HiTrap Q XL column and protein was eluted using a 0-1 M (0-100%) NaCl gradient (green line). Elution was monitored using UV absorbance at 280 nm (blue line). (B) Prior to mass identification, protein from the HiTrap Q column was separated using liquid chromatography and shown is the UV absorbance profile at 280 nm. QToF mass identification for species contained in the peaks at (C) 20.3 min and at (D) 20.4 min.

The success of the LC column in separating the acetylated and mistranslated protein on an analytical scale prompted the use of a reverse phase-high performance liquid chromatography (RP-HPLC) column to separate preparative amounts of acUbK48 from mistranslated Ub. In comparison to the analytical sample shown in Figure 2.2B, the chromatogram for the larger preparative amount of protein showed an elution profile containing 3 peaks (Fig. 2.3A). Immediately after the column had finished running, the collected fractions were injected into the QToF mass spectrometer to identify the mass of protein species contained in each fraction. We found that mistranslated Ub eluted from the LC column with a shorter retention time than acUbK48, and that cross contamination of samples could be avoided by manually collecting fractions for each new peak. The first fraction collected at 35.5 min corresponded to a protein with a mass of 8818.2 Da (Fig. 2.3B), and the middle fraction collected at 36.4 min showed a mass of 8818.1 Da (Fig. 2.3C). These two fractions correspond to mistranslated Ub, and although the sequence of the mistranslated products was not confirmed, the ability to resolve the species on RP-

HPLC indicates they contain two different sequences. The last fraction (36.9 min) showed a major component with a mass of 8860.0 Da and a smaller contaminant at 8818.3 Da, indicating acUbK48 made up over 90% of the protein collected in the last fraction (Fig. 2.3D). We therefore concluded that despite the relatively small amount of mistranslated Ub present in the last RP-HPLC fraction, the acUbK48 protein could be effectively purified using two nickel columns to remove untagged bacterial proteins followed by RP-HPLC to separate the mistranslated Ub. This protocol could then be applied to purify the other six acUb proteins.
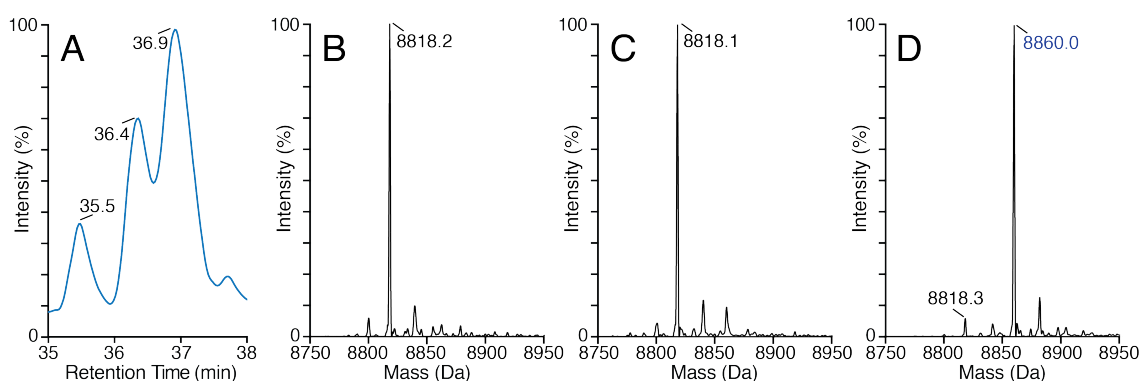
Figure 2.3. RP-HPLC separates acUbK48 from mistranslated Ub.
Following the double Ni^{2+}-NTA affinity purifications, protein was subjected to preparative RP-HPLC to separate the major components. (A) The UV absorbance (280 nm) chromatogram from the RP-HPLC column showed three peaks, and the masses were identified using QToF mass spectrometry. Masses corresponding to proteins contained in the peaks at (B) 35.5 min, (C) 36.4 min, and (D) 36.9 min are identified.

2.3.2   Optimization of bacterial growth conditions for acUb expression

Although acUbK48 could successfully be separated from mistranslated protein using preparative RP-HPLC, the process was time consuming and cost ineffective. Further, the large proportion of mistranslated side product separated out was not usable and discarded, leaving poor yield of the final acUbK48. Therefore, we decided to try to optimize the protein expression conditions during bacterial growth and protein induction to minimize the proportion of mistranslated side product at the onset of protein translation. We chose to test a range of acK concentrations in the expression medium while keeping the concentration of IPTG constant. Since the initial expressions with maximum 5 mM acK proved ineffective, we chose to increase amounts up to 100 mM acK in separate small-

scale growths. These small-scale expressions were subsequently followed by measuring the amounts of acUbK48 and mistranslated product using mass spectrometry. We noted a clear dose dependence between the amount of acK added and the incorporation of acK into
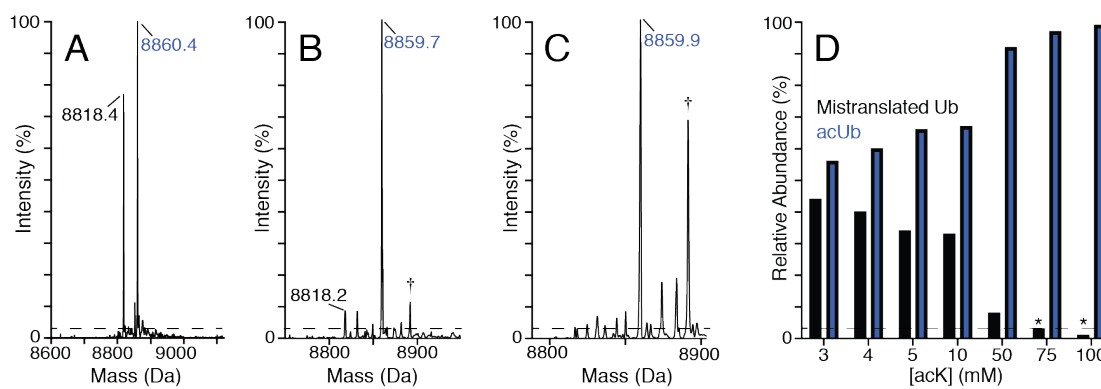
Figure 2.4. Homogeneous acUbK48 translation depends on the concentration of acK. Full length mass identification for protein species purified from an expression of acUbK48 with (A) 3 mM acK, (B) 50 mM acK, and (C) 75 mM acK supplemented in growth media. Signals labeled † correspond to minor oxidation artifacts of acUbK48. (D) The proportion of mistranslated Ub and acUb proteins is shown for expression of acUbK48 over a range of acK concentrations added to the media. The relative amounts of mistranslated Ub (black) compared to acUb (blue) were determined by measuring their appropriate signals in QToF mass spectra and calculating the relative abundance as a fraction of the total combined signal. A dashed line at 3% intensity indicates the detection limit of the mass spectrometer. At 75 mM acK and above, the amount of mistranslated Ub falls under the detection limit of the instrument (*). Truncated products were not considered in this analysis.

the acUbK48 protein. Below 5 mM acK, there was approximately 55% acUbK48 and 45% mistranslated protein (Fig. 2.4A). Increasing the acK to 50 mM resulted in a dramatic decrease in the amount of mistranslated product. The signal for acUbK48 (8859.7 Da) increased to 91% leaving the signal for mistranslated product (8818.2 Da) at 9% of the total protein (Fig. 2.4B). At 75 mM acK, the mass spectrometry signal for mistranslated product was detected at 3% of the signal for acUbK48, was indistinguishable from the noise, and fell below the detection limit of the instrument (Fig. 2.4C). Figure 2.4D shows the concentration dependent increase in acUbK48 expression at the tested acK concentrations. As the detection limit of the mass spectrometer is constant, concentrations of acK higher than 75 mM proved to be ineffective at significantly reducing the 3%

mistranslated product. We therefore concluded that 75 mM was the optimal amount of acK to add to the expression medium to produce homogeneous acUbK48 and could be applied to the other six acUb variants.

2.3.3   Acetylation modifies bacterial growth and protein expression

The determination that acUbK48 requires 75 mM acK for homogeneous protein expression initiated small test expressions for the other six acetylation sites in Ub. Small growths (100 mL) for each of the seven acUb proteins and Ub were done in parallel to study the effects of the acetylation plasmid and the addition of acK on bacterial growth. Figure 2.5A shows the bacterial growth curves associated with the 100-mL growths. Noticeably, the growth
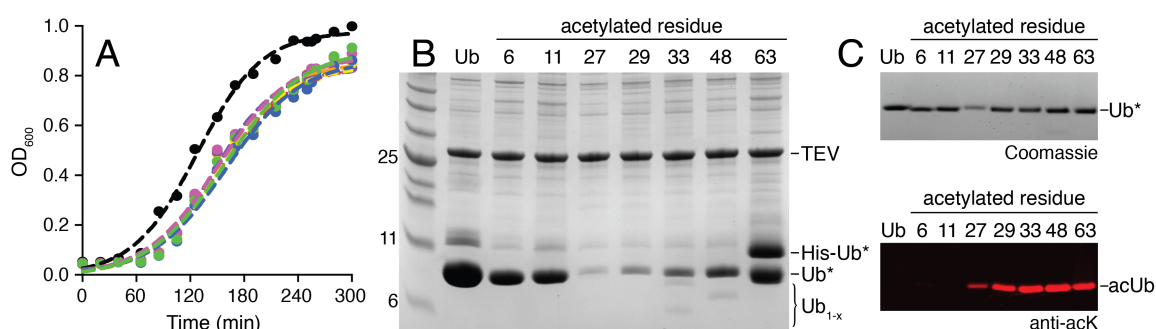
Figure 2.5. Genetic code expansion for acetyl-lysine incorporation modifies cell growth and protein expression.
(A) Growth curves for *E. coli* BL21(DE3) cells transformed with plasmids for Ub (black) and each acUb variant; acUbK6 (orange), acUbK11 (red), acUbK27 (purple), acUbK29 (yellow), acUbK33 (pink), acUbK48 (blue), and acUbK63 (green) are shown based on OD_{600} measurements. Data shown are an average of two experiments. In these experiments, 75 mM acetyl-lysine was added at $OD_{600}= 0.4$. (B) Expression levels of Ub and acUb proteins following initial Ni^{2+}-NTA affinity purification and cleavage with TEV protease. Proteins were separated on SDS-PAGE and stained with Coomassie dye. Ub_{1-x} denotes truncation products of the orthogonal translation system. Ub^* refers to the band containing both Ub and acUb. The positions of specific acetylated residues are indicated along the top of the gel. (C) The final purified proteins from an optimized expression of each construct were examined via SDS-PAGE and Coomassie staining (top) in parallel with anti-acK immunoblotting (bottom) as described in Materials and methods. The positions of specific acetylated residues are indicated along the top of each panel.

for Ub was 30% faster compared to the growths containing the acetylation system evidenced by the faster doubling time (black vs. coloured curves). Cell densities for the acUb growths reached 80-90% of wild-type Ub based on final OD_{600} values. There was no difference between growths for the expression between any of the acUb proteins: The curves were right-shifted to a similar degree.

To visualize and compare total protein expression, each 100-mL growth was harvested and lysed as indicated in the Materials and methods. The soluble fractions were incubated with TEV protease to cleave the His-tag to ensure all Ub or acUb protein was at the correct molecular weight. The protein solutions were then concentrated to a 1-mL final volume and analyzed by SDS-PAGE (Fig. 2.5B). These experiments consistently showed the acUb variants had lower protein expression levels than wild-type Ub, ranging from about 10% (acUbK27) to 40% (acUbK6, acUbK11, acUbK63) of that for Ub. Further, all acUb variants had different quantities of protein truncated at the acK position, which is a side product of the orthogonal translation system. This was most evident for acUbK63, which consistently showed at least 50% of the protein was truncated. In comparison, the expression of truncated products from other acK variants such as acUbK33 and acUbK48 appeared at lower levels than the full-length product. Truncation products for acUbK6, acUbK11, acUbK27, and acUbK29 were too small to observe by this method.

To confirm the incorporation of the acK residue, final purified protein samples were subjected to SDS-PAGE followed by immunoblotting with an anti-acK antibody and a fluorescent secondary antibody (Fig. 2.5C). Most of the acUb proteins were detected by this method; just those closest to the N-terminus showed poor reactivity (acUbK6, acUbK11). We attributed this to steric hindrance in the Ub structure or sequence variation from the original acK epitope.

To further confirm position-specific incorporation of acK, each purified acUb protein was subjected to a trypsin enzymatic digest followed by LC-ESI-MS/MS and subsequent peptide identification. For example, acUbK48 showed a monoisotopic residue mass of 170.1 Da, corresponding to lysine (128.09 Da) plus 42.01 Da, at position 48 of the protein,

which is a positive identification of acetyl-lysine (Fig. 2.6). Similar mass spectrometric identification was used to confirm site-specific acetylation for the other six acUb proteins.
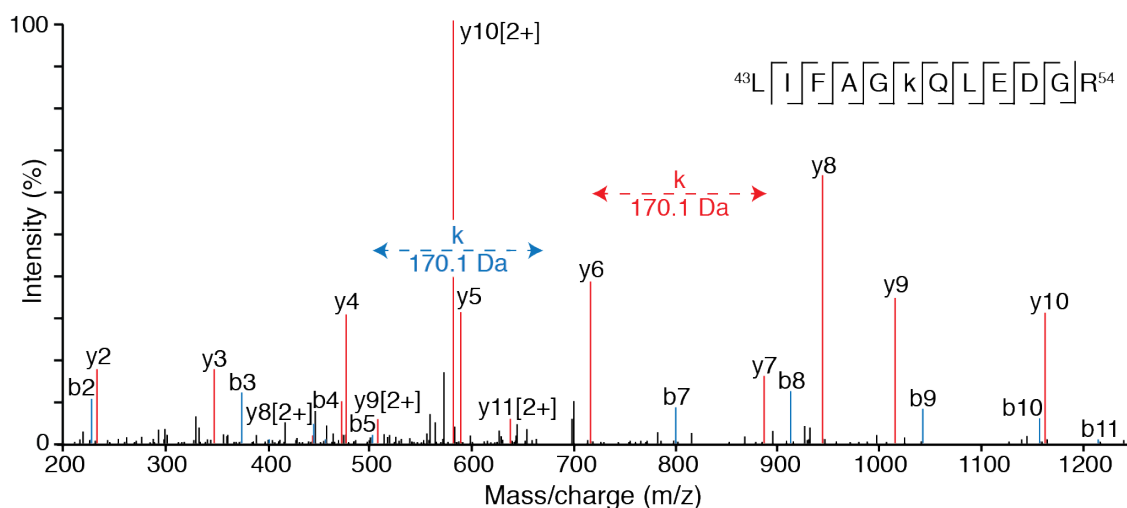
Figure 2.6. Identification of position-specific acetyl-lysine incorporation in purified acUb.
Purified acUbK48 protein from an optimized expression and purification experiment was analyzed via LC-ESI-MS/MS to confirm sequence-specific acetyl-lysine incorporation at position 48. Lowercase 'k' denotes modified lysine; in this case, the monoisotopic residue mass of 170.1 Da indicates acetyl-lysine. Data were analyzed using PEAKS X software and a complete list of observed ions is provided in Table 2.1.

Table 2.1. Complete list of y and b ions for an acK48-containing peptide.
ESI-MS/MS data corresponding to acUbK48 demonstrates a monoisotopic mass of 170.1 Da at position 48.

#	Immonium	b	b-H_2O	b-NH_3	b (2+)	Seq	y	y-H_2O	y-NH_3	y (2+)	#
1	86.0969	114.0919	96.0813	97.0649	57.5459	L					12
2	86.0969	227.1400	209.4820	210.8150	114.0880	I	1275.6290	1258.0830	1258.0830	638.4370	11
3	120.0812	374.1720	356.3140	357.2173	187.6222	F	1162.5500	1144.5640	1145.5581	581.9950	10
4	44.0499	445.3000	427.3370	428.3580	223.1407	A	1015.4920	997.5150	998.4897	508.4450	9
5	30.0343	502.3220	484.1310	485.3100	251.5020	G	944.4980	926.4460	927.4526	472.9320	8
6	143.1183	672.5100	654.4230	655.3815	336.7042	k(+42.01)	887.4950	869.4475	870.4311	444.3930	7
7	101.0714	800.4170	782.4860	783.4401	401.1990	Q	717.3650	699.3730	700.3550	359.3130	6
8	86.0969	913.4670	895.5450	896.5241	457.2690	L	589.2940	571.3720	573.0090	295.1470	5
9	102.0554	1042.5420	1024.6360	1025.5667	522.1040	E	476.2130	458.2750	459.1829	239.2750	4
10	88.0398	1157.5310	1139.5010	1140.5936	578.9390	D	347.1990	329.2270	330.1404	174.0837	3
11	30.0343	1214.5060	1196.3600	1197.0350	607.8210	G	232.1530	214.1450	215.2010	116.5702	2
12	129.1139					R	175.1189	157.1084	158.0919	88.0595	1

2.3.4   Acetylated Ub proteins generate unique ubiquitination patterns

To study the effects of different acUb variants along parts of the ubiquitination cascade, we chose to use human UBA1 and a subset of E2 and E3 enzymes. For E2 enzymes, we purified three E2 enzymes: UBE2D1 (ubcH5a), a promiscuous E2 known to interact with various E3 enzymes to build multiple types of Ub signals; UBE2L3 (ubcH7), a Cys-specific E2 that interacts with E3 enzymes of the HECT and RBR type; and UBE2N:UBE2V2 (ubc13:mms2), a Lys-specific E2 that synthesizes K63-linked polyUb in the presence of a RING E3 protein. For the E3 step in the mechanism, we focused on the C-terminal catalytic region of IPAH3 (residues 270-571), a bacterial HECT-like E3 protein established to synthesize primarily K48-linked polyUb in the presence of UBE2D1 [127], and the RING domain of RNF8 (residues 345-485) that builds K63-linked polyubiquitin chains using UBE2N:UBE2V2 [81]. Figure 2.7 shows SDS-PAGE corresponding to the purification of each of the mentioned proteins. In all cases, final protein yield was sufficient for enzyme assays and purity was excellent at working concentrations.
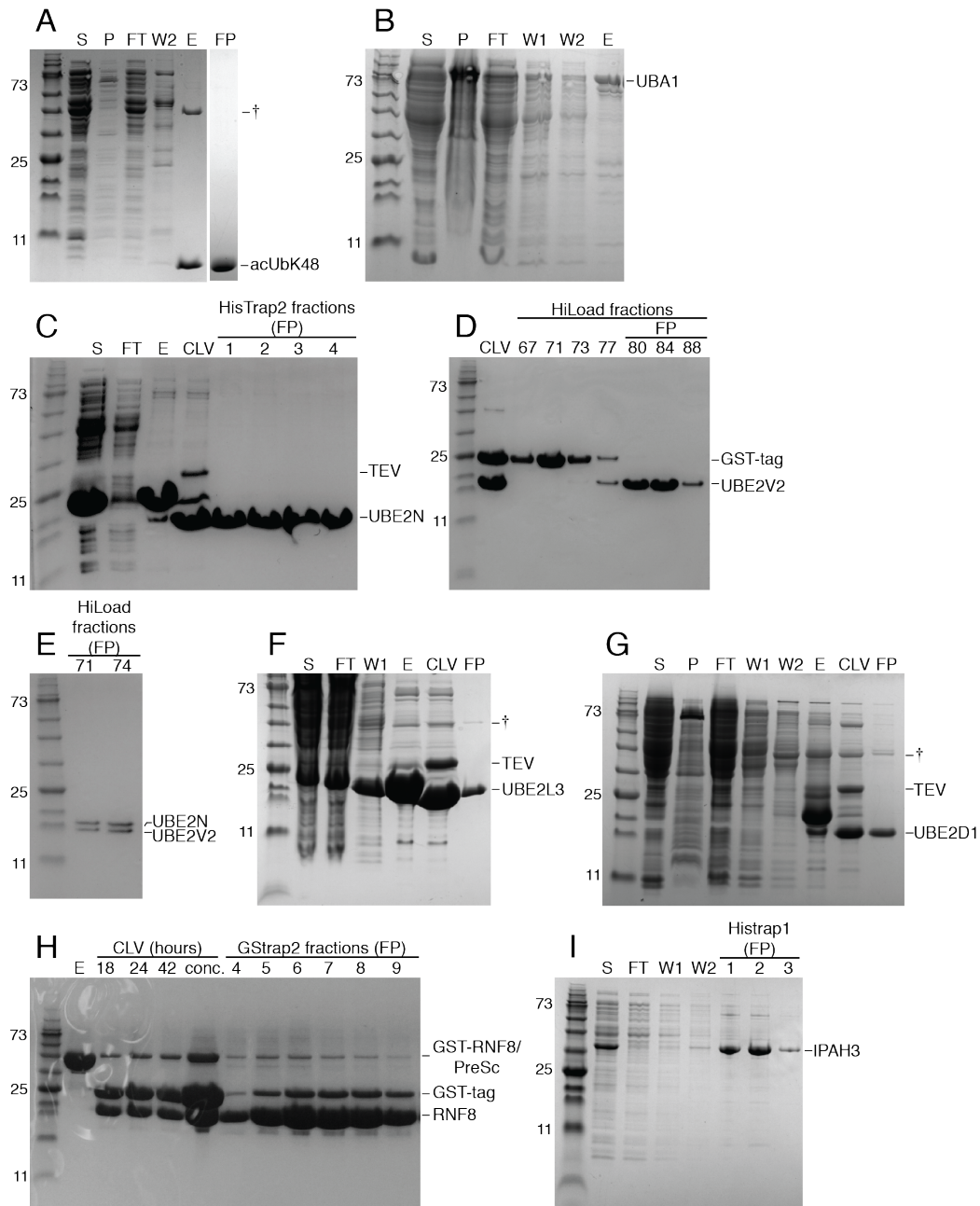
Figure 2.7. Purification of ubiquitination proteins.
SDS-PAGE illustrating the final step(s) in purification for (A) acUbK48, (B) UBA1, (C) UBE2N, (D) UBE2V2, (E) UBE2N/UBE2V2, (F) UBE2L3, (G) UBE2D1, (H) RNF8, and (I) IpaH3 are shown. Lanes labeled with numbers correspond to fractions collected during purification, or in the case of (G) a cleavage time course. All other lanes are as follows: S-highspeed supernatant, FT- flowthrough, W1- wash with 10 mM imidazole, W2- wash with 35 mM imidazole, E- elution from affinity column, CLV- TEV or PreSc cleaved protein, FP-final protein. Proteins of interest are labeled to the right of each gel, and the bands labeled † correspond to a contaminant protein commonly observed in Ni^{2+}-NTA affinity purification.

Initial experiments did not use UBE2L3 as we chose to only focus on two well established E2:E3 pairs in the HECT and RING ubiquitination mechanisms. We hypothesized that acUbK48 would prevent polyubiquitination for IPAH3, while K63 chain building would be eliminated for RNF8 using acUbK63. For IPAH3, the wild-type Ub protein exhibited a robust ubiquitination pattern at 10 min based on the depletion of Ub and the appearance of higher molecular weight bands observed by SDS-PAGE (Fig. 2.8). As expected, the E2:E3 pair of UBE2D1:IPAH3 demonstrates poorer ubiquitination using acUbK48 showing little depletion of the initial acUbK48 pool (Ub* band in the gels) and decreased intensities for many of the higher molecular weight bands. In contrast, acUb proteins (acUbK6, acUbK11, acUbK29, and acUbK33) appear to have strong ubiquitination patterns similar to Ub (Fig. 2.8A), indicating that K48 ubiquitination is minimally altered by these acetylated variants.
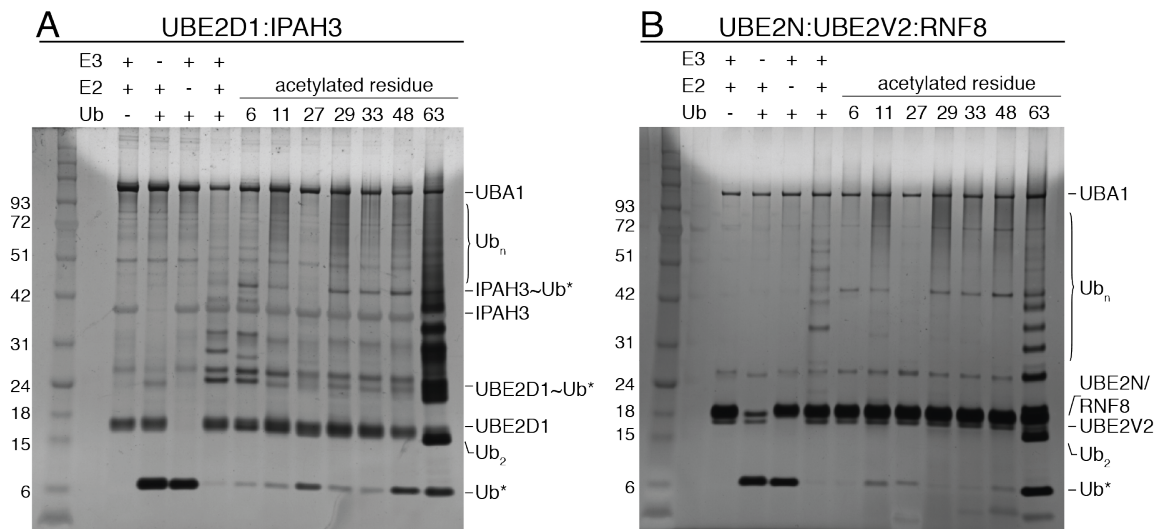
Figure 2.8. Acetylated ubiquitin proteins can alter ubiquitination patterns.
Ubiquitination assays for (A) IPAH3 and (B) RNF8 with their respective E2 enzymes. Wild-type and acUb variants were used in each assay. Experiments used 0.2 µM UBA1 (E1), 8 µM Ub or specific acUb, 1 µM UBE2D1 or UBE2N:UBE2V2 (E2), 2 µM IPAH3 or RNF8 (E3), 5 mM MgATP, and 50 mM HEPES at pH 7.4. Ubiquitination occurred for 10 min prior to analysis by SDS-PAGE. Other details are provided in the Materials and methods. Bands marked Ub* correspond either to Ub or to one of the acUb proteins indicated at the top of each gel.

Similarly, ubiquitination assays using RNF8 along with its preferred E2 UBE2N:UBE2V2 show a strong ubiquitination pattern with Ub (Fig. 2.8B). The acUb variants acUbK6,

acUbK11, acUbK29, acUbK33, and acUbK48 appear to have similar ubiquitin depletion levels and show the appearance of high molecular weight species. Remarkably, acUbK63 demonstrates an obvious ubiquitination pattern with UBE2N:UBE2V2 and RNF8. Since this acUb species is unable to build K63-linked polyubiquitin chains, it may be possible that another lysine in Ub becomes more active for chain building or the acUbK63 protein multiply mono-ubiquitinates either the E2 or E3 enzyme. Interestingly, acetylation at K27 appears to reduce the overall ubiquitination in both experiments, which might be indicative of a problem unique to acUbK27. These experiments suggests that acetylation at some positions in Ub may alter the types of polyubiquitin chains built by a given E2:E3 combination.

2.4 Discussion

The characterization of acUb and its regulation are poorly understood. The identification of acUb peptides from mass spectrometry has become more sensitive with the development of detection and enrichment equipment. However, current approaches are limited by the fact that ubiquitination is a PTM as well; that is, many datasets either examine ubiquitination or acetylation, but not both. As a result, these datasets can be quite incomplete. The best way to determine the full extent of acetylation on ubiquitin lysine residues would be to enrich for acetyl-lysine in all peptides, without exclusion.

While many of the datasets available in the PRIDE database [128] (wwwdev.ebi.ac.uk/pride) do not include Ub peptides, they do manage to cover other proteins involved in ubiquitination. Enzymes involved in every step of the ubiquitination cascade have been observed to be acetylated or phosphorylated. The E1- activating enzyme UBA1, the E2-conjugating enzymes UBE2L3 and UBE2N, and a vast majority of deubiquitinating enzymes are highly acetylated following DNA damage [112]. Further, many RING and HECT E3 ligases undergo acetylation as a result of DNA damage. Acetylation of E2 enzymes and E3 Ub ligases is also abundant as a result of rapamycin-induced autophagy [111], indicating that cell stress-induced acetylation may act as a means of ubiquitination regulation. Other than the notion that K11- and K48- branched chains

function better at targeting substrates to the proteasome [129], there is little evidence in the literature about branched polyubiquitin that might be guided by acetylation. It could be that cells simply need an external signal such as an acetylated lysine so that E2/E3 pairs are able to discriminatively build various polyubiquitin linkages.

Recent studies of the phosphorylation of Ub and its necessity for the functioning of the E3 ligase parkin have identified PINK1 as the requisite protein kinase [130,131]. Purified versions of this kinase have been successfully used to enzymatically phosphorylate purified ubiquitin [123,132]. However, other serine residues have been observed to be phosphorylated in Ub and are only reachable using orthogonal methods until the corresponding kinase proteins have been identified. In the case of acetylation, the upstream KATs are widely uncharacterized and unmatched to specific acetylation events. In Ub even though six of the seven possible lysine residues have been observed to be acetylated under different cellular conditions, the KATs that specifically give rise to these variants are unknown. This being said, we have successfully used genetic code expansion with tRNA$^{Pyl-opt}$ and acKRS, which are orthogonal to those pairs found naturally in *E. coli*, to synthesize all possible acK variants of Ub. Few studies have used this system to produce acetylated proteins. However, from these studies it appears that efficient incorporation of acetyl-lysine is strongly dependent on exogenous acetyl-lysine addition; thus, the need to assay acetyl-lysine concentrations becomes system-dependent. For example, only 1 mM acetyl-lysine was required to synthesize acetylated myoglobin [117], but other reports required 2.5–50 mM acetyl-lysine for various other proteins [118,119]. In the current work, the higher expression of Ub by the *E. coli* system likely results in a higher concentration of acetyl-lysine.

Here, we have successfully used genetic code expansion to synthesize all possible acetylated lysine variants for Ub and developed protocols to eliminate mistranslated products allowing for the purification of position-specific, stoichiometrically acetylated Ub proteins. We have also provided evidence that these acUb proteins may direct unique ubiquitination patterns with HECT or RING E3 ligases. Our approach should pave the way for future biochemical experiments that focus on the impact of acetylation in ubiquitination.

3

Acetylation of Ub modulates UBA1 transthiolation to E2 proteins[†]

3.1 Introduction

The qualitative nature of the experiments used to study ubiquitination often show long timepoints (minutes to hours) that indicate a reaction end point. These types of experiments, while great at demonstrating ubiquitination patterns and overall function, neglect the small differences and preferences of the system that might only be visible in the initial stages of the reaction. Various techniques to quantitatively monitor ubiquitination like SDS-PAGE with band densitometry or autoradiography require discrete timepoints to be collected. Traditional gel-based techniques are often still useful in complicated multi-protein systems like full ubiquitination experiments. However, these methods are more limited for rapid time point collection. The development of high-throughput methods including Förster resonance energy transfer (FRET) experiments or fluorescence polarization now allow the monitoring of ubiquitination reactions to occur in real-time using many (ie. 96-well plates) samples.

To examine how acetylation of Ub alters the transthiolation between the E1 UBA1 and E2 proteins, we synthesized all seven acetylated forms of Ub and examined the kinetics of

formation for the E2~Ub conjugate with the E2 proteins UBE2D1 and UBE2L3. We used kinetics approaches to unmask small differences in rates that sometimes can be hidden in steady-state experiments. To do so, we utilized FRET experiments that provide a robust method for quantifying Ub and Ub-like protein−protein interactions [133,134]. Our experiments show that acetylation of Ub can have a significant effect on the rate of transthiolation between UBA1 and an E2 protein. Overall, these experiments provide insights into the general impact of protein acetylation on the Ub pathway.

3.2 Materials and methods

3.2.1   Plasmids and cloning

pET28 plasmids containing Ub^{CyPet} or $^{YPet}UBE2D1$ were a kind gift from J. Liao (University of California, Riverside, CA). Site-directed mutagenesis was used to insert an amber stop codon at the desired position in the ubiquitin sequence to generate $acUbKx^{CyPet}$ (where x denotes the acetylated residue) constructs. Restriction-free (RF) cloning was used to swap the UBE2D1 gene for that of UBE2L3 to create $pET28-^{YPet}UBE2L3$. Successful polymerase chain reaction products were confirmed with DNA sequencing. The pTech plasmid was prepared as indicated in section 2.2.1.

3.2.2   Protein expression and purification

$pET28-His-Ub^{CyPet}$ and $pET28-His-^{YPet}UBE2D1$, $pET28-His-^{YPet}UBE2L3$ constructs were expressed and purified as previously reported [133]. Acetylated Ub (acUb) constructs were generated from a fresh cotransformation of $pET28-His-acUbKx^{CyPet}$ with pTech into *E. coli* BL21(DE3). Acetylated ubiquitin $acUbK63^{CyPet}$ was expressed in *E. coli* BW25141(λDE3) as previously established [135]. All acetylated ubiquitin proteins were expressed like His-TEV constructs prepared previously [136]. Briefly, after a fresh cotransformation of the orthogonal translation system and the $acUbKx^{CyPet}$ construct of interest, a colony was transferred into selective Luria broth (LB) (30 µg/mL kanamycin, 34 µg/mL chloramphenicol, and 0.2% glucose) and grown at 37 °C overnight. This culture was then inoculated into a larger culture of selective LB, and bacteria grew until the OD_{600} reached 0.4. The cells were pelleted and resuspended in selective LB without glucose. To express

acetylated proteins, 75 mM acetyl-lysine (acK) and 10 mM nicotinamide (NAM) were added to the medium and the cells were grown at 37 °C until the OD_{600} reached 0.8. Protein expression was induced with 0.2 mM isopropyl β-D-1-thiogalactopyranoside (IPTG) overnight at 25 °C. His-acUbKx^{CyPet} proteins were purified by Ni^{2+}-affinity chromatography using 50 mM Tris pH 8.0, 500 mM NaCl, and 250 μM tris(2-carboxyethyl)- phosphine (TCEP) with either 10 mM imidazole and 15 mM NAM (lysis and binding buffer), 35 mM imidazole (wash buffer), or 250 mM imidazole (elution buffer). Purified proteins were dialyzed into 25 mM Tris pH 8.0, 250 mM NaCl, and 250 μM TCEP for storage. The yield of acUbKx^{CyPet} proteins was significantly lower than that of Ub^{CyPet} arising from the insolubility of some side products. The acetylated ubiquitin proteins were validated by mass spectrometry and SDS-PAGE.

3.2.3   Measurement of E2∼Ub conjugation by FRET

UBE2D1 and UBE2L3 loading assays were conducted in triplicate using 5 μM Ub^{CyPet} or 5 μM acUb^{CyPet}, 0.1 μM UBA1, 1−25 μM ^{YPet}E2, 5 mM MgATP, and 50 mM Hepes (pH 7.4). Samples were measured using black 96-well plates placed in a Synergy H1 microplate reader controlled by Gen5 software (Biotek). Each sample well was measured discretely using a 100 ms delay following plate movement. The system was temperature controlled to 30 °C, and the instrument was set to fluorescence end-point mode with an excitation wavelength of 420 nm using a xenon flash lamp. Fluorescence was monitored at 528 nm using read heights of 4.50 mm for the equilibration kinetic loop (90 μL volume) and 4.75 mm for the conjugation loop (100 μL volume). A system gain of 50 was used for all measurements. Two kinetic loops were used for data collection: (1) 10-s time points for 30 min (equilibration) and (2) 10-s time points for 90 min (conjugation). MgATP was added manually with a multi-channel pipette immediately before the start of the second loop.

3.2.4   Data Analysis

Data were processed initially using Microsoft Excel to subtract background fluorescence attained during the equilibration loop. Fluorescence data were then converted to product formed in GraphPad Prism 8, and linear regression was used to determine initial rates. Three independent replicates were performed that were globally fit to determine the

average initial rates of E2~Ub conjugate formation. The resulting rates [average ± the standard error of the mean (SEM)] were then evaluated as a function of ^{YPet}E2 concentration in a separate sheet. Sixteen rates were used to derive the initial Michaelis−Menten plot, and 15 of these rates were used to finalize the plots. The three highest ^{YPet}E2 concentrations exhibited apparent rates resulting from the inner filter effect. As described previously, the inner filter effect has a significant influence on a system when the concentration of the detected fluorophore nears 20 μM [137]. The highest concentration of ^{YPet}E2 was eliminated from K_M, k_{cat}, and catalytic efficiency (k_{cat}/K_M) calculations due to the strong influence this data point had on the errors of calculated parameters.

Statistical analysis was performed in GraphPad Prism 8 using the Student's *t* test to compare the average ± SEM for K_M and k_{cat} between each acUb and Ub. In all cases, statistical significance was assigned if the adjusted *p* value was $0.05 > p \geq 0.0005$ (one asterisk) and $p < 0.0005$ (two asterisks).

3.3 Results

UBE2D1 is a promiscuous E2 enzyme that has been observed to interact and function with RING, HECT, and RBR subclasses of E3 ligases. Accordingly, UBE2D1 has been observed to build numerous unspecific types of lysine-linked poly-Ub chains with an array of interacting partners [45]. For example, UBE2D1 in complex with CHIP E3 ligase shows little preference for lysine position [138], but polyubiquitination with APC/C preferentially builds K6-, K11-, K48-, or K63-linked chains [94]. We chose to study UBE2D1 to provide insight as to how Ub acetylation alters the loading of the promiscuous UBE2D family of proteins. Conversely, as a well-accepted cysteine-preferring E2 enzyme, UBE2L3 functions with numerous HECT E3 ligases like E6AP or ITCH and RBR type E3 ligases such as parkin or HHARI [139–141] and has little influence on lysine preference for polyubiquitination. The two chosen E2 proteins provide contrast to study the effects of Ub acetylation on promiscuous and specific ubiquitin conjugating enzymes. Genetic code expansion was used to incorporate acetyl-lysine into each of the seven lysine positions in Ub [136].

3.3.1   Design and validation of FRET experiments

Each acetylated Ub and wild-type Ub was tagged at its N-terminus with the CyPet fluorophore (Ub^{CyPet}) and used in combination with an E2 protein tagged with the YPet fluorophore at its N-terminus (^{YPet}E2; ^{YPet}UBE2D1 or ^{YPet}UBE2L3). Acetylated Ub^{CyPet} proteins were expressed and purified from *E. coli* BL21(DE3) or BW25141(λDE3) cells and analyzed with quadrupole time-of-flight (QToF) mass spectrometry to ensure the final purified protein solutions did not contain substitutions or truncations. The FRET system was designed so that Ub^{CyPet} acts as the donor an ^{YPet}E2 acts as the acceptor [133,134] (Fig. 3.1A). To determine the best wavelengths for excitation and emission, absorbance and fluorescence spectra were evaluated. Ub^{CyPet} exhibited a strong absorbance centered at 430 nm that overlapped with the absorbance profile for the ^{YPet}E2 proteins between 450 and 475 nm. To minimize indirect excitation of the YPet fluorophore, the Ub^{CyPet} excitation wavelength was set at 420 nm where minimal absorbance of ^{YPet}E2 occurs. Characteristic
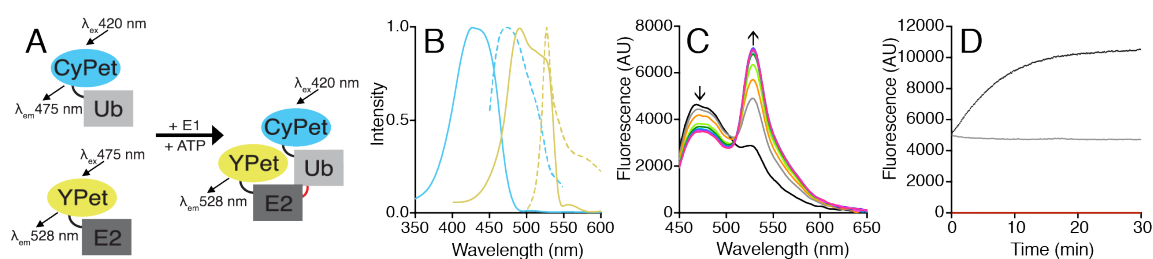
Figure 3.1. FRET characteristics of an E2 loading assay.
(A) Schematic diagram showing the E1-mediated reaction of Ub^{CyPet} with a ^{YPet}E2 to form the ^{YPet}E2~Ub^{CyPet} conjugate. The excitation (λ_{ex}) and emission (λ_{em}) wavelengths for each protein are shown. (B) Spectral profiles of CyPet (blue) and YPet (yellow) contained in Ub^{CyPet} and ^{YPet}UBE2D1. Absorbance curves are shown as solid lines, and emission profiles as dashed lines. Each spectrum was normalized internally to the highest intensity. (C) Spectral scans of a real-time E2 loading assay involving a 1:1 Ub^{CyPet}:^{YPet}UBE2D1 ratio. The black curve indicates the measured fluorescence at t= 0 min, and the arrows represent the changes in the spectra over a 10 min time period. Spectra were measured using an excitation wavelength of 420 nm and show a FRET maximum near 528 nm. (D) Time dependent increase in fluorescence at 528 nm during a full E2 loading assay involving a 1:1 Ub^{CyPet}:^{YPet}UBE2D1 ratio (black), a 1:1 Ub^{CyPet}:^{YPet}UBE2D1 ratio without ATP or UBA1 (grey), and reaction buffer (red).

of FRET, the emission profile of Ub^{CyPet} efficiently overlaps with the absorbance curve for ^{YPet}E2 enzymes. For example, the emission maximum for ^{YPet}UBE2D1 (528 nm) corresponds to a low background fluorescence of Ub^{CyPet} (Fig. 3.1B). The selection of optimal wavelengths for excitation of Ub^{CyPet} and emission of ^{YPet}UBE2D1 enabled excellent spectra to be acquired where a strong FRET signal from the CyPet/YPet fluorophores occurs in the E2~Ub conjugate due to an expected distance of <50 Å [142]. Thus, the FRET signal obtained from the excitation of Ub^{CyPet} and fluorescence of ^{YPet}E2 in the presence of UBA1 and ATP provides a direct measure of Ub^{CyPet} conjugation to ^{YPet}E2 that can be measured in a time-dependent manner. E2~Ub formation was marked by a decrease in emission for Ub^{CyPet} (λ = 475 nm) and a concomitant increase in fluorescence for ^{YPet}E2 at 528 nm, as demonstrated for ^{YPet}UBE2D1 (Fig. 3.1C), expected for the real-time formation of the ^{YPet}UBE2D1~Ub^{CyPet} covalent conjugate. Monitoring the formation of the E2~Ub conjugate at 528 nm over time demonstrated a robust signal increase dependent on UBA1 and ATP addition (Fig. 3.1D). The full reaction (black) demonstrated a fluorescence signal double the magnitude of the reaction without UBA1 and ATP (grey curve). The constant fluorescence signal obtained in the reaction without UBA1 and ATP indicates the background signal from the two fluorophores being in solution together. For reference, the red curve demonstrates the fluorescence signal in a reaction containing only 50 mM Hepes pH 7.4. From this initial experiment, we concluded that our experimental design had high sensitivity for the formation of the E2~Ub species.

To verify that the FRET signal was derived from the formation of the E2~Ub conjugate and to quantify this reaction, a series of parallel experiments were used to detect the E2~Ub conjugate by fluorescence and SDS-PAGE. Figure 3.2 shows the time-dependent increase in the intensity of the FRET signal for a reaction using equal amounts of ^{YPet}UBE2D1 and Ub^{CyPet} where the background fluorescence has been subtracted. In the initial phases of the reaction (0−600 sec), the curve was nearly linear, demonstrating the time-dependent accumulation of the E2~Ub conjugate. At longer time points, the slope decreased, and beyond 30 min, the curve plateaued, indicating conjugation was complete and a maximum amount of the E2~Ub conjugate had formed. End-point samples were removed at 37 min and examined by SDS-PAGE using thioester-preserving conditions. The data show the
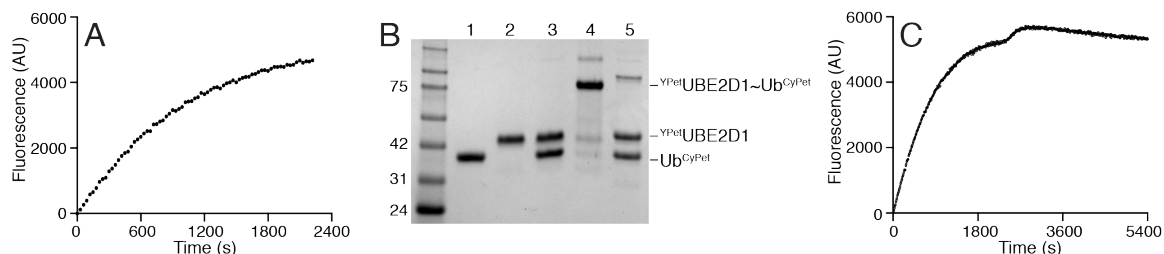
Figure 3.2. Real-time measurement of E2~Ub conjugation using FRET.
(A) FRET fluorescence measured at 528 nm generated with equimolar concentrations of Ub^{CyPet} and ^{YPet}UBE2D1. Samples were equilibrated to light and temperature for 15 min prior to the addition of MgATP. Following the addition of MgATP, the fluorescence was measured every 10 s until the curve began to plateau. (B) End-point samples from panel A were quenched with 3× SDS sample buffer and separated via 10% Bis-Tris SDS-PAGE in MES running buffer [50 mM MES, 50 mM Tris, 0.1% SDS, and 1 mM EDTA (pH 7.4)]: lane 1, Ub^{CyPet} only; lane 2, ^{YPet}UBE2D1 only; lane 3, E1, Ub^{CyPet}, and ^{YPet}UBE2D1 without MgATP; lane 4, end-point sample from panel A showing full E2 loading (acidified with 0.001% Trifluoroacetic acid); lane 5, E2 loading (reduced with 50 mM DTT). (C) FRET fluorescence measured at 528 nm similar to panel A, but with a longer time frame showing the decrease in fluorescence due to minor hydrolysis of the ^{YPet}UBE2D1~Ub^{CyPet} thioester.

appearance of an intense band above the 75 kDa marker, consistent with the expected size of the E2~Ub conjugate (84.2 kDa) carrying both YPet and CyPet fluorophores. Also noticeable are two much less intense bands for ^{YPet}UBE2D1 and Ub^{CyPet}, indicating these proteins were nearly completely consumed during thioester formation. In addition, the thioester formed was easily reduced with the addition of DTT to yield the initial reactants. At extended times beyond the plateau region, we frequently observed a decrease in FRET intensity. We attributed this to hydrolysis of a small portion of the E2~Ub conjugate, previously observed for ubc1 and ubc13 [143,144]. Alternatively, it is possible that some back transfer of Ub to UBA1 occurs once Ub^{CyPet} is exhausted in reactions with limiting Ub^{CyPet}. The intensity changes at extended periods of time accounted for <5% of the total change in FRET intensity. Overall, these data show that the FRET signal at saturation corresponds to maximum formation of the E2~Ub conjugate in a reaction.

3.3.2 Real-time formation of E2~Ub conjugates using acetylated Ub variants

Using these approaches, a series of experiments were completed to quantify the formation of the UBE2D1~Ub and UBE2L3~Ub conjugates using Ub and the seven acetylated Ub variants. The first data point was collected <5 s after MgATP addition, and subsequent data points were collected in 10-s intervals. The kinetic loop used to monitor conjugation lasted 90 min, and 541 individual data points were collected during this time. Multiple experiments were completed by varying the concentration of the ^{YPet}E2 proteins (1−25 μM) using the different acetylated Ub^{CyPet} proteins. Together, these experiments showed the magnitude of the FRET signal was dependent on the concentration of the ^{YPet}E2 for both UBE2D1 and UBE2L3 using either Ub (Fig. 3.3A, D) or acetylated Ub (Fig. 3.3B, E). For example, reactions using 5 μM ^{YPet}UBE2D1 and Ub^{CyPet} (Fig. 3.3A) or acUbK6^{CyPet} (Fig. 3.3B) yielded FRET signals following maximal E2~Ub conjugation (plateau region) that were 2.3−2.5-fold larger than those of similar reactions using 2 μM ^{YPet}UBE2D1. When the maximum FRET signal (ΔFRET) was plotted as a function of UBE2D1 concentration, a nearly linear correlation was observed for the formation of the UBE2D1~Ub conjugate (Fig. 3.3C). In addition, the slopes using acetylated Ub derivatives were very similar to that for Ub. As an example, the slopes of the correlations for Ub^{CyPet} and acUbK6^{CyPet} were 11.7 ± 1.1 and 11.0 ± 0.8, respectively. This indicates that the acetylation of Ub did not impact the absolute FRET signal observed for the different UBE2D1~Ub conjugates. The similarity in response with respect to UBE2D1 concentration allowed a common conversion of ΔFRET to UBE2D1~Ub conjugate concentration (nanomolar) to be used for all reactions.

Similarly, reactions using 5 μM ^{YPet}UBE2L3 and Ub^{CyPet} (Fig. 3.3D) or acUbK6^{CyPet} (Fig. 3.3E) demonstrated FRET signals at maximal E2~Ub conjugation that were between 2.0-2.5-fold larger than the signals obtained from reactions with 2 μM ^{YPet}UBE2L3. Consistent across all concentrations of ^{YPet}UBE2L3, we noticed a striking decrease in the FRET signal after maximum E2~Ub formation. We attributed this difference from UBE2D1 experiments to the identity of the E2 protein and the subtle differences that might occur during E2~Ub formation by UBA1. Further, the decrease in intensity could result from the
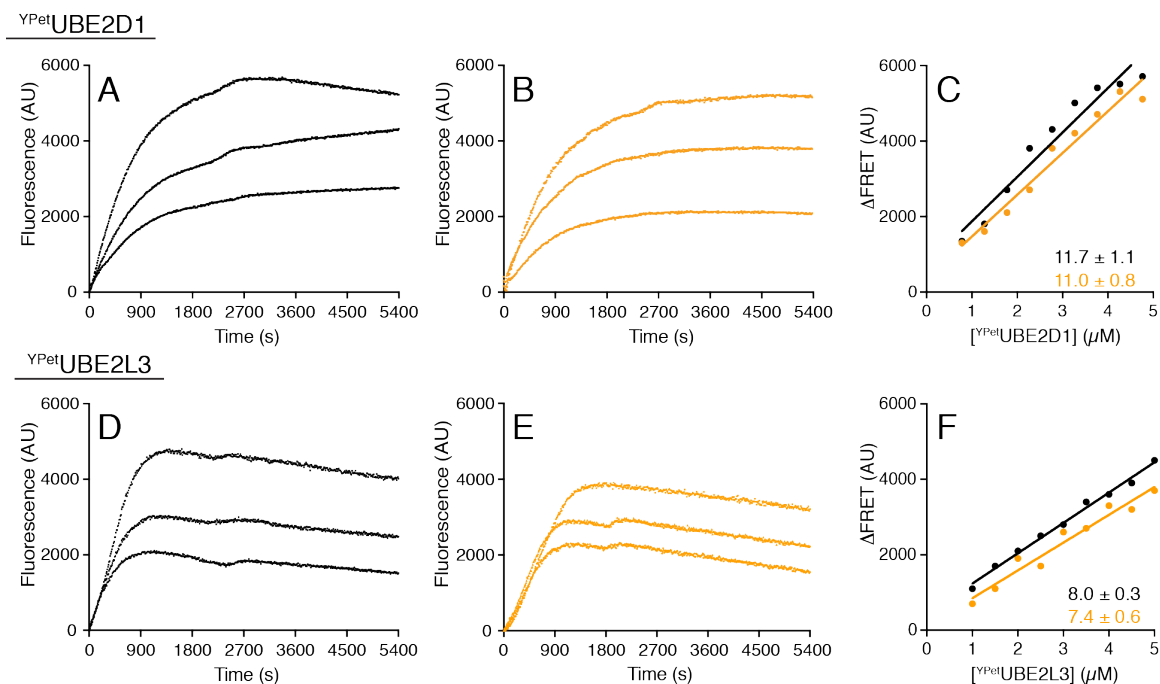
Figure 3.3. ^{YPet}E2 concentration influences fluorescence signal.
After the addition of MgATP, ^{YPet}UBE2D1~Ub^{CyPet} (top panels) or ^{YPet}UBE2L3~Ub^{CyPet} (bottom panels) conjugate formation was monitored via a kinetic loop that measured fluorescence at 528 nm every 10 s. Data were corrected by subtracting the background fluorescence obtained during the equilibration period and then referencing the data set minimum as zero. Shown are three different concentrations of ^{YPet}E2 (2, 3, and 5 μM; corresponding to the bottom, middle, and top curves, respectively, in panels A, B, D, and E). ^{YPet}E2 loading for the indicated E2 protein with (A, D) Ub^{CyPet} and (B, E) acUbK6^{CyPet}. (C, F) Visualization of the FRET signal as a function of ^{YPet}E2 concentration. The maximum FRET signal observed at each concentration was plotted for Ub^{CyPet} (black) and acUbK6^{CyPet} (orange). The insignificant variation in the slopes (indicated in the bottom right of the panels, slope ± SEM) enabled a common factor to be used for Ub^{CyPet} and acUb^{CyPet} proteins for each ^{YPet}E2 system.

hydrolysis of the ^{YPet}UBE2L3~Ub^{CyPet} conjugate, as this E2 protein is susceptible to hydroxyl- and thiol-mediated reactions. Regardless, the ΔFRET to nanomolar conversion could be applied for these experiments as well (Fig. 3.3F). The slopes of the correlations using the acUb proteins were very similar to that for Ub and allowed a common conversion factor to be applied for all reactions using ^{YPet}UBE2L3. For example, the slopes for ^{YPet}UBE2L3 with Ub^{CyPet} or acUbK6^{CyPet} were 8.0 ± 0.3 and 7.4 ± 0.6, respectively. Although the magnitude of the conversion factor for the ^{YPet}UBE2L3 experiments is

smaller than that for UBE2D1 experiments, the correlation is linear, indicating that Ub acetylation does not alter the total FRET signal in reactions with ^{YPet}UBE2L3. Therefore, these distinct conversion factors can be applied to their specific systems to effectively convert FRET signal to E2~Ub concentration.

To obtain kinetic curves, data from the first 20% of E2~Ub conjugate formation were used. At the lowest concentrations of ^{YPet}E2, ≤ 12 min was required to reach 20% conjugation, while conjugation was 20% complete in as little as 1.5 min at the highest concentrations of ^{YPet}E2. In all cases, the first 20% of each reaction demonstrated a nearly linear response for the FRET signal. Some experiments, particularly those at the lowest concentrations of ^{YPet}E2, experienced a "lag time" immediately after the addition of MgATP. For this reason, we treated all experiments the same and began rate determination at 2 min (Fig. 3.4). This allowed between 20 and 50 individual data points to be used for each data set. Regardless of the E2 protein used and the Ub acetylation state, FRET data showing E2~Ub conjugate formation were very reproducible with low fitting errors ($< 2.5\%$). The data show that the rate of formation of the UBE2D1~Ub conjugate is most rapid for wild-type Ub and is strongly dependent on ubiquitin acetylation (Fig. 3.4A-D). For example, ^{YPet}UBE2D1 conjugation of Ub^{CyPet} occurs ~1.25 times faster than that of acUbK6^{CyPet} and 2.2 times faster than that of acUbK33^{CyPet}. For ^{YPet}UBE2L3, Ub^{CyPet} conjugation occurred ~1.36 times faster than acUbK6^{CyPet} and ~1.43 times faster than acUbK33^{CyPet} (Fig. 3.4E-H). Strikingly, the different acUb proteins did not exhibit the same alterations to loading between the two E2 proteins. This is most evident for acUbK33^{CyPet}, where this acUb protein impairs UBE2D1 loading to a larger extent than it impairs UBE2L3 loading. These results indicate that Ub acetylation will influence E2~Ub formation uniquely for each individual E2 protein.
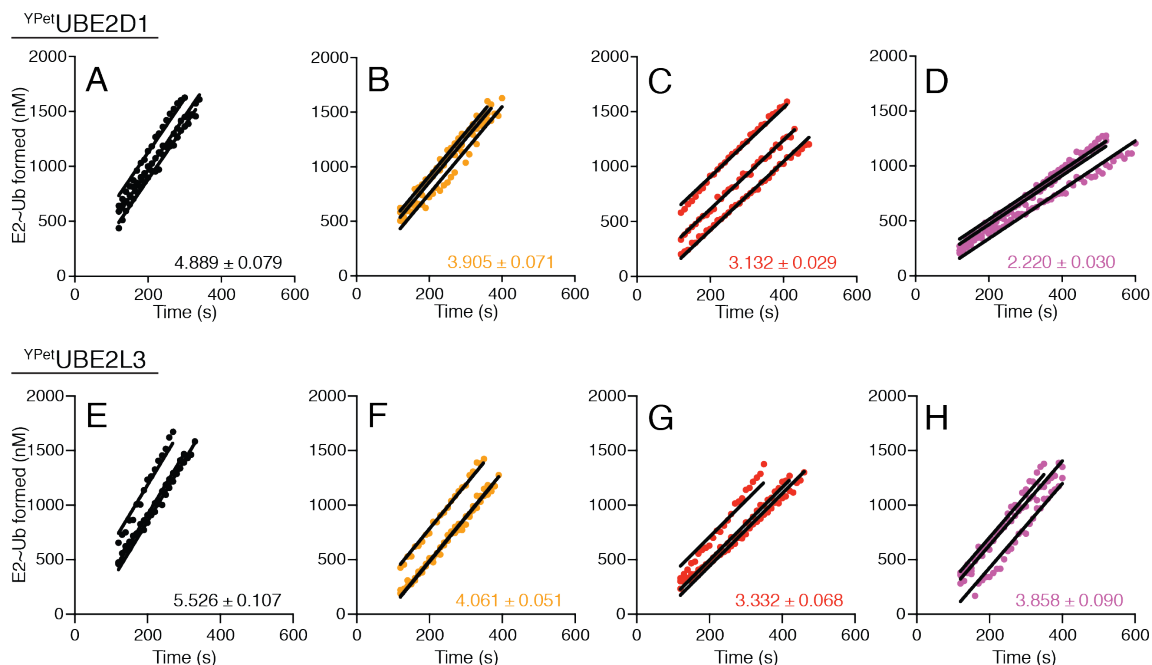
Figure 3.4. The initial rate of E2~Ub conjugation varies for different acUb proteins. (A, E) Ub^{CyPet}, (B, F) acUbK6^{CyPet}, (C, G) acUbK11^{CyPet}, and (D, H) acUbK33^{CyPet} were conjugated using equimolar amounts of ^{YPet}UBE2D1 (top) or ^{YPet}UBE2L3 (bottom) and monitored using fluorescence at 528 nm. The conversion of fluorescence data to the amount of product formed (nanomolar) allowed initial rates to be fit in the linear region. Data were fit globally for three replicates over the first 20% of each reaction to determine the slope ± SEM, shown in the bottom right of each panel.

3.3.3 Acetylation modulates Ub loading by E2 proteins

The observed initial rates for E2~Ub conjugate formation were plotted as a function of ^{YPet}E2 concentration to derive Michaelis-Menten kinetic parameters using a nonlinear regression (eq. 1).

$$v_0 = \frac{V_{max}[S]}{K_M+[S]} \quad (1) \qquad k_{cat} = \frac{V_{max}}{[E]_t} \quad (2) \qquad cat_{eff} = \frac{k_{cat}}{K_M} \quad (3)$$

In these systems, the ^{YPet}E2 protein acts as the substrate, and the enzyme UBA1 has formed its active complex with two Ub molecules. The Michaelis complex forms through noncovalent interactions between the E2 protein and the UBA1 active complex. For simplicity, the kinetic scheme is indicated below without the fluorophore tags on the Ub and the E2 proteins (reaction A).

$$\text{UBA1}{\sim}\text{Ub(t)} : \text{Ub(a)} + \text{E2} \rightleftharpoons \text{UBA1}{\sim}\text{Ub(t)} : \text{Ub(a)} : \text{E2} \rightarrow \text{UBA1}{\sim}\text{Ub(t)} : \text{Ub(a)} + \text{E2}{\sim}\text{Ub} \quad \text{(A)}$$
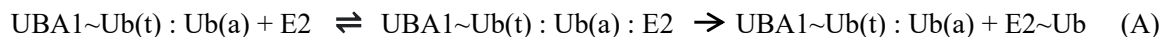
To evaluate the effects that acUb has on UBE2D1 loading, kinetic curves were analyzed as a function of $^{\text{YPet}}$UBE2D1 concentration and compared with those of Ub (Fig. 3.5 A, B). The K_M values for most of the acUb$^{\text{CyPet}}$ constructs were similar within error to that of Ub$^{\text{CyPet}}$ (Fig. 3.5C), indicating that the association of $^{\text{YPet}}$UBE2D1 with the E1 loaded with each acUb$^{\text{CyPet}}$ is not altered by acetylation. In contrast, acUbK48$^{\text{CyPet}}$ exhibited an average
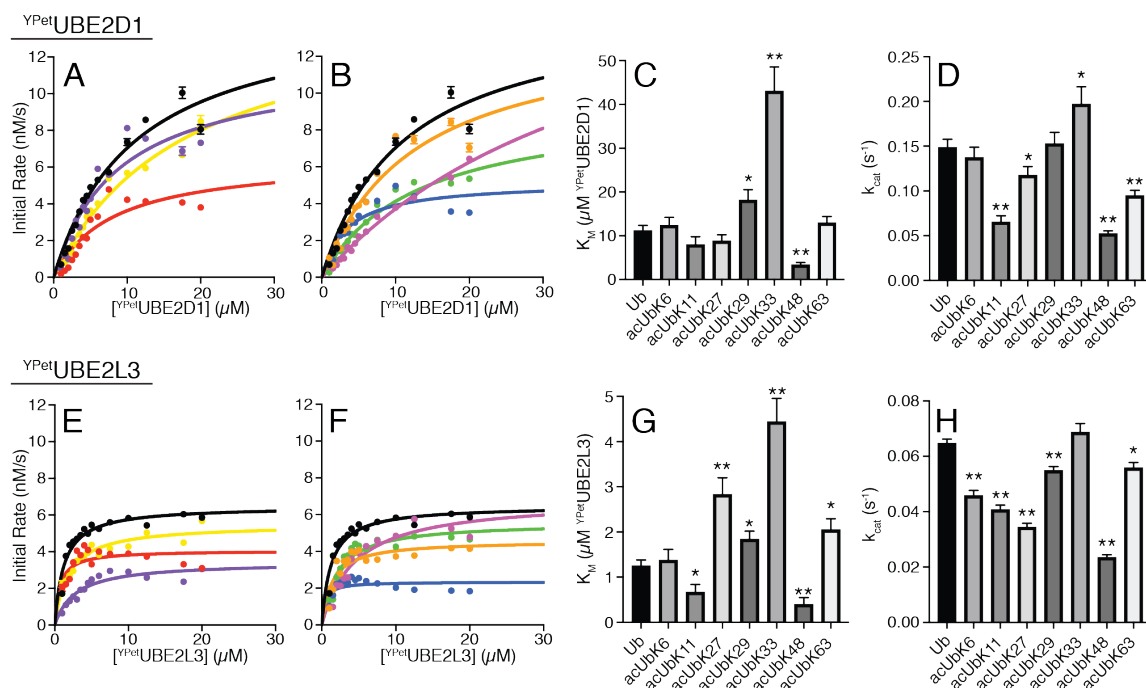
Figure 3.5. Ubiquitin acetylation modifies kinetic curves for UBE2D1 and UBE2L3. Initial rates for E2$\sim$Ub conjugate formation using 1−20 μM $^{\text{YPet}}$UBE2D1 or $^{\text{YPet}}$UBE2L3 were plotted and fit. Individual data points represent the average initial rates of three individual replicates per concentration. Error bars are shown for each point ($\pm$ SEM). Curves are coloured as follows: black for Ub$^{\text{CyPet}}$, (A, E) red for acUbK11$^{\text{CyPet}}$, purple for acUbK27$^{\text{CyPet}}$, and yellow for acUbK29$^{\text{CyPet}}$, and (B, F) orange for acUbK6$^{\text{CyPet}}$, pink for acUbK33$^{\text{CyPet}}$, blue for acUbK48$^{\text{CyPet}}$, and green for acUbK63$^{\text{CyPet}}$. The curves were used to derive the Michaelis-Menten kinetic parameters (C, G) K_M and (D, H) k_{cat} for the transthiolation from UBA1 to the indicated E2 protein, and bars represent the average $\pm$ SEM of each parameter. A Student's t test was used to determine which acUb constructs were significantly different from Ub: $0.05 > p \geq 0.0005$ (one asterisk), and $p < 0.0005$ (two asterisks).

K_M (3.31 μM) that was 70% lower than that of Ub^{CyPet} (11.11 μM), and the K_M of acUbK33^{CyPet} (43.02 μM) was nearly 300% higher, both suggesting that acetylation of Ub at these sites alters the interaction of UBE2D1 with Ub-loaded UBA1. The turnover number (k_{cat}, eq. 2) obtained from the Michaelis-Menten curves demonstrated more variation between the acUb variants and Ub (Fig. 3.5D). Ubiquitin acetylated at K6 or K29 demonstrated k_{cat} values within 10% of Ub. The acUbK33^{CyPet} protein was the only construct to have a higher turnover number (0.197 s^{-1}). Four acUb variants showed significantly lower k_{cat} values that ranged from 15% (acUbK27^{CyPet}) to 70% (acUbK11^{CyPet} and acUbK48^{CyPet}) poorer than that of Ub^{CyPet}. These translated to catalytic efficiencies (k_{cat}/K_M, eq. 3) for four acetylated ubiquitin proteins (acUbK11^{CyPet}, acUbK29^{CyPet}, acUbK33^{CyPet}, and acUbK63^{CyPet}) that were significantly decreased compared to that of Ub. Surprisingly, the consistently lower K_M and k_{cat} values for acUbK48^{CyPet} resulted in a catalytic efficiency that was indistinguishable from that of Ub^{CyPet}.

The same methodology was used to compare the kinetics of E2~Ub formation with ^{YPet}UBE2L3. Figure 3.5 E, F shows the Michaelis-Menten curves associated with the FRET experiments collected for the acetylated Ub proteins with UBE2L3. Intriguingly, the significant variation in the K_M values (Fig. 3.5G) derived from these experiments indicate that ubiquitin acetylation influences the binding of ^{YPet}UBE2L3 to the active UBA1 complex. While acUbK11^{CyPet} and acUbK48^{CyPet} reduce the K_M between 50-75%, most other acUb proteins increase the K_M. Numerically, acUbK29^{CyPet} and acUbK63^{CyPet} increase the K_M between 150-165%, while acUbK27^{CyPet} (230%) and acUbK33^{CyPet} (350%) have a more drastic influence on ^{YPet}UBE2L3 binding. This variation demonstrates that the different acetylated lysine residues modify distinct regions or binding conformations in the UBA1 active complex that can either promote or deter ^{YPet}UBE2L3 recruitment. Further, six of the seven acUb proteins impaired catalytic turnover evidenced by the reduction in k_{cat} (Fig. 3.5H). Ub acetylated at K33 was the only protein that did not modify catalytic turnover with ^{YPet}UBE2L3. The other acUb proteins caused between a 15% (acUbK29^{CyPet} and acUbK63^{CyPet}) to 64% (acUbK48^{CyPet}) reduction in k_{cat}. Together, the variation in K_M and k_{cat} correlated to significantly different k_{cat}/K_M values for all seven acUb proteins with ^{YPet}UBE2L3. Ub acetylated at K11 or K48 showed ~1.15-fold higher

k_{cat}/K_M values, while the other acUb proteins ranged from 23% (acUbK27$^{\text{CyPet}}$) to 64% (acUbK6$^{\text{CyPet}}$) that of Ub$^{\text{CyPet}}$.

3.4 Discussion

In this work, we used programmed acetylation to express and purify all possible acetylated lysine variants in the post-translational modifier protein Ub (acUb). These proteins were used to identify whether acetylation of ubiquitin alters the ability of the E1-activating enzyme UBA1 to catalyze the formation of an E2~Ub conjugate with UBE2D1, a promiscuous E2-conjugating enzyme, or UBE2L3, a cysteine specific E2-conjugating enzyme. For UBE2D1, our work shows that acetylation of most lysine residues yields K_M values that are similar to that of Ub, indicating that acetylation of Ub does not significantly disrupt the interaction of the UBA1 ternary complex with UBE2D1 for these proteins. In contrast, acetylation of Ub appears to have a larger impact on k_{cat}, showing that five acUb proteins (acUbK11, acUbK27, acUbK33, acUbK48, and acUbK63) have k_{cat} values that are significantly different from that of Ub for the formation of the UBE2D1~Ub conjugates. Overall, this results in four acUb proteins (acUbK11, acUbK29, acUbK33, and acUbK63) that have catalytic efficiencies that were ~50% worse than that of Ub with UBE2D1. Conversely, our data indicates that ubiquitin acetylation impairs recruitment and binding of UBE2L3, as the K_M values for all but acUbK6 were significantly different than the K_M for Ub. A similar trend was observed with k_{cat} values, where all acUb proteins except acUbK33 had significant influence on the turnover number of the UBA1-ternary complex with UBE2L3. These trends resulted in reduced catalytic efficiencies for the formation of UBE2L3~Ub species with five out of the seven acUb proteins (ranging from 37-77% poorer than Ub); acUbK11 and acUbK48 demonstrated a modest increase in catalytic efficiency. In general, the reduction in catalytic efficiency for the different acUb proteins is consistent regardless of E2 identity. That is, a given acUb protein reduces the parameter in both systems. One acUb protein, acUbK27, has contrasting effects on catalytic efficiency. Ub acetylated at K27 has no influence on the efficiency for UBE2D1 loading, but catalytic efficiency decreases for UBE2L3 loading by 77%. This variation is largely due to the differences in K_M values for the two E2 proteins. Although the general trends for catalytic efficiency are the same, a similar contrast is evident with acUbK29 where the

k_{cat} for UBE2D1 turnover is unchanged, while the turnover number for UBE2L3 has a 15% reduction. These trends likely reflect changes linked to E2 identity in addition to Ub acetylation.

The absolute values for K_M and k_{cat} for the transthiolation of ubiquitin by UBA1 to UBE2D1 or UBE2L3 are larger than previously described [48,145,146]. This could be due to differences in the protein constructs or assays used. Our work utilized a C-terminal His-tagged variant of UBA1, while previous studies used an N-terminal GST-tagged copy of the enzyme. On the basis of three-dimensional structures [37–41,47], neither of these modifications is expected to alter the fold of UBA1, the interactions of ubiquitin, or the recruitment of the E2 protein. Our work also demonstrated that the K_M for UBE2D1 was larger than that for UBE2L3, which disagrees with other findings [146]. However, we did find that although the magnitude of our values for k_{cat} for Ub with UBE2D1 or UBE2L3 were smaller than previously described, the k_{cat} for UBE2D1 was approximately 2.0-2.5-times larger than the k_{cat} for UBE2L3 in our work, a ratio that is similar to previous findings [145]. It is unclear why our experiments showed these differences in kinetic values. In our assays, we utilized N-terminal FRET tags attached to Ub and UBE2D1 or UBE2L3 [134]. It is possible that these large β-barrel fluorophores might cause some steric hindrance for E2 or ubiquitin binding that could alter the absolute values of K_M and k_{cat}. In most structures of UBA1 in complex with Ub, the N-terminus, where the FRET tag is located, faces the solvent. Any minimal effects are expected to contribute consistently for each acUb and still allow comparison of the different proteins.

Three acetylated Ub proteins, acUbK6, acUbK33 and acUbK48, showed the same trend in terms of K_M regardless of E2 identity. For both UBE2D1 and UBE2L3, acUbK6 did not alter the binding of the E2 protein, evidenced by the insignificant 10% increase in K_M compared to that for Ub. Conversely, acUbK33 caused over a 300% increase in the K_M for the binding of UBE2D1 and UBE2L3 in their separate systems, and acUbK48 reduced the K_M for the binding of each individual E2 protein by 70%. The k_{cat} of both E2 systems with acUbK48 was reduced 65%. These similarities likely reflect influences that these acUb proteins have on the UBA1-ternary complex, as they are not specific to a given E2 protein.

Many of the other acUb proteins had kinetic parameters that were modulated with varying magnitude along the same directionality between E2 systems. For example, acUbK11 reduced the k_{cat} 56% and 37% for UBE2D1 and UBE2L3, respectively, and reduced the K_M 28% and 47% for UBE2D1 and UBE2L3, respectively. The differences in magnitude but the conserved directionality between systems with UBE2D1 and UBE2L3 indicate that these acUb proteins likely have influences on both the UBA1-ternary complex and the stability of the E2~Ub product.

Finally, two acUb proteins displayed kinetic parameters that had opposing directionality between the UBE2D1 and UBE2L3 systems. The k_{cat} for acUbK29 was insignificantly increased with UBE2D1, but this Ub protein demonstrated a 15% reduction in the same parameter with UBE2L3. The inconsistent influence that acUbK29 has on the formation of E2~Ub with different E2 proteins indicates that acetylation of K29, in addition to the E2 identity, has a role in E2~Ub formation. A more drastic difference between the UBE2D1 and UBE2L3 systems was observed with acUbK27, where the K_M values were 22% reduced and 230% increased, respectively. This major difference indicates that acetylation of Ub at K27 directly influences the binding of an E2 protein and could have further implications in E2~acUbK27 product stability.

We attempted to rationalize the modified catalytic activities of UBA1 with different acUb proteins using structures of UBA1. The E1 enzyme UBA1 contains five domains and a four-helix bundle that are utilized to load Ub onto an E2. Multiple three-dimensional structures [37,38,41,47] show that the initial adenylation of Ub results in a complex in which the adenylated Ub [Ub(a)] is bound near the juncture of the IAD (inactive adenylation), AAD (active adenylation), and FCCH (first catalytic cysteine half) domains (Fig. 3.6A). Formation of the E1 thioester-linked Ub species [Ub(t)] is accomplished by a large hinge-like motion of the second catalytic cysteine half (SCCH) domain that positions the catalytic cysteine (C593, *Schizosaccharomyces pombe*; C600, *Saccharomyces cerevisiae*) near the C-terminus of the adenylated Ub(a) to facilitate the transfer [39,147]. It has been shown that the fully activated E1 enzyme is loaded with both Ub(a) and Ub(t) molecules that continually cycle (Fig. 3.6A) and that this complex has maximal affinity for an E2 enzyme [92]. Structures show that E2 binding is accommodated by movement of the

UFD (Ub fold domain) to allow an E2 enzyme to bind the space between the UFD and the SCCH domain of UBA1 [38,47,148,149]. The positioning of the E2 by the UFD provides
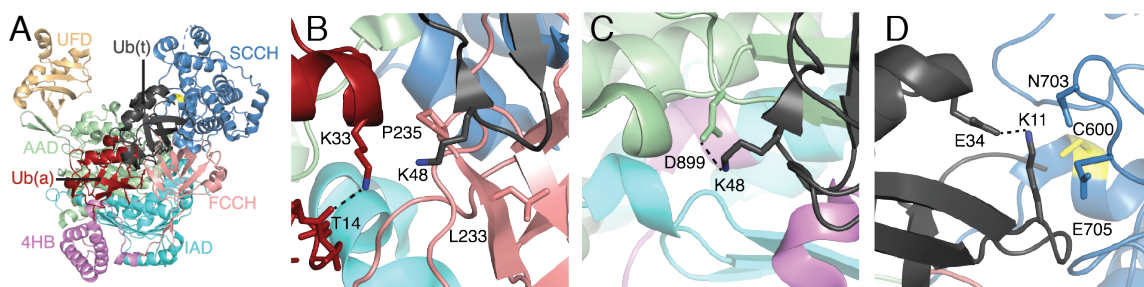
Figure 3.6. Specific interactions between UBA1 and two bound acUb molecules could cause variation in transthiolation rates.
(A) Structure of UBA1 in complex with Ub(a) (red) and Ub(t) (dark grey) proteins crystallized as part of the asymmetric unit from [41] (PDB ID: 4NNJ). The domains of *S. cerevisiae* UBA1 are labeled as follows: UFD, ubiquitin fold domain (wheat); SCCH, second catalytic cysteine half domain (blue); FCCH, first catalytic cysteine half domain (pale pink); IAD, inactive adenylation domain (cyan); 4HB, four-helix bundle (magenta); AAD, active adenylation domain (pale green). (B) Interaction of K48 of Ub(t) with L233 and P235 of the FCCH domain. K48 in Ub(t) sits across from K33 in Ub(a) (red) that is hydrogen bonded to the backbone carbonyl of T14 in Ub(a). (C) Interaction between K48 in Ub and D899 of *S. pombe* UBA1 as demonstrated in the closed capture complex (PDB ID: 6O83). (D) Specific regions of interaction around K11 of Ub(t) (dark grey) with N703 and E705 of the SCCH domain. The side chain of K11 is hydrogen-bonded to the carboxylate of E34 of Ub(t). Dashed lines represent polar contacts involving the lysine residue of Ub as per the indicated X-ray structure.

some specificity that places Ub(t) near helix α2 of the E2 enzyme in a conformation that resembles the closed E2~Ub conformation. It is possible that differences in k_{cat} could reflect any of the Ub transfer states from Ub to Ub(a), the E1~Ub(t) conjugate, and the E2~Ub conjugate. To limit these possibilities, our experiments were performed using excess amounts of Ub and ATP relative to UBA1. We expect that the initial steps are masked in our experiments and kinetic differences would be most apparent in the stability of the fully loaded E1~Ub(t):Ub(a) complex and in the formation of the E2~Ub(t) conjugate. Further experiments will be needed to confirm this.

Ub acetylated at position K48 shows the most significant decreases in k_{cat} values compared to that of Ub, regardless of E2 identity. Among the seven lysines in Ub, this residue has

some of the most obvious interactions with UBA1 that could impede transfer to an E2 enzyme. The side chain of K48 in Ub(t) lies near L233 and P235 of the hydrophobic β11−β12 loop (V232−F236) in the FCCH domain of UBA1 and across from the side chain of K33 of Ub(a) (Fig. 3.6B). While residues in the FCCH domain do not appear to have any charged interactions with K48 in Ub(t), the closed UBA1−Ub capture complex (PDB ID: 6O83) provides evidence for ionic interactions (<4 Å) between K48 in the covalently linked Ub and D899 (*S. pombe*; E910 in *S. cerevisiae*) in the AAD domain [38,39,41] that would be compromised upon acetylation of K48 (Fig. 3.6C). Thus, the diminished turnover (k_{cat}) upon acetylation at K48 of Ub may result from possible enhanced hydrophobic interactions due to lysine side chain neutralization in Ub(t) or loss of charged interactions in the closed UBA1−Ub complex that could inhibit transfer to the catalytic cysteine in UBA1.

Acetylation of five residues resulted in differences in k_{cat} compared to that of Ub for E2~Ub conjugate formation, where the magnitude of the difference was dependent on E2 identity, but the overall directionality of the difference was conserved. In multiple structures, the side chains of two of these proteins, acUbK6 and acUbK63, are exposed to solvent in Ub(a) and Ub(t) [37–39,41,47]. For acUbK6, the influence that acetylation at this residue has on E2~Ub formation is dependent on E2 identity, as there is insignificant variation in the k_{cat} in the UBE2D1 system compared to Ub. Previous work has shown that modification at K6 with the fluorescent label Oregon green increases the K_M and decreases the k_{cat} for UBE2D1~Ub formation [150]. Thus, it is likely that acUbK6 modifies k_{cat} in an E2-dependent manner and does not have much influence on the UBA1-ternary complex itself. The side chains of K63 in Ub(a) and Ub(t) lie on the exterior of the UBA1 enzyme complex. In addition, multiple structures of E2~Ub conjugates display K63 as a solvent-facing residue regardless of the conformation [52,57,151,152] making it unclear how acetylation at this residue can alter UBE2D1~Ub and UBE2L3~Ub conjugate formation. It is possible that our observations, where acetylation at K63 impairs E2~Ub conjugate formation, may result from differences earlier on in Ub activation that cannot be detected in our experiments. Acetylation at K11 in Ub reduced the k_{cat} of UBE2D1~Ub and UBE2L3~Ub formation by 56% and 37%, respectively. The β1−β2 loop in Ub(t) is central

for interactions with the SCCH domain in UBA1, contacting the extended αH24−αH25 loop C-terminal to crucial E2-binding residues [38]. Following the β1−β2 loop in Ub, K11 in Ub(t) sits across from N703/E705 (*S. cerevisiae*, corresponding to T697/Q699 for *S. pombe*) of the SCCH domain (Fig. 3.6D), supporting the interaction [41]. As expected, substitutions in this region of UBA1 show decreased levels of E2~Ub conjugate formation [38,39,47]. However, the largest alteration from acetylation at K11 would likely be the disruption of an intramolecular ionic interaction with the side chain of E34 in Ub(t) that is observed in nearly all Ub structures [153]. Acetylation at K11 would likely change the conformation of the β1−β2 loop in Ub(t), destabilizing this necessary interaction with the SCCH domain needed to facilitate transfer to the E2 enzyme. Previous experiments have indicated that neutralization or charge swapping at E34 of Ub inhibits diubiquitin formation and increases yeast sensitivity to DNA-damaging agents [36,154]. Ub acetylation at K27 caused a more drastic decrease in the k_{cat} for UBE2L3~Ub formation compared to UBE2D1~Ub formation (48% vs. 21% reduced). In the available structures, K27 and K33 in Ub(a) or Ub(t) make little obvious contact with UBA1 [37–41,47]. Similar to K11 and E34 of Ub, the side chain of K27 is positioned for an intramolecular ionic interaction with D52 that acetylation would clearly disrupt. It is possible the loss of this ionic interaction in acUbK27 influences the small decrease (21%) in k_{cat} for UBE2D1~Ub formation with acUbK27. In contrast, the most reasonable explanation for the smaller turnover number for UBE2L3 is the much larger K_M (230% higher than Ub in this system), indicating that the formation of a productive E1:E2 transthiolation complex is already impaired by worsened E2 binding. The side chain of K33 in Ub(a) is intramolecularly hydrogen bonded to the backbone carbonyl of T14. Although the side chain extends toward a primarily negatively charged pocket just below the β11−β12 loop in the FCCH, further hydrogen bonds are not evident. Curiously, this region is near the same pocket where K48 in Ub(t) sits (Figure 3.6B). It is possible that acetylation at K33 in Ub(a) promotes the transfer of Ub to the Ub(t) position correlating to the increased turnover number (k_{cat}) described here. The inconsistent magnitude change in k_{cat} between E2 proteins likely reflects the interactions the SCCH domain uses to position helix α3 of the bound E2 protein that might be distal to the position of K11, K27, or K33. The composition of helix α3 is quite different between UBE2D1 and UBE2L3. Except for a few conserved aspartate residues, helix α3 in UBE2L3

contains more charged residues compared to helix α3 in UBE2D1. This variation provides evidence as to why the magnitude change of k_{cat} could be dependent on E2 identity.

Intriguingly, acetylation of K29 is the only residue that has not been observed in Ub, yet this species of Ub demonstrated the most obvious dependence of k_{cat} on E2 identity. For UBE2D1, the k_{cat} for transthiolation from UBA1 was an insignificant 3% higher than Ub, but for UBE2L3, the k_{cat} was reduced 15%. In the available E1 structures [37–41,47], the sidechain of K29 extends into solvent and has no obvious interactions with any of the proteins in the complexes. Additionally, in sampled E2~Ub structures, the sidechain of K29 extends outwards into solvent and makes no contact with the E2 protein [52,57,151,152]. Together, these structures indicate that K29 has no significant interaction with any of the proteins involved in catalytic complexes used in our studies. Further experiments with other E2 proteins may highlight a more defined involvement of K29 and could provide explanation as to how acetylation of this residue selectively impairs the formation of various E2~Ub species.

The available X-ray structures used to examine positioning of acetylated lysine residues capture multiple snapshots of UBA1, Ub, and an E2 protein. It is clear, however, that Ub transfer is a very dynamic process in solution. UBA1 mutagenesis experiments to complement structural work identify two main regions of UBA1 that are crucial for complex remodeling. The closed E1 structure required for E1~Ub(t) conjugate formation demonstrates contacts between the FCCH and SCCH domains [39,40] while the open structure (which is favored in Ub adenylation and E2~Ub conjugate formation) maintains contacts between the SCCH and AAD domains [37,38,41,47]. The remodeling events required for E2~Ub conjugate formation rely heavily on the uninterrupted dynamics of the SCCH domain. We have used kinetic experiments to show that acetylated lysine residues in Ub(t) have the potential to impair the rearrangement necessary for E2~Ub conjugate formation in our experiments, resulting in poorer catalysis. Although further experiments are required, we expect that the poorer catalysis for acUb variants observed here will have downstream effects on substrate ubiquitination.

4

Ub acetylation affects E2~Ub conjugate conformation and alters HECT-mediated ubiquitination

4.1 Introduction

The previous chapters have provided evidence that Ub acetylation alters the transthiolation between the E1 protein UBA1 and the two E2 proteins UBE2D1 and UBE2L3. How acetylation modulates steps downstream of E2~Ub formation remains unevaluated, but it could be the result of multiple influences. Primarily, lysine acetylation of Ub blocks ubiquitination sites, thereby preventing the formation of polyUb chains by E2:E3 ubiquitination pairs. Can E2:E3 pairs compensate for lysine acetylation at their preferred polyubiquitination site, or does acetylation limit the function of certain enzymes? Secondly, the conformation of the E2~Ub conjugate required by the different classes of E3 ligases could be altered by Ub acetylation. To visualize the range of conformations that an E2~Ub conjugate can adopt, crystal structures of various E2 proteins with a Ub covalently attached to its catalytic cysteine have been solved. Further, some structures capture E2~Ub species non-covalently bound to select E3 proteins where the extreme conformations become evident. For example, the open conformation of E2~Ub observed in the structure of UBE2D2~Ub bound to the HECT E3 ligase NEDD4-2 shows no non-covalent interaction between the Ub protein and UBE2D2 [56]. Conversely, in the closed

conformation observed with the RING E3 ligase RNF4, the Ub protein folds onto helix α2 of UBE2D1 [59], an interaction that is mediated by the I44 hydrophobic patch of Ub. The other available structures show snapshots of E2~Ub species populating conformations between these two extremes, indicating there is a large distribution of potential conformations. To understand solution properties of E2~Ub conjugates, NMR spectroscopy and other biophysical techniques have been used [53,60]. Previous work has identified key residues such as K48 and Q49 in Ub that are diagnostic of particular E2~Ub conformations that can be tracked in NMR experiments.

Unfortunately, how acetylated Ub proteins alter E2~Ub conformations remains unclear. Acetylation of K6 or K48, which lie in proximity to the I44 hydrophobic patch, are expected to have the largest influence on E2~Ub conformation because they would extend the hydrophobic surface. Other acetylated residues such as K29 and K33 protrude into solution in all available structures and would be expected to have little impact on conformation. Here, we used traditional gel-based experiments to monitor E2 unloading with two catalytic cysteine-containing E3 proteins IPAH3 and HUWE1. We show that acetylation at the preferred polyubiquitination sites by these E3 proteins limits E2~Ub discharge. Further, we highlight how Ub acetylation at K6 or K33 might alter the conformation of the UBE2L3~Ub conjugate. Together, our findings indicate that certain acetylation sites influence the UBE2L3~Ub conjugate to adopt a more closed structure and provides evidence that Ub acetylation impairs polyubiquitination by cysteine-dependent E3 ligases.

4.2 Materials and methods

4.2.1 Protein expression and purification

All proteins were expressed and purified as indicated in sections 2.2.2.3 and 2.2.2.4 with the exception that LB medium was replaced with minimal medium (M9) for Ub and acUb expressions to be used in Nuclear Magnetic Resonance (NMR) experiments. To isotopically label Ub and acUb proteins, M9 medium was supplemented with 1 g $^{15}NH_4Cl$ with or without 2 g ^{13}C-glucose. In growths without isotopically labeled glucose, 0.4% glucose was added to the medium. In labeled acUb growths, use of the orthogonal system

required unlabeled (^{14}N) acetyl-lysine to be added to the medium, so the acetyl-lysine residue is not visible in NMR experiments.

UBE2L3 C86K was purified using the same method described for UBE2L3. The HECT domain of HUWE1 (residues 4006-4374; herein referred to as HUWE1) was expressed in *E. coli* BL21(DE3) overnight at 16 °C with 1 mM IPTG. Cells were harvested and resuspended in 50 mM Tris pH 7.5, 500 mM NaCl, 10 mM imidazole, 10% glycerol (wash buffer). Cells were lysed and debris was removed using high speed ultracentrifugation. The cleared supernatant was applied to Ni^{2+}-NTA resin and batch bound for 1 hour at 4 °C. The resin was washed with wash buffer and His-HUWE1 was eluted using 50 mM Tris pH 7.5, 200 mM NaCl, 250 mM imidazole, 10% glycerol. Overnight dialysis was used to remove the imidazole and HUWE1 protein was aliquoted and frozen at -80 °C.

4.2.2 Nucleophile discharge assays

Discharges of the UBE2D1~Ub conjugates in the presence of nucleophilic amino acids were conducted on preloaded UBE2D1 [155]. A 500 mM stock solution of L-lysine monohydrochloride and a 125 mM stock of L-cysteine were prepared in 50 mM Hepes (pH 7.35 and 7.2, respectively). The E2~Ub and E2~acUb conjugates were formed for 50 min at 30 °C in reaction mixtures containing 1 μM UBA1, 10 μM UBE2D1, 90 μM Ub or acUb, and 5 mM MgATP in 50 mM Hepes (pH 7.4). The accumulation of the UBE2D1~Ub conjugate was terminated by the addition of 5 mM N-ethylmaleimide for 10 min at 30 °C to alkylate the catalytic cysteines of UBA1 and any unconjugated UBE2D1. After incubation with N-ethylmaleimide, 50 mM L-lysine or 6 mM L-cysteine was added, and the reactions proceeded at 30 °C. Samples were taken at the indicated time points after nucleophile addition and quenched in 3x SDS sample buffer containing 20 mM EDTA. Protein species were resolved via Bis-Tris SDS-PAGE in MES running buffer (50 mM MES, 50 mM Tris, 0.1 % SDS, and 1 mM EDTA at pH 7.4) and Coomassie stained. A longer time course experiment was conducted with Ub to choose the appropriate time points. The methodology was repeated for UBE2L3 discharge experiments except that the concentrations of Ub and acUb proteins in the reactions was reduced to 15 μM, and the concentration of UBA1 was reduced to 0.7 μM.

4.2.3   E3-mediated E2 discharge

Discharges of the UBE2D1~Ub conjugates in the presence of the HECT-like E3 IPAH3 were conducted on preloaded UBE2D1. Reaction mixtures containing 0.7 μM UBA1, 15 μM Ub or acUb, 20 μM UBE2D1 and 5 mM MgATP in 50 mM Hepes (pH 7.4) were incubated at 30 °C for 50 minutes and immediately transferred into an ice bath (0 °C) for 10 minutes for temperature equilibration. To find the optimal concentration of IPAH3, multiple tests were done with the Ub protein at 30 °C and 0 °C. The optimal concentration of IPAH3 was determined to be 0.75 μM. The IPAH3 protein was simultaneously pre-equilibrated on ice prior to its addition to the UBE2D1~Ub or UBE2D1~acUb conjugate. To determine if IPAH3 induced discharge of the UBE2L3~Ub conjugate, we tested conditions identical to those optimized for UBE2D1~Ub. We then increased the concentration and temperature of the reaction as indicated. Reactions were sampled at the chosen timepoints over 5 minutes and separated on 15% Bis-Tris SDS-PAGE in MES running buffer. Gels were then stained with Coomassie, destained, and imaged using a BioRad ChemiDoc imaging system.

HUWE1-mediated E2 discharge for both UBE2D1~Ub and UBE2L3~Ub conjugates were optimized similarly to the IPAH3 reaction. Briefly, the respective E2~Ub conjugates were pre-formed at 30°C for 1 hour prior to the addition of HUWE1. HUWE1 was pre-warmed to room temperature prior to its addition to the reaction. Initial reactions used various concentrations of HUWE1. The final experiments used 0.7 μM UBA1, 15 μM Ub or acUb, 20 μM UBE2D1 or UBE2L3, 5 μM HUWE1, and 5 mM MgATP in 50 mM Hepes (pH 7.4). Optimized unloading experiments were conducted at 30 °C for 10 minutes after accumulation of the E2~Ub conjugate. Samples were removed at the desired time points and protein species were resolved on 15% Bis-Tris SDS-PAGE in MES running buffer. Gels were stained, destained, and imaged as indicated above.

4.2.4   Data analysis

To determine the relative amounts of E2~Ub throughout the discharge reactions, SDS-PAGE for each Ub or acUb protein were Coomassie stained and destained as usual. Gels were imaged using a BioRad ChemiDoc system using the pre-set Coomassie Blue protein

gel filter. Image Lab software was used to manually select bands and band densitometry measurements were obtained using the Volume function. The data for each Ub protein were normalized internally to the volume of the band at t= 0 min representing 100% of the E2~Ub conjugate. Data were fit using either a one-phase decay, logistic decay, or linear regression as indicated. Curves for E3-mediated discharge experiments represent the average for two individual reactions.

4.2.5   Formation of thioester E2~Ub species

To examine the NMR spectra of ^{15}N-Ub or ^{15}N-acUb containing E2~Ub complexes, a slight excess of E2 (UBE2L3) was reacted with ^{15}N-Ub or ^{15}N-acUb at 30 °C for 1 hour using 5 mM MgATP and 1 µM UBA1 in 50 mM Hepes pH 7.4. The 1-mL reaction volume was then injected onto a Superdex75 gel filtration column pre-equilibrated in 25 mM Hepes pH 7.0, 50 mM NaCl. The column was run at 0.3 mL/min to ensure separation of any remaining unconjugated ^{15}N-Ub or ^{15}N-acUb protein. SDS-PAGE was used to resolve protein species contained in each fraction, and those fractions containing primarily UBE2L3~^{15}N-Ub or UBE2L3~^{15}N-acUb were pooled and concentrated using a Millipore 3K MWCO centrifugal device. The concentrated sample was used in NMR experiments immediately following preparation.

4.2.6   Formation of a stable isopeptide linked E2–Ub species

4.2.6.1. *Isopeptide conjugation.* To form a stable E2–Ub species, UBE2L3 C86K was purified using the methods established for the wild-type proteins described in section 2.2.2.4. Prior to conjugation, all reaction components (UBA1, UBE2L3, ^{13}C^{15}N-His-Ub or ^{13}C^{15}N-His-acUb) were dialyzed against 200 mL of 50 mM Ches pH 9.5, 150 mM NaCl, 10 mM MgATP (Ches buffer) for two hours at room temperature. A second 200 mL of the buffer was pre-warmed to 37 °C during this time. After two hours, a slight excess of E2 protein, as determined by SDS-PAGE and Coomassie staining, was mixed with the ^{13}C^{15}N-His-Ub or ^{13}C^{15}N-His-acUb protein in a dialysis bag, and a final concentration of 50 µM UBA1 was added. Initially, only half of the UBA1 protein was added to the reaction; the other half was added in hourly increments for the first four hours. The reaction was left at

37 °C for 18 hours with slow shaking, and conjugation progress was monitored by SDS-PAGE.

4.2.6.2. *Purification of the isopeptide-linked UBE2L3–$^{13}C^{15}N$-His-Ub species.* Following conjugation, the reaction mixture was batch bound to Ni^{2+}-NTA resin prewashed with 50 mM Tris pH 8.0, 250 mM NaCl, 250 µM TCEP (UbW2 buffer). Binding occurred at 4 °C for 1 hour with constant mixing. The flowthrough (containing unconjugated E2 protein) was then removed, and the beads were washed extensively with UbW2 buffer. His-tag-containing species (UBA1-His, UBE2L3–$^{13}C^{15}N$-His-Ub, and $^{13}C^{15}N$-His-Ub) were eluted from the resin with UbE buffer (50 mM Tris pH 8.0, 250 mM NaCl, 250 µM TCEP, 250 mM imidazole) in increments of 2 mL. All fractions were monitored by SDS-PAGE to determine protein composition. Fractions containing UBE2L3–$^{13}C^{15}N$-His-Ub were incubated with TEV protease (2.5 mg) to remove the His-tag and dialyzed overnight into UbW2 buffer at 4 °C. Following cleavage, the protein solution was passed through the Ni^{2+}-NTA resin and the flowthrough was collected. Extensive washing with UbW2 buffer ensured all unbound proteins came off the column. The flowthrough and the wash fractions were pooled and concentrated to a 1-mL final volume and injected into a Superdex75 gel filtration column pre-equilibrated with 25 mM Hepes pH 7.0, 50 mM NaCl, 500 µM TCEP (NMR buffer). Separated species were visualized with SDS-PAGE and fractions containing UBE2L3–$^{13}C^{15}N$-Ub were pooled and concentrated for NMR.

4.2.7   Nuclear Magnetic Resonance (NMR) spectroscopy

4.2.7.1. *Sample preparation.* All protein samples were soluble in NMR buffer prior to sample preparation. The NMR samples were made up using 90% protein solution, 5% 1 mM DSS in 99.9% D_2O, and 5% of 99.9% D_2O. Imidazole was used as an internal pH indicator at a final concentration of 3 mM. In all NMR spectra presented, the Ub or acUb molecule is the NMR visible component of the sample (either ^{15}N-labeled or $^{13}C^{15}N$-labeled).

4.2.7.2. *Data collection, processing, and analysis.* All NMR experiments were collected on a Varian Inova 600-MHz NMR spectrometer equipped with a triple-resonance probe temperature controlled to 25 °C. $^1H^{15}N$-HSQC experiments were collected using either a

room temperature or cryogenic probe depending on instrument availability. All ^{1}H^{15}N-HSQC experiments were no longer than 1.5 hours in length, and the pH was measured between 6.95-7.05 for each sample. For signal assignments, the HNCA experiment [156] was collected using the cryogenic probe for the free Ub proteins Ub and acUbK27, and UBE2L3–Ub conjugates containing Ub, acUbK6, and acUbK33. For most experiments, the ^{1}H spectral window was set at 7000 Hz centered around 4.77 ppm and the ^{15}N spectral window was 1944 Hz centered around 120.15 ppm. For triple-resonance HNCA experiments, the ^{1}H spectral window was 7000 Hz centered around 4.77 ppm, the ^{15}N spectral window was 1632 Hz centered around 118.15 ppm, and the ^{13}C spectral window was 4524 Hz centered around 56.12 ppm. All samples were referenced internally to DSS. All data were processed using NMRPipe [157] and analyzed using NMRViewJ [158]. In ^{1}H^{15}N-HSQC experiments used to evaluate the conformation of the UBE2L3–Ub isopeptide conjugates expected to be in fast exchange, the proportion closed was calculated using $f_{closed} = (\delta_{obs} - \delta_{open})/(\delta_{closed} - \delta_{open})$, where f_{closed} is the fraction occupying the closed conformation and δ_{obs}, δ_{open}, and δ_{closed} refer to the chemical shifts of the observed, open, and closed signals, respectively. In ^{1}H^{15}N-HSQC experiments used to evaluate the conformation of the UBE2L3~Ub conjugates expected to be in slow exchange, the proportion closed was calculated using signal intensity where $f_{closed} = V_{closed}/(V_{closed} + V_{open})$, where V_{closed} and V_{open} represent the volume of the closed and open signals, respectively.

4.2.8   Analytical ultracentrifugation

A Beckman XL-A analytical ultracentrifuge equipped with an An60-Ti rotor and double sector cells (1.2 cm) with quartz windows were used for sedimentation velocity experiments. Samples were prepared in NMR buffer and referenced appropriately. All data were collected in 25 mM Hepes pH 7.0, 50 mM NaCl, 0.5 mM TCEP at 25 °C. All velocity experiments were performed at 55,000 rpm (236,000 × g), and protein absorbance was measured at 280 nm scanned 30 times over 6 hours. Scans were acquired in duplicate. SEDFIT [159] was used to generate c(s) distribution data using a partial specific volume (vbar) of 0.73 mL/g, buffer density (ρ) of 1.0064 g/mL, and viscosity of 0.0103 P.

Qualitative observations for acUbK48 were made by comparing distribution data to that of Ub.

Sedimentation equilibrium data were collected using the same instrument using the An60-Ti rotor set up with six-channel Epon-charcoal centerpieces. Protein samples were prepared in NMR buffer and absorbance data were recorded at 280 nm. Experiments were run at 25 °C using rotor speeds of 20 000, 24 000, 28 000, 32 000, and 45 000 RPM. Analyses were done using the data collected at 24 000, 32 000, and 45 000 RPM, and the data were fit using a single ideal species model [160].

4.2.9 Size Exclusion Chromatography- Multi-Angle Light Scattering (SEC-MALS)

A Superdex75 gel filtration column was used with an AKTA FPLC (GE Healthcare) to evaluate protein samples for Ub and acUbK48. The AKTA was connected to a Dawn Heleos light scattering instrument, and both instruments were stored and operated at 10 °C. The systems were controlled using AKTA and ASTRA 7.1.4 software for UV and light scattering data collection. Protein samples were injected onto the Superdex75 at 600 μM for Ub and 220 μM for acUbK48 in degassed NMR buffer. For data processing, the refractive index 1.331 was used.

4.2.10 X-ray crystallography

The acUbK48 protein was expressed and purified as described in section 2.2.2.3 to a stock concentration of 10 mg/mL in 25 mM Tris pH 8.0, 250 mM NaCl, 250 μM TCEP. Crystallization trays were set up using the HR2-133 screen (Hampton Research) using a 1:1 mixture of reservoir to protein solution. Crystals were obtained in 0.18 M ammonium sulfate, 0.09 M sodium acetate trihydrate pH 4.6, 27% PEG MME 2000, 10% glycerol. Crystals were fished without cryoprotectant and sent to the Canadian Light Source (CLS) for data collection. Diffraction data were collected on a beamline rotating 0.2° every 3 sec to cover 180° total. The data were processed using iMosflm in the CCP4 suite, and molecular replacement with Ub (PDB: 1UBQ) in Phenix [161] was used to fit the electron density. The acetyl-lysine at position 48 (code ALY) was manually added in Coot [162].

4.3 Results

4.3.1 Ub acetylation increases UBE2D1~Ub conjugate sensitivity to nucleophilic cysteine

To assess changes downstream of E2~Ub conjugate formation that might arise due to an acetylated Ub molecule, we used nucleophile reactivity assays [155]. UBE2D1~Ub and each UBE2D1~acUb conjugates were assembled at 30 °C using limiting amounts of UBE2D1 and the appropriate Ub protein. After conjugation for 50 min, the forward reaction was inhibited using N-ethylmaleimide to alkylate the catalytic cysteines of the UBA1 and any unconjugated E2. Initially, a 1 h time course was used to monitor the disappearance of the E2~Ub conjugate band to ensure a steady decrease in the amount of conjugate at the chosen nucleophile concentrations (Fig. 4.1A) and to choose appropriate time points to monitor UBE2D1 unloading of acUb proteins. Under these steady-state conditions, reactions showed that all UBE2D1~Ub conjugates were formed at approximately the same level (Fig. 4.1B, C). Following treatment with N-ethylmaleimide, UBE2D1 unloading was initiated with the addition of 50 mM L-lysine or 6 mM L-cysteine at 30 °C and monitored via SDS-PAGE. Figure 4.1B shows that the lysine-mediated
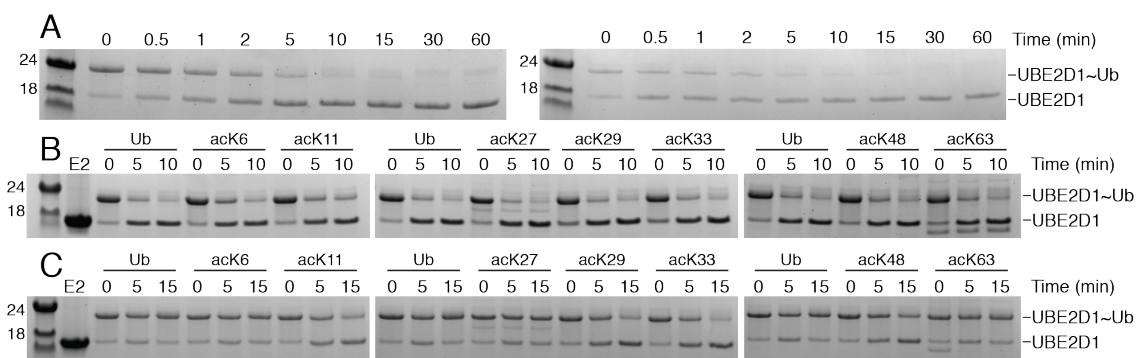
Figure 4.1. Ub acetylation alters the unloading of UBE2D1~Ub conjugates.
Reaction mixtures containing 1 µM UBA1, 10 µM UBE2D1, and 90 µM Ub or acUb in the presence of 5 mM MgATP and 50 mM Hepes (pH 7.4) were used to form the UBE2D1~Ub or UBE2D1~acUb conjugates. (A) A 1 h time course was used to observe the steady decrease in the level of the UBE2D1~Ub conjugate over time using 50 mM L-lysine (left) or 6 mM L-cysteine (right) at 30 °C. Appropriate time points for the unloading of acUb from UBE2D1 in the presence of (B) 50 mM L-lysine or (C) 6 mM L-cysteine were chosen. Proteins were resolved via non-reducing Bis-Tris SDS-PAGE for all reactions.

disappearance of the UBE2D1 conjugate with all acetylated Ub proteins occurs over the first 10 min of the reaction. Visually, there is little difference between the intensities of bands for UBE2D1 for the aminolysis of the UBE2D1~Ub conjugate compared to any of the UBE2D1~acUb variant conjugates, indicating that acetylation of Ub does not impair nucleophilic lysine discharge in these experiments. Conversely, cysteine discharge experiments with UBE2D1~Ub conjugates were influenced by the acetyl modification of Ub (Fig. 4.1C). Band densitometry analysis of the gels in Figure 4.1B, C was used to confirm the qualitative findings (Fig. 4.2). Our data show that acetylation at K11, K29, K33, or K48 increases the reactivity of the UBE2D1~acUb conjugates to nucleophilic cysteine by 30-50% (Fig. 4.2C, D). These findings may indicate that acetylation of certain Ub residues may play a role in thioester reactivity in the various steps of ubiquitination.
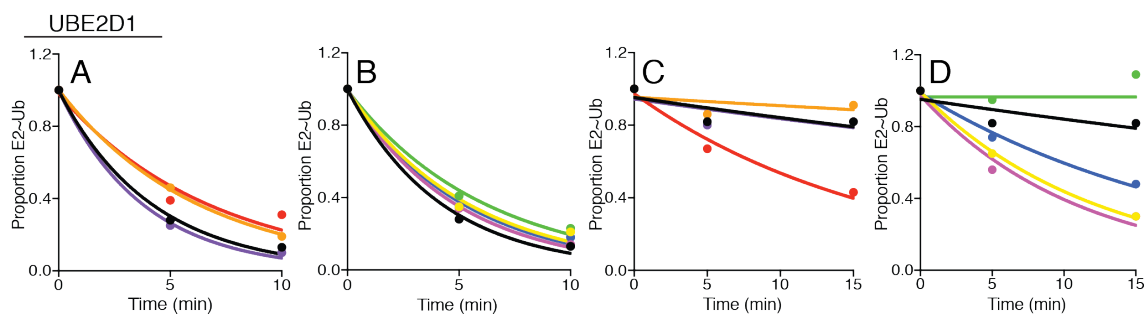
Figure 4.2. Band densitometry of nucleophile induced UBE2D1~Ub unloading details modifications due to acUb proteins.
The intensities of the bands from gels presented in Figure 4.1 were evaluated using BioRad ImageLab software. Each reaction was normalized internally to the intensity of the band at the t= 0 min timepoint for (A, B) 50 mM L-lysine reactions, and (C, D) 6 mM L-cysteine reactions. In all cases, curves were fit with a one-phase decay with a plateau of zero E2~Ub using GraphPad Prism 9.0. Colours throughout the panels are as follows: black- Ub, orange- acUbK6, red- acUbK11, purple- acUbK27, yellow- acUbK29, pink- acUbK33, blue- acUbK48, and green- acUbK63. Curves shown here represent a single experiment for each of the Ub proteins.

4.3.2 Ub acetylation does not alter UBE2L3~Ub conjugate sensitivity to amino acid nucleophiles

To understand the downstream effects of Ub acetylation on another E2 protein, UBE2L3, nucleophile reactivity assays were also used. The UBE2L3~Ub conjugate and each

UBE2L3~acUb species were pre-made similar to the UBE2D1~Ub conjugates. An hour-long time course was initially done using either 6 mM L-cysteine or 50 mM L-lysine to determine the appropriate timepoints (Fig. 4.3A). In the presence of 6 mM L-cysteine, the UBE2L3~Ub conjugate was completely unloaded after 60 minutes. As expected, the UBE2L3~Ub conjugate did not unload in the presence of 50 mM L-lysine at timepoints up
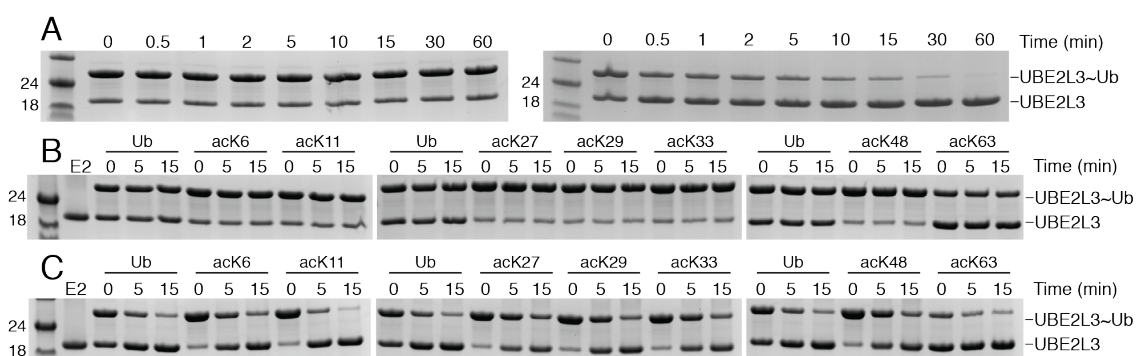
Figure 4.3. Acetylation of Ub has little influence on UBE2L3~Ub small nucleophile-mediated discharge.
The UBE2L3~Ub and indicated UBE2L3~acUb conjugates were pre-formed using 0.7 μM UBA1, 10 μM UBE2L3, 15 μM Ub or acUb, 5 mM MgATP in 50 mM Hepes pH 7.4. (A) Initially, a 1 h time course at 30 °C was used to confirm no reactivity towards 50 mM L-lysine (left) and reactivity towards 6 mM L-cysteine (right). Timepoints were selected from these time courses and the unloading of UBE2L3~Ub conjugates with each of the acUb proteins was observed for (B) 50 mM L-lysine and (C) 6 mM L-cysteine. Protein species were resolved on 15% Bis-Tris SDS-PAGE in MES running buffer and visualized using Coomassie staining.

to 1 hour. For this reason, the timepoints from the cysteine reaction were used for lysine-mediated unloading of UBE2L3~acUb conjugates (Fig. 4.3B). For each UBE2L3~acUb conjugate, there was approximately an equal amount of conjugate formed in each reaction, indicated by the intensity of the band at the zero timepoints. The UBE2L3~acUbK63 conjugate appeared less intense due to the large amount of truncated Ub_{1-62} that was present in the acUbK63 preparation. As expected, we observed no unloading in the presence of nucleophilic lysine regardless of Ub species, indicating that acetylation of Ub does not prompt UBE2L3 discharge onto lysine (Fig. 4.3B). In cysteine-mediated discharge experiments, there visually appeared to be little influence on UBE2L3 unloading due to Ub

acetylation (Fig. 4.3C). These qualitative findings were corroborated using band densitometry analysis. In the presence of lysine, the UBE2L3~Ub conjugates with Ub or each acUb remained over 80% intact (Fig. 4.4A, B). In cysteine experiments, the discharge of the UBE2L3~Ub conjugate was stimulated nearly 2-fold faster with acUbK11 achieving over 90% discharge compared to the approximately 75% discharge of the UBE2L3~Ub conjugate (Fig. 4.4C). Surprisingly, acUbK27, acUbK33, and acUbK63 (Fig. 4.4C, D) only reached 60% unloading, evidenced by the larger proportion of E2~Ub present at the final timepoint. Overall, these data suggest that selected acUb proteins have a minor influence on UBE2L3~Ub unloading with small nucleophiles.
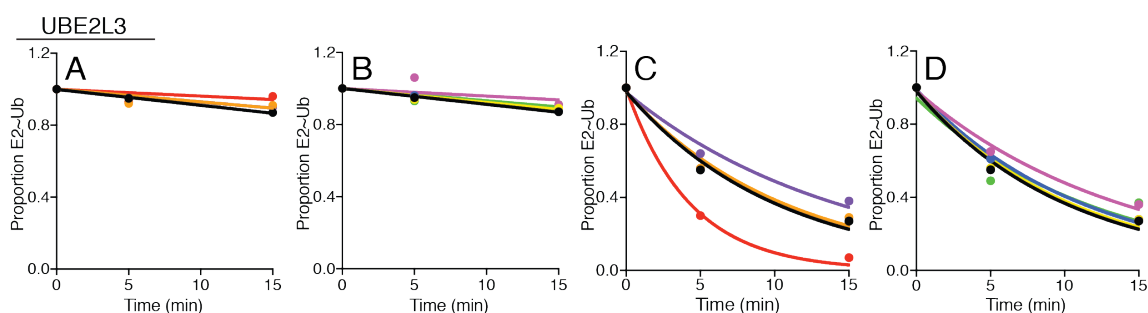
Figure 4.4. Band densitometry accentuates minor differences in cysteine-mediated unloading of UBE2L3~acUb conjugates.
BioRad ImageLab software was used to determine the intensities of the bands from gels presented in Figure 4.3. Each reaction was normalized internally to the intensity of the band at the t= 0 min timepoint for (A, B) 50 mM L-lysine reactions, and (C, D) 6 mM L-cysteine reactions. For lysine-mediated reactions, curves were fit with a linear regression, and curves for the cysteine reactions were fit with a one-phase decay with a plateau of zero E2~Ub using GraphPad Prism 9.0. Colours throughout the panels are as follows: black-Ub, orange- acUbK6, red- acUbK11, purple- acUbK27, yellow- acUbK29, pink- acUbK33, blue- acUbK48, and green- acUbK63. Curves shown here represent a single experiment for each of the Ub proteins.

4.3.3   UBE2L3~Ub conjugates are not reactive with bacterial HECT-like E3 IPAH3

To determine how acetylated Ub influences events downstream of E2~Ub formation with either UBE2D1 or UBE2L3, we examined the discharge of the conjugate in the presence of an E3 ligase. The HECT-like IPAH3 is a bacterial effector protein that utilizes the UBE2D family of E2 proteins to synthesize K48-linked polyUb chains via the formation

of an IPAH3~Ub intermediate [127]. The UBE2D1~Ub conjugate was pre-formed at 30°C for 1 hour. Initially, unloading experiments were conducted at 30°C, but the activity of IPAH3 in the presence of the UBE2D1~Ub conjugate was extremely high, as indicated by the complete loss of UBE2D1~Ub within 15 seconds (Fig. 4.5A). We then chose to decrease the temperature (0 °C) but still observed a fast decrease in UBE2D1~Ub (Fig. 4.5B). Accordingly, we reduced the amount of IPAH3 in the solution to 20-times less than that of the UBE2D1~Ub conjugate and kept the reaction at 0 °C (Fig. 4.5C). For experiments conducted at 0 °C, we introduced a 10-min equilibration period to drop the temperature of the reaction from 30 °C (for conjugation) to 0 °C (for unloading). At 0 °C, high activity was still observed in the unloading of the UBE2D1~Ub conjugate, evidenced by the complete disappearance
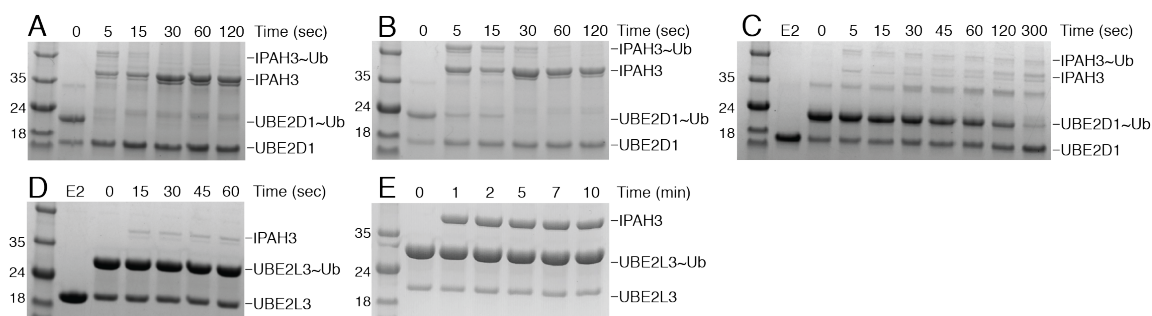
Figure 4.5. IPAH3 is competent with UBE2D1 but not UBE2L3.
Optimization of the IPAH3-mediated unloading of the E2~Ub conjugates was accomplished through modifying the concentration of IPAH3 and temperature of the reaction. In panels A-C, the UBE2D1 protein was 20 µM and the Ub was 15 µM for (A) 7.5 µM IPAH3 at 30 °C, (B) 7.5 µM IPAH3 at 0 °C, and (C) 0.75 µM IPAH3 at 0 °C. For panels D and E, 20 µM UBE2L3 was used with 15 µM Ub for (D) 0.75 µM IPAH3 at 0 °C, and (E) 5 µM IPAH3 at 30 °C. For each reaction, the E2~Ub conjugate was pre-formed at 30 °C and unloaded for the indicated timepoints. Protein species were resolved on 15% Bis-Tris SDS-PAGE with MES running buffer. Bands were visualized using Coomassie staining and the gels were imaged using a BioRad ChemiDoc system. Lanes labeled "E2" were included to show where the unconjugated UBE2D1 or UBE2L3 protein runs.

of the UBE2D1~Ub band after 5 minutes (Fig. 4.5C). We observed a steady decrease in UBE2D1~Ub intensity over the full experiment instead of the sudden unloading observed at 30 °C. We then repeated IPAH3-mediated unloading experiments with UBE2L3~Ub. However, we observed no reaction between UEB2L3~Ub and IPAH3 at the appropriate

conditions described for UBE2D1 (Fig. 4.5D). As UBE2L3 is a cysteine specific E2 protein that reacts with both HECT and RBR E3 ligases [139], we decided to increase the temperature to 30 °C and the concentration of IPAH3 to 5 µM to mimic the initial conditions tested for UBE2D1. Intriguingly, these modifications had no effect on the discharge of the UBE2L3~Ub conjugate in the presence of IPAH3 (Fig. 4.5E), providing further evidence that UBE2L3:IPAH3 is not a competent E2:E3 pair in ubiquitination [127].

4.3.4 K11, K27, or K48 acetylation in Ub impairs UBE2D1 unloading with IPAH3

The bacterial E3 protein IPAH3 has been studied with E2 proteins from the UBE2D family. We chose to use UBE2D1 as the cognate E2 protein in IPAH3-mediated unloading experiments to evaluate how acetylation might influence this step in ubiquitination. Experiments were optimized for Ub with the following final reaction conditions: 50-minute UBE2D1~Ub pre-formation at 30 °C under limiting Ub, 10-min equilibration to 0 °C, followed by addition of IPAH3 at 0 °C. The reaction progress was monitored by SDS-PAGE and following the UBE2D1~Ub conjugate band over time. Figures 4.6A-C show exemplary gels from the reactions with Ub and two acUb proteins (acUbK27, acUbK48). The UBE2D1~Ub conjugate band had completely disappeared by 5 minutes, indicating the reaction was complete. The time courses for acUbK27 and acUbK48 show reduced disappearance of the UBE2D1~acUb conjugate band, indicating a slower reaction between UBE2D1~acUb and IPAH3. Band densitometry and subsequent fitting using a one-phase decay showed that most of the acUb proteins discharged similarly to Ub in the presence of IPAH3, evident by curves that resemble the overall shape of the Ub curve (Fig. 4.6D). Most acUb proteins achieved over 90% completion, demonstrated by the <10% UBE2D1~acUb conjugate band remaining at 5 minutes. However, acetylation at K11, K27, or K48 caused impaired unloading of the UBE2D1~acUb conjugate. While acUbK11 and acUbK27 ultimately achieved 50% discharge, there was no significant discharge of the UBE2D1~acUbK48 conjugate, and over 80% of the acUbK48 protein remained conjugated to UBE2D1. These findings suggest that acetylation at K11, K27, or K48 impair the transthiolation step between UBE2D1 and the HECT-like protein IPAH3.
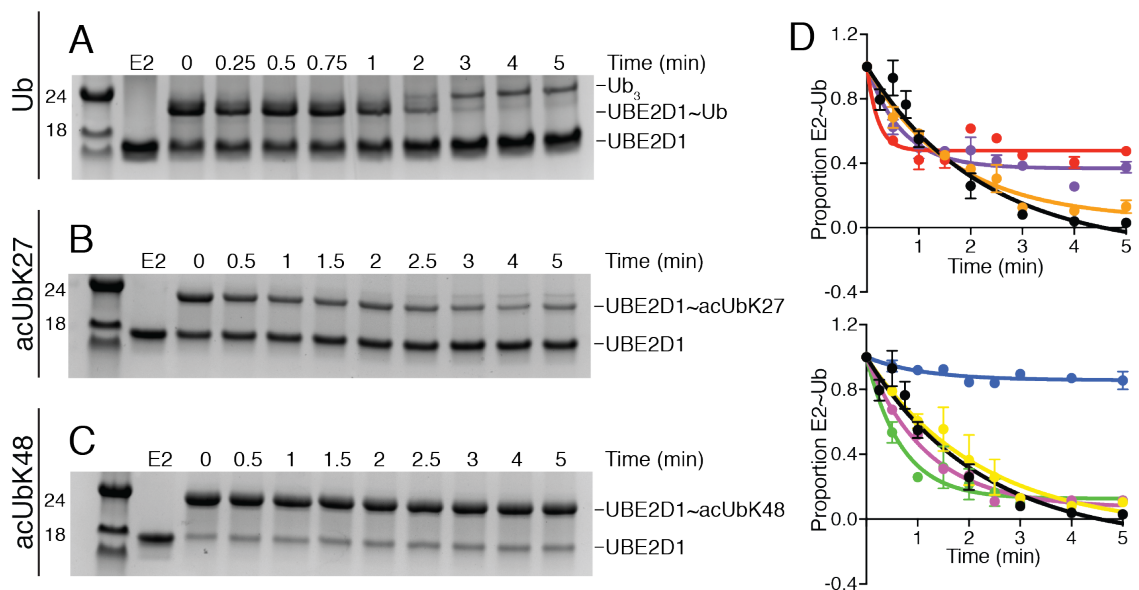
Figure 4.6. Acetylation at K11, K27, or K48 impairs the IPAH3-induced unloading of UBE2D1~Ub.

Reactions containing 20 µM UBE2D1, 15 µM Ub or acUb, 0.7 µM UBA1 were incubated with 5 mM MgATP in 50 mM Hepes pH 7.4 at 30 °C to pre-form saturating amounts of the UBE2D1~Ub or UBE2D1~acUb conjugate. Mixtures were then incubated in an ice bath for 10 minutes prior to the addition of 0.75 µM IPAH3. Unloading was monitored at the indicated time points and protein species were resolved on SDS-PAGE. Exemplary gels for (A) Ub, (B) acUbK27, and (C) acUbK48 are shown. The "E2" lane shows UBE2D1 only. (D) Band densitometry measurements were taken using BioRad ImageLab software and each reaction was referenced internally to the intensity of the UBE2D1~Ub conjugate band present at the t= 0 min time point: This band corresponds to the whole fraction (100%) of UBE2D1~Ub or acUb conjugate. One-phase decay curves were used to fit the data and represent experiments collected in duplicate (n=2). Colours are as follows: black- Ub, orange- acUbK6, red- acUbK11, purple- acUbK27, yellow- acUbK29, pink- acUbK33, blue- acUbK48, and green- acUbK63.

4.3.5   Ub acetylated at K6 or K11 impairs UBE2D1 unloading with HUWE1

Next, to determine how the acUb proteins might influence HECT-mediated discharge of UBE2D1 with a human HECT E3 protein, we turned to mitochondrial ligase HUWE1 that has established interactions with the UBE2D family of E2 proteins [163]. The end reaction conditions were: 60-minute pre-conjugation of UBE2D1~Ub with limiting Ub at 30 °C, followed by the addition of HUWE1 for 10 minutes at 30 °C. As done for the UBE2D1~Ub

and IPAH3 reactions, SDS-PAGE was used to monitor reaction progress. We found that the UBE2D1~Ub conjugate was completely unloaded at 8 minutes (Fig. 4.7A). Figure 4.7B, C show two examples of reactions for acUb proteins (acUbK6 and acUbK29). The reactions with acUbK6 demonstrated impaired UBE2D1 discharge, shown by the intense band corresponding to UBE2D1~acUbK6 at the 10-minute timepoint (Fig. 4.7B). Conversely, the reaction with acUbK29, while slow to get started, reached completion around the 6-minute timepoint (Fig. 4.7C). The reasonable conditions (high temperature and fast reaction) prompted us to attempt to utilize our FRET system (^{YPet}UBE2D1, Ub^{CyPet}) with the optimized UBE2D1:HUWE1 reaction to monitor unloading; however, we observed no change in FRET up to an hour after HUWE1 addition (data not shown). SDS-PAGE of these reactions provided evidence that the ^{YPet}UBE2D1~Ub^{CyPet} had not unloaded. As we had used reaction conditions identical to those optimized for the gel-based experiments, we attributed the lack of UBE2D1 unloading to the N-terminal YPet on UBE2D1 that would be expected to alter UBE2D1~Ub conjugate recruitment and binding by HUWE1.

To quantify the HUWE1-mediated discharge of UBE2D1~Ub or acUb conjugates, we instead used band densitometry (Fig. 4.7D). Surprisingly, these reactions did not appear to follow a one-phase decay model like the UBE2D1:IPAH3 reactions did. Instead, a logistic decay (sigmoidal curve) was used to fit the data due to the slow reaction at the beginning and end of the time course and accelerated rate in the 3–6-minute range. We observed that Ub acetylated at K29, K33, or K48 all showed complete turnover of the UBE2D1~acUb conjugate, evident by 0% of the conjugate band at the final time points. Acetylation at K27 or K63 showed moderately impaired turnover, reaching levels between 85-90% of the UBE2D1~acUb discharged; albeit, slower than the Ub reaction. Finally, acetylation at K6 or K11 severely impaired the reaction between UBE2D1~Ub and HUWE1, evidenced by 50% of the conjugate remaining at 10 minutes. Together, these results show that the UBE2D1:HUWE1 reaction is impaired by Ub acetylation at K6 or K11, and to a lesser extent, K27 and K63.

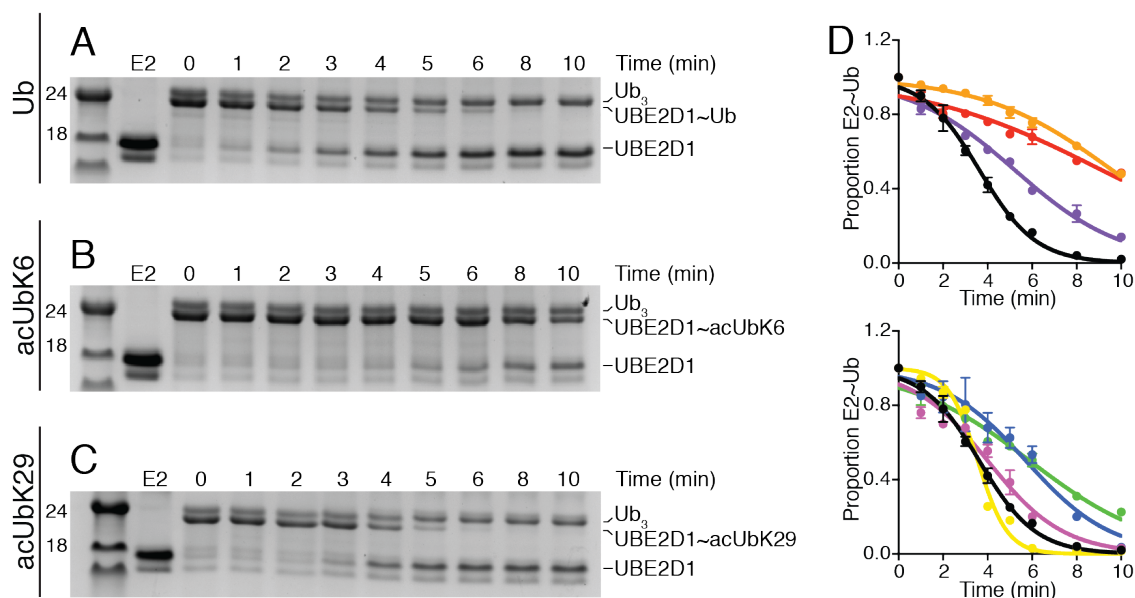**Figure 4.7. Acetylation of Ub modulates the unloading of UBE2D1~Ub with HUWE1.** Reactions containing 20 µM UBE2D1, 15 µM Ub or acUb, 0.7 µM UBA1 were incubated with 5 mM MgATP in 50 mM Hepes pH 7.4 at 30 °C to pre-form saturating amounts of the UBE2D1~Ub or UBE2D1~acUb conjugate. The unloading part of the experiment was initiated after one hour by the addition of 5 µM HUWE1. Unloading was monitored at the indicated time points and protein species were resolved on SDS-PAGE. Exemplary gels for (A) Ub, (B) acUbK6, and (C) acUbK29 are shown. The lane labeled "E2" shows where UBE2D1 runs when unconjugated. (D) Band densitometry measurements were taken using BioRad ImageLab software and each reaction was referenced internally to the intensity of the UBE2D1~Ub conjugate band present at the t= 0 min time point: This band corresponds to the whole fraction (100%) of UBE2D1~Ub or acUb conjugate. Data were fit to a logistic decay curve and represents experiments collected in duplicate (n=2). Colours are as follows: black- Ub, orange- acUbK6, red- acUbK11, purple- acUbK27, yellow- acUbK29, pink- acUbK33, blue- acUbK48, and green- acUbK63.

4.3.6 Ub acetylation modulates UBE2L3 unloading with HUWE1

To study how the acUb proteins alter HUWE1-mediated discharge of the E2 protein with a different E2, we used UBE2L3. The UBE2L3:HUWE1 ubiquitination pair has been well used in the literature in vitro and the interaction between these two proteins has been observed in cells [68,163]. Reactions containing UBE2L3 in place of UBE2D1 were set up identically to those described above: 60 minutes pre-conjugation and 10 minutes unloading, all at 30 °C. Visually, we observed a steady decrease in the amount of UBE2L3~Ub conjugate over the 10-minute period (Fig. 4.8A). The reaction conditions

were then replicated for the acUb reactions using the indicated acUb substituted for the Ub protein. Figure 4.8B, C show examples of the SDS-PAGE from monitoring the reactions containing acUb proteins. We observed that the intensity of the UBE2L3~acUbK11 conjugate decreased less drastically than the reactions for the Ub protein. Further, the UBE2L3~acUbK33 conjugate initially appeared visually similar to the Ub protein; however, at the longest timepoints (8 and 10 minutes), the band corresponding to the UBE2L3~acUbK33 conjugate is less intense than the corresponding band in the Ub reaction.
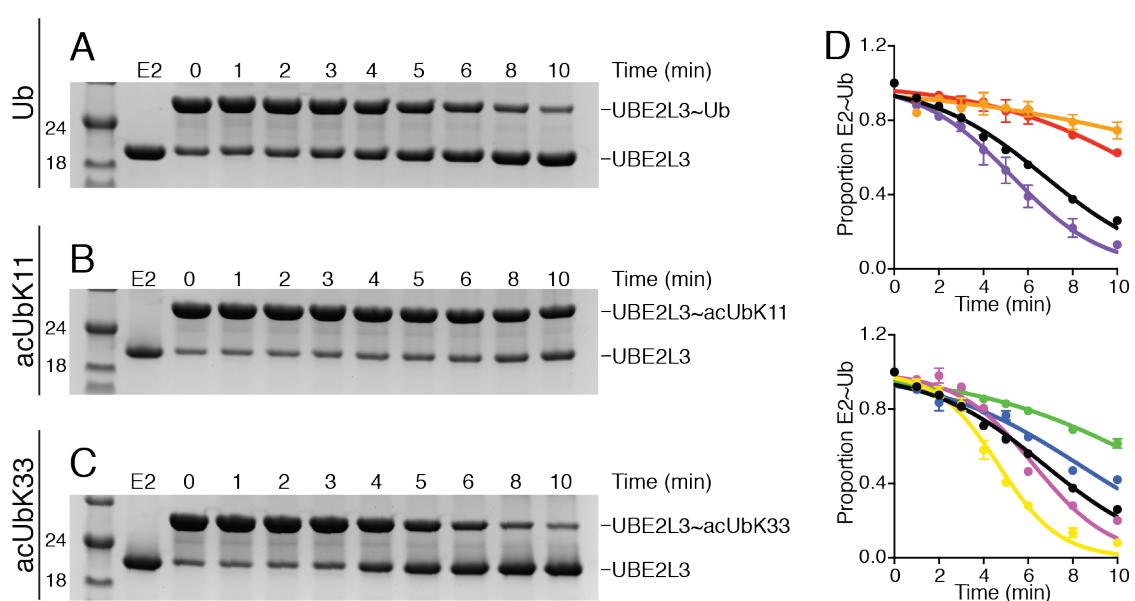
Figure 4.8. Acetylation of Ub modulates the unloading of UBE2L3~Ub with HUWE1. Reactions were conducted identically to those described for UBE2D1 except that UBE2L3 was used as the E2 protein in these experiments. The UBE2L3~Ub and UBE2L3~acUb conjugates were pre-formed at 30 °C and the unloading part of the experiment began with the addition of 5 µM HUWE1 to the reaction. Exemplary gels show the unloading of the UBE2L3~Ub conjugate for (A) Ub, (B) acUbK11, and (C) acUbK33. Lanes labeled "E2" show where unconjugated UBE2L3 migrates. (D) Band densitometry was used to quantify the unloading reaction by referencing the UBE2L3~Ub or UBE2L3~acUb conjugate band intensity at t= 0 min as 100% conjugate. Data were fit to logistic decay curves, and in all cases, best fits represent experiments collected in duplicate (n=2). Colours are as follows: black- Ub, orange- acUbK6, red- acUbK11, purple- acUbK27, yellow- acUbK29, pink- acUbK33, blue- acUbK48, and green- acUbK63.

We then quantified the bands using band densitometry to follow the proportion of UBE2L3~Ub or acUb over time (Fig. 4.8D). We again noticed that the curves could not be

fit with a one-phase decay and were instead fit with a logistic decay. Most of the data in the short timepoints (less than 2 minutes) were clustered around each other, indicating that acetylation does not appear to immediately alter the rate of UBE2L3 discharge. There appears to be more variation in the rates further into the time course where the curves start to disperse. Reactions with acUbK27, acUbK29, or acUbK33 all have parts of their discharge profiles that are faster than the Ub reaction. Ub acetylated at the other four residues (K6, K11, K48, or K63) all show impaired turnover of the UBE2L3~Ub conjugate ranging from 40% (acUbK48) to 80% (acUbK6) conjugate still remaining at the 10-minute timepoint. Our results indicate that Ub acetylated at K27, K29, or K33 improve the discharge of the UBE2L3~Ub conjugate in the presence of HUWE1, while acetylation at K6, K11, or K63 most severely compromise HUWE1-mediated UBE2L3~Ub discharge.

4.3.7   Most acUb proteins are structurally similar to Ub

Our finding that various acUb proteins alter the rates of transthiolation to and from the E2 proteins UBE2D1 and UBE2L3 suggest there might be some structural influence due to the unique acetylation sites. We previously discussed how Ub acetylation could modify interactions with the E1 protein UBA1 to alter the rate of E2~Ub conjugate formation. In addition to protein-protein interactions, Ub acetylation could alter the fold or stability of Ub itself, resulting in a species that might be handled sub-optimally by ubiquitination enzymes. To gain insight into the effects of acetylation on Ub structure, we used Nuclear Magnetic Resonance (NMR) spectroscopy. Individually acetylated proteins were isotopically labeled using $^{15}NH_4Cl$ with or without ^{13}C-glucose as described in section 4.2.1. Use of the orthogonal translation machinery to incorporate acetyl-lysine at the position of interest resulted in a single residue that was unlabeled and therefore, NMR invisible (Fig. 4.9).
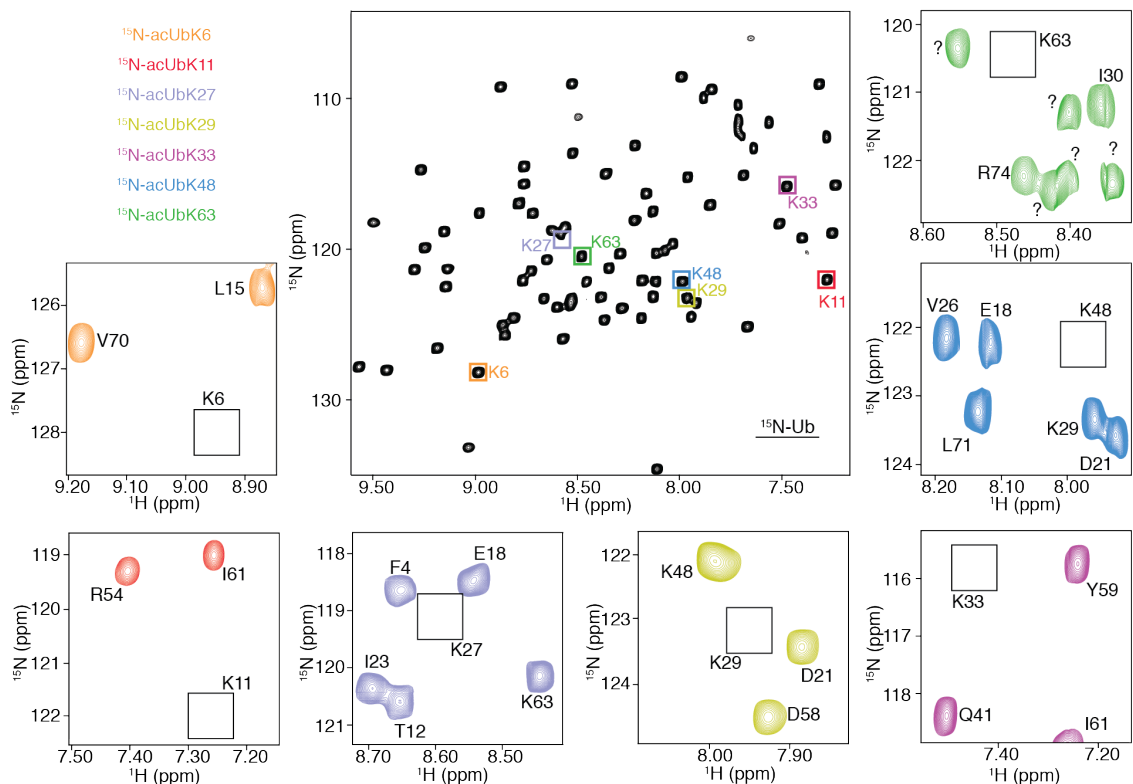
Figure 4.9. ^{1}H^{15}N-HSQC of acUb variants.
The two-dimensional NMR spectrum for ^{15}N-Ub is shown in black (center) with the location of the signals for the seven lysine residues outlined in coloured boxes and labeled. The smaller panels show regions of the spectra collected for each of the ^{15}N-acUb proteins where the colours of the spectra match the labels in the center panel. Black boxes outline the expected location of the lysine residue and other residues that overlap with those found in the ^{15}N-Ub spectrum are labeled. The signal for each acetylated residue is not visible due to unlabeled (^{14}N) acetyl-lysine used in the labeling technique. Signals labeled with a question mark (?) are unassigned and only present in samples containing large amounts of truncated ^{15}N-Ub$_{1-62}$.

In all acUb ^{1}H^{15}N-HSQC spectra, there were a significant number of signals that overlapped with signals from the spectrum for Ub. Figure 4.9 demonstrates regions surrounding the acetyl-lysine residue of interest and shows nearby signals that overlap with those from the ^{15}N-Ub spectrum. Initial NMR experiments used samples that contained a proportion of the truncated products from each acUb protein: These ^{1}H^{15}N-HSQC spectra showed a mix of folded acUb protein (signals that overlapped with those of Ub) and unfolded acUb protein (signals that had collapsed to the center of the spectrum). We

noticed that the unfolded signals were more obvious in acetylation sites closer to the C-terminus of the protein. These correlated to the acetylated residues that yielded the highest level of truncated product, namely acUbK63. Subsequent preparations of acUb samples for NMR required slow-run size exclusion chromatography to remove as much truncated product as possible. We also detected some slight modifications to the fold of acUbK27 in the ^{1}H^{15}N-HSQC spectrum. While many of the signals in the ^{1}H^{15}N-HSQC spectrum for acUbK27 overlap with those in Ub, there were several signals that had shifted position (Fig. 4.10). Lysine 27 is contained in helix α1 of Ub: We observed signals corresponding to others in the helix (I23-S28) had shifted position due to acetylation at K27. We also
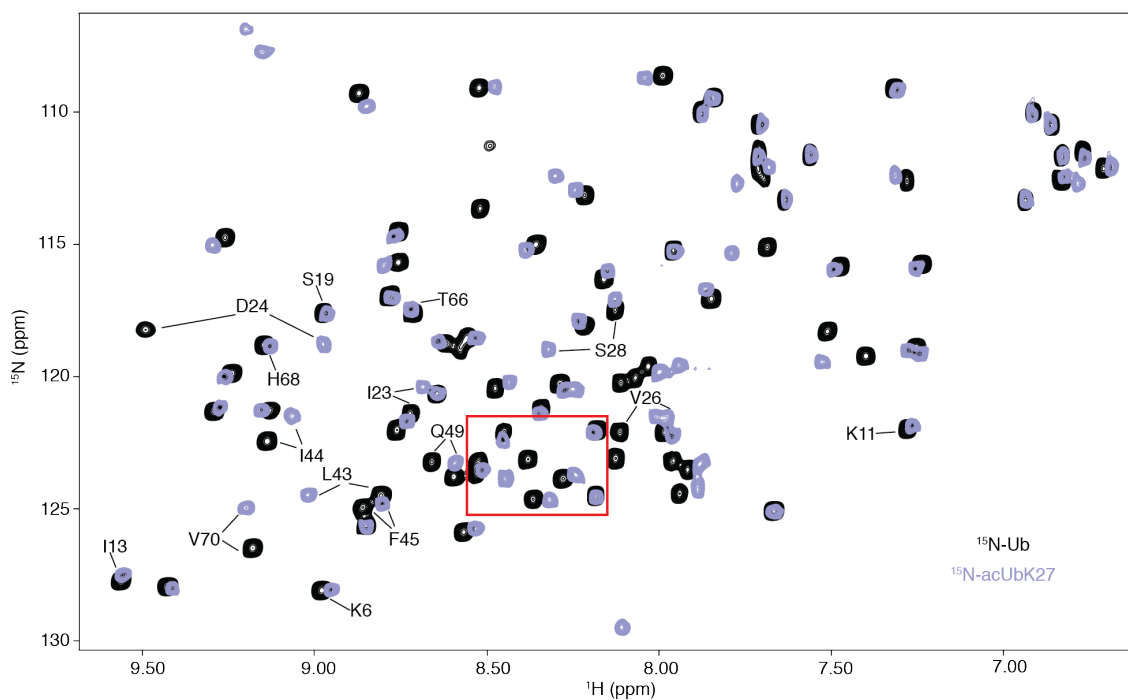
Figure 4.10. The ^{1}H^{15}N-HSQC spectra for ^{15}N-acUbK27 and ^{15}N-Ub differ.
^{1}H^{15}N-HSQC spectra were acquired, processed, and are shown for Ub (black) and acUbK27 (purple). Signals were assigned using triple-resonance HNCA experiments collected at the same time as each ^{1}H^{15}N-HSQC. Signals that are labeled are assigned with high confidence in both spectra and includes signals in conserved positions and those that have moved in the acUbK27 protein. The red box outlines signals difficult to assign for ^{15}N-acUbK27 but expected to include regions of the C-terminal tail (L71-R74) and the loop containing E51-L56 based on assignments for ^{15}N-Ub.

observed changes in structurally nearby residues including those in β3 (R42-F45). Finally, we were unable to confidently assign a few residues (primarily E51-L56 and L71-R74) due to the large distance between their signal in the ^{15}N-Ub spectrum and the positions of the remaining signals in the ^{15}N-acUbK27 spectrum. Although interesting, we did not explore this further.

4.3.8   Evidence for acUbK48 dimerization

In addition to NMR spectroscopy, we attempted to crystallize the individual acUb proteins. Protein crystals were obtained for both acUbK11 and acUbK48; however, only acUbK48 crystals gave excellent diffraction data. The diffraction data (summarized in Table 4.1) for acUbK48 suggested a structure with two acUbK48 monomers packed together, burying their I44 hydrophobic patches against each other (Fig. 4.11). The interface observed in our diffraction data is
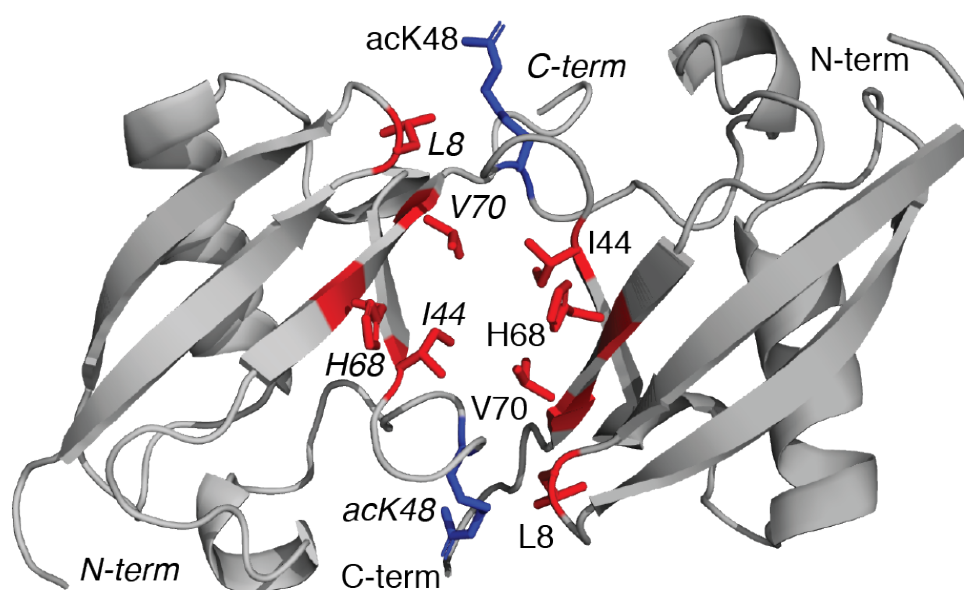
Figure 4.11. acUbK48 crystals bury the I44 hydrophobic patch.
Purified acUbK48 was crystallized as indicated in the Materials and methods. Diffraction data was collected at the Canadian Light Source with resolution to 1.3 Å. Molecular replacement was done using the PDB coordinates for Ub (1UBQ) and the structure was refined using Refmac 5.8. Shown are two monomers (each grey) of acUbK48 from the asymmetric unit. The acetylated K48 residue is shown in blue, and residues comprising the I44 hydrophobic patch are shown in red. Labels corresponding to monomer 1 (left) are indicated in italics, and those corresponding to monomer 2 (right) are regular font.

Table 4.1. Crystallographic data for acUbK48.

Diffraction data	
Space group	P 1 21 1
Resolution range (Å)	44.85-1.17
Cell dimensions	
a,b,c (Å)	29.48, 55.39, 44.98
α, β, γ (˚)	90, 99.574, 90
Total reflections	100054
Unique reflections	27518
Multiplicity	3.6
Completeness (%)	99
R_{means}	6.3
Mosaicity	0.38
$I/\sigma(I)$	13.8
CC half (%)	99.8
Refinement data	
Resolution range (Å)	29.09-1.39
Completeness (%)	96.9
Number of reflections	25418
R_{work}/R_{free}	0.19745/0.22487
RMS deviations	
Bonds	0.0115
Angles	1.916
Ramachandran favoured (%)	99.3

similar to interfaces found in various other structures including closed E2~Ub conjugates [52,59], compact polyUb chains [164], and compact K48-linked diUb [89]. We hypothesized that the dimer structure we observed could either have biological implications or could be an artifact of crystallization. To determine if the dimeric structure we observed was biologically relevant, we used in solution experiments to study acUbK48 at lower concentrations (< 500 µM). Sedimentation velocity analytical ultracentrifugation showed similar c(s) curves between Ub and acUbK48, indicating that acUbK48 behaves similar to Ub in solution (Fig. 4.12A). Further, size exclusion chromatography coupled to multi-angle light scattering (SEC-MALS) revealed similar retention volumes for Ub and acUbK48 (13.735 mL and 13.666 mL, respectively) (Fig. 4.12B). This experiment provided evidence that the molecular weights of the protein species from the single peaks were 8.59 ± 2%
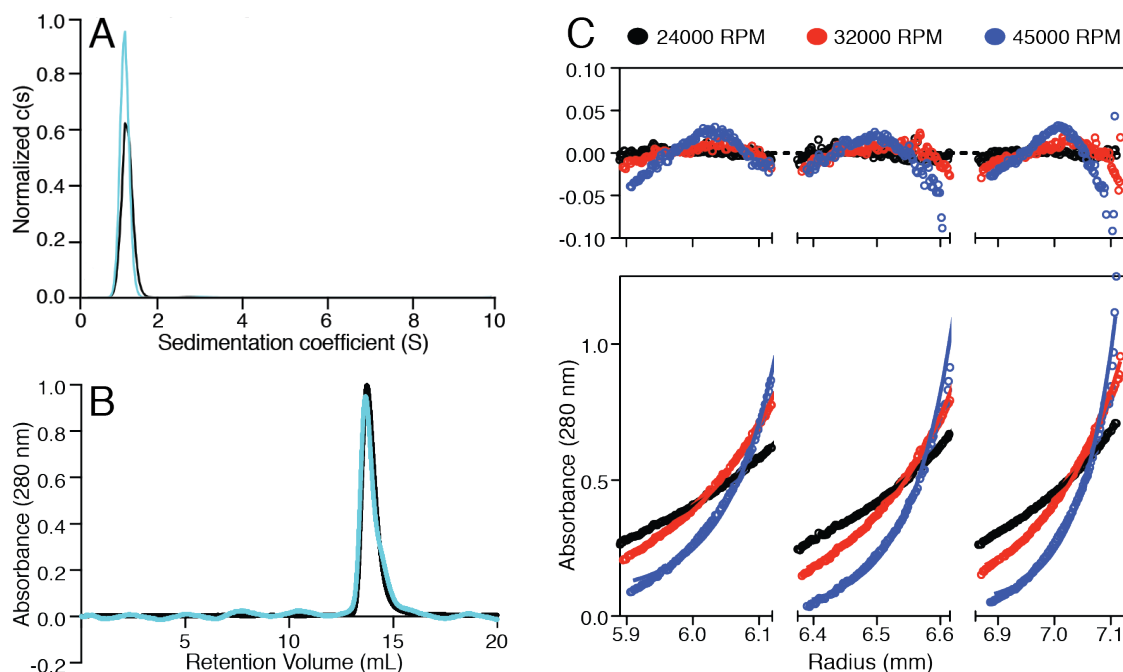
Figure 4.12. Solution experiments show no sign of acUbK48 dimerization.
(A) Normalized c(s) distribution curves from sedimentation velocity analytical ultracentrifugation experiments for Ub (black) and acUbK48 (cyan). (B) Ub and acUbK48 proteins were purified and further subjected to SEC-MALS experiments. Elution profiles are shown for Ub (black) and acUbK48 (cyan). (C) Sedimentation equilibrium data (bottom) and residuals (top) for acUbK48 are shown in triplicate. Data was collected at the indicated speeds and fit to a global single ideal species model. Each of these experiments described were collected with a minimum of two different preparations of material; results shown here were similar across each preparation.

kDa and 8.82 ± 6% kDa for the Ub and acUbk48 samples, respectively. These results indicate that acUbK48 behaves as a monomer in solution. Sedimentation equilibrium experiments confirmed these findings: Figure 4.12C shows the data and residuals for acUbK48. Using the indicated speeds for both Ub and acUbK48, a global single ideal fit was used to determine the molecular weight of each species. The calculated molecular weights were 9213 ± 152.1 Da and 9250 ± 129.5 Da for Ub and acUbK48, respectively, corresponding to a monomer ($MW_{expected}$ 8818 Da (Ub) and 8860 Da (acUbK48)). Finally, to confirm that various NMR samples of acUbK48 were monomeric, a series of dilution NMR experiments were set up. Three different concentrations of ^{15}N-acUbK48 were prepared through serial dilution at measured concentrations of 370 µM, 230 µM, and 100

µM. A 40-minute ^{1}H^{15}N-HSQC spectrum was collected for each sample (Fig. 4.13). As expected, the intensity of the signals decreased with decreasing concentration, but they
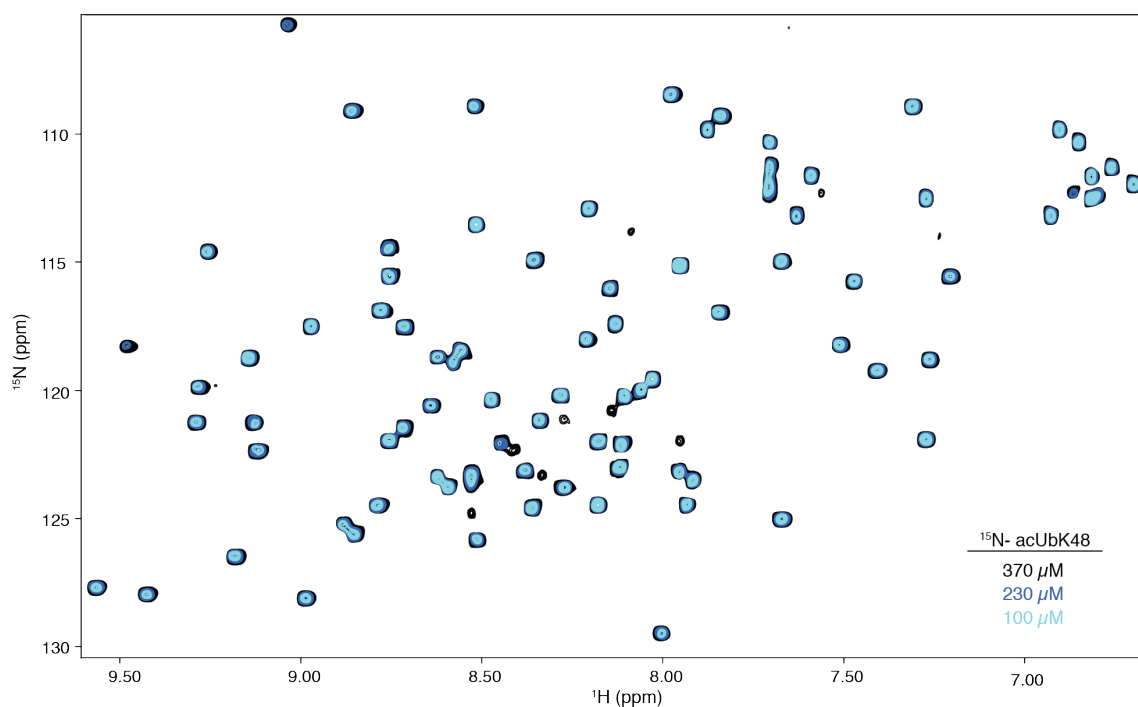
Figure 4.13. Dilution NMR of ^{15}N-acUbK48 shows no sign of dimerization.
^{15}N-acUbK48 was expressed and purified as described in section 4.2.1. The protein sample was concentrated to the smallest volume possible for NMR experiments and a two-dimensional ^{1}H^{15}N-HSQC spectrum was acquired (black spectrum). The sample was removed, diluted 1:2 with NMR buffer, and a second ^{1}H^{15}N-HSQC spectrum was collected (dark blue spectrum). This process was repeated to collect a third spectrum with a total dilution of 1:4 (cyan spectrum). The measured working concentrations of the samples are indicated. Data were processed using NMRPipe and visualized using NMRViewJ.

remained in the same position. The most concentrated sample of acUbK48 showed less than 10 extra signals. Comparison of these signals to a spectrum collected for the mix of truncated Ub$_{1-47}$ and acUbK48 confirmed that these extra signals corresponded to some unfolded protein product that might have been too weak to observe in the more dilute samples. Therefore, various in solution techniques on multiple preparations of acUbK48 provide evidence that the dimer interface observed in our diffraction data was an artifact of crystallization, and that acUbK48 exists as a predominantly monomeric species in solution.

4.3.9 Acetylation of Ub alters the conformation of UBE2L3~Ub conjugates

To study the influences that an acUb protein has on the conformation of a UBE2L3~Ub conjugate, we utilized NMR spectroscopy and chemical shift tracking for reporter residues described previously. The UBE2L3~Ub conjugate adopts a variety of conformations ranging from an open conformation (with little noncovalent interaction between Ub and UBE2L3) to a closed conformation (with extended contact between Ub and UBE2L3 through the I44 hydrophobic patch and crossover helix α2, respectively) (Fig. 1.6). Previous work has elegantly described how reporter residues in Ub, namely K48 and Q49 in addition to residues towards the C-terminus of Ub, can be monitored via NMR spectroscopy to provide insight onto the conformation of the UBE2L3~Ub conjugate [53]. Briefly, in the open conformation, the signal for the reporter would be in the same position as it is found in unconjugated Ub. In the closed conformation, the reporter signal shifts in a predictable direction to occupy a new position in the ^{1}H^{15}N-HSQC spectrum (Fig. 4.14).
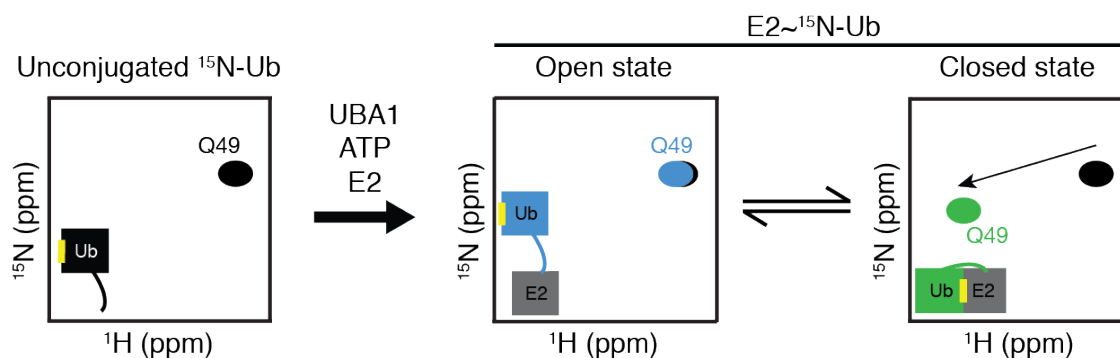
Figure 4.14. Ub signals in ^{1}H^{15}N-HSQC spectra report on E2~Ub conjugate conformations.
Various reporter residues (for example, Q49) in the Ub or acUb protein report on conformation of Ub in an E2~Ub conjugate. The signal for Q49 in the unconjugated Ub protein occupies a distinct position (black). Conjugation to an E2 protein like UBE2L3 produces the E2~Ub conjugate that adopts an array of conformations. The two extreme conformations are shown. In the open state (blue), there is no non-covalent interaction between the Ub and E2 protein. Conversely, in the closed state (green), the Ub folds back against the E2 protein, forming significant non-covalent interaction using the I44 hydrophobic patch (shown in yellow). Notably, an equilibrium exists between these two states and the signals reflect on the population in each state.

To generate a baseline to compare the acUb conjugates to, the wild-type UBE2L3~Ub conjugate was studied. ^{15}N-Ub was conjugated to UBE2L3 at 30 °C in a heat block using UBA1 and ATP with limiting Ub. The UBE2L3~^{15}N-Ub conjugate was separated from the remaining components using a Superdex75 size exclusion chromatography column pre-equilibrated in NMR buffer without TCEP (25 mM Hepes pH 7.0, 50 mM NaCl). Fractions were evaluated by SDS-PAGE and those containing the UBE2L3~^{15}N-Ub species were pooled and concentrated for an NMR sample. Upon conjugation to UBE2L3, we observed significant overlap with the free ^{15}N-Ub spectrum for many signals (Fig. 4.15A). The same finding was observed for many UBE2L3~^{15}N-acUb conjugates. Figure 4.15B shows the full spectra for ^{15}N-acUbK6 before and after conjugation to UBE2L3, for example. In the UBE2L3~^{15}N-Ub conjugate, there were <10 signals present that moved due to conjugation.
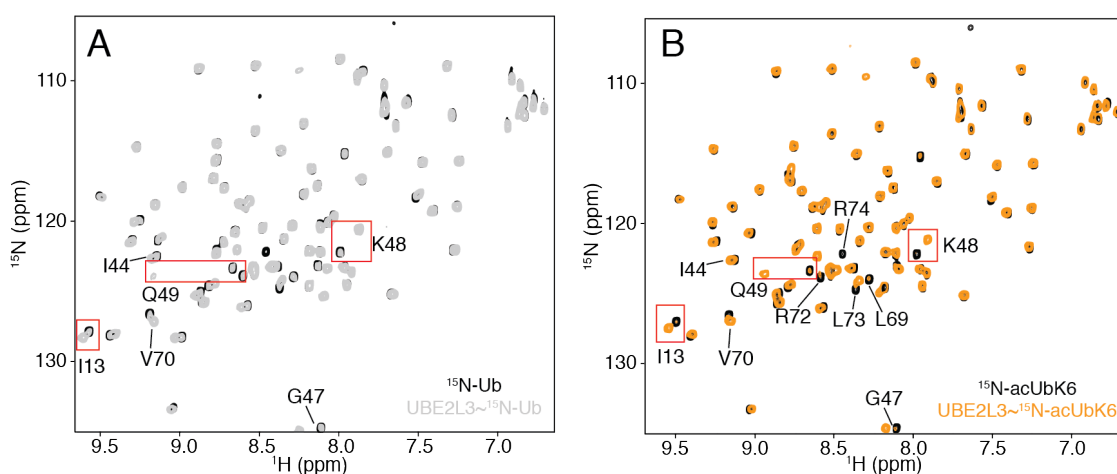
Figure 4.15. Conjugation of Ub or acUb to UBE2L3 modifies the ^{1}H^{15}N-HSQC spectrum of the Ub protein.
^{15}N-Ub or ^{15}N-acUb was expressed and purified to homogeneity as described in the Materials and methods. A two-dimensional ^{1}H^{15}N-HSQC spectrum was acquired before and after conjugation to UBE2L3 for each of the Ub proteins. The Ub proteins were conjugated to UBE2L3 in a heat block and separated from unconjugated protein using a Superdex75 gel filtration column. In each panel, the black spectrum corresponds to the unconjugated ^{15}N-Ub or ^{15}N-acUb protein, and the non-black spectrum corresponds to the UBE2L3~^{15}N-Ub or UBE2L3~^{15}N-acUb conjugate for (A) Ub, and (B) acUbK6. Red boxes highlight the reporter residues I13, K48, and Q49, and other discussed residues are labeled.

Some of these signals likely correlate to new locations due to the closed UBE2L3~Ub conformation, resulting in multiple signals for a given residue (G47, K48, Q49) (Figure 4.16). We also observed signal broadening that could result from the higher molecular weight of the E2~Ub species compared to Ub alone. Interestingly, some of the broadened residues would be buried against the UBE2L3 protein (I13, I44, V70, for example) in the closed conformation. The presence of both dual signals and signal broadening provides evidence for both slow and fast exchange between the open and closed conformation. Interestingly, the signal that corresponds to the open conformation of Q49 is more intense than that of the closed conformation, but the signal for the closed conformation of K48 is more intense than that of the open conformation (Figure 4.16). To determine the population distribution between the open and closed states, we used the signal intensities in the slow exchange formula $f_{closed} = V_{closed}/(V_{closed} + V_{open})$. Together, these results indicate that the UBE2L3~Ub conjugate exists in an equilibrium between open and closed conformation, and the Ub-containing conjugate is approximately 60% closed.
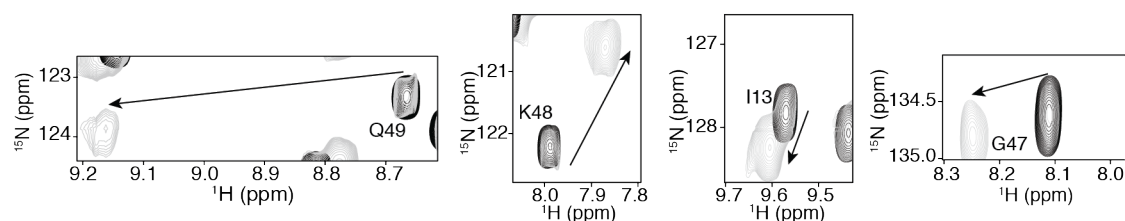
Figure 4.16. The UBE2L3~^{15}N-Ub conjugate is 60% closed.
Two dimensional ^{1}H^{15}N-HSQC NMR spectra were acquired for ^{15}N-Ub (black) and UBE2L3~^{15}N-Ub (grey) and analyzed using NMRViewJ. Shown are regions of the spectra for reporter residues I13, G47, K48, and Q49. Arrows represent the direction of shift upon conjugation to UBE2L3.

Similar to the UBE2L3~Ub conjugate, the acUb-containing conjugates were pre-formed and purified using size exclusion chromatography prior to the collection of an ^{1}H^{15}N-HSQC spectrum. Figure 4.15B shows the full NMR spectrum for UBE2L3~^{15}N-acUbK6. In the UBE2L3~^{15}N-acUbK6 spectrum, we again observed dual signals for some of the residues (I13, G47, K48, Q49) corresponding to the open and closed states (Fig. 4.17).

Additionally, the signals for some residues (L43, I44, V70) appear broader than other signals in the spectrum, while others are almost completely broadened or disappeared (L69,
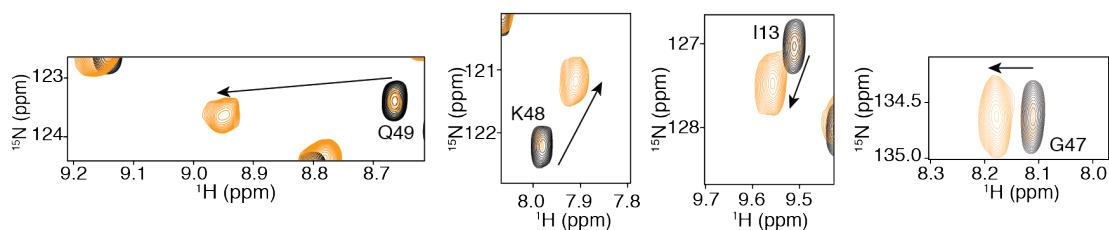
Figure 4.17. Acetylation at K6 causes the UBE2L3~Ub conjugate to populate a more closed state.
^{1}H^{15}N-HSQC spectra were collected for ^{15}N-acUbK6 before (black) and after (orange) conjugation to UBE2L3. Signals for the reporter residues I13, G47, K48, and Q49 are shown, and arrows show direction of shift due to the formation of the UBE2L3~^{15}N-acUbK6 conjugate.

R72, L73, R74). For the residues that exhibit two signals, the signal corresponding to the closed conformation was stronger in each case, indicating the UBE2L3~^{15}N-acUbK6 conjugate favours the closed conformation. Using the intensities of the signals, we approximated that >90% of the acUbK6-containing conjugate occupies a closed conformation. Similar observations were seen for the UBE2L3~^{15}N-acUbK33 conjugate. Here, there appear to be no obvious dual signals corresponding to two different conformations of conjugate. Most of the reporter residues described previously as containing two resonance signals (I13, G47, K48) display a single, strong signal, which corresponds to the closed conformation of UBE2L3~^{15}N-acUbK33 conjugate (Fig. 4.18).
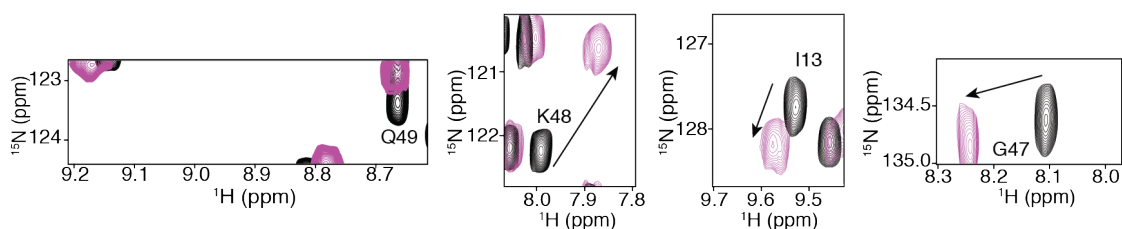
Figure 4.18. Ub acetylation at K33 promotes the closed conformation of UBE2L3~Ub.
Reporter residues I13, G47, K48, and Q49 are shown for the ^{15}N-acUbK33 (black) and UBE2L3~^{15}N-acUbK33 conjugate (pink) ^{1}H^{15}N-HSQC NMR spectra. Arrows represent the path of shift for signals in the UBE2L3~^{15}N-acUbK33 conjugate.

Curiously, in this spectrum, the signal for Q49 has disappeared from its position in free Ub and does not reappear in its predicted position in the closed conformation of UBE2L3~^{15}N-acUbK33, likely indicating this signal has broadened completely and cannot be distinguished above the noise of the instrument. The appearance of a single signal for these reporter residues indicates that acetylation at K33 stabilizes the UBE2L3~^{15}N-acUbK33 conjugate in a closed conformation. The graphs shown in Figure 4.19 quantify the UBE2L3~Ub populations for conjugates containing Ub, acUbK6, and acUbK33. Quantification using the intensities of the signals demonstrates that both acUb proteins promote the closed conformation of UBE2L3~Ub conjugate, where the Ub conjugate is 60% closed, but the acUbK6 and acUbK33 conjugates are 90% and 100% closed, respectively.
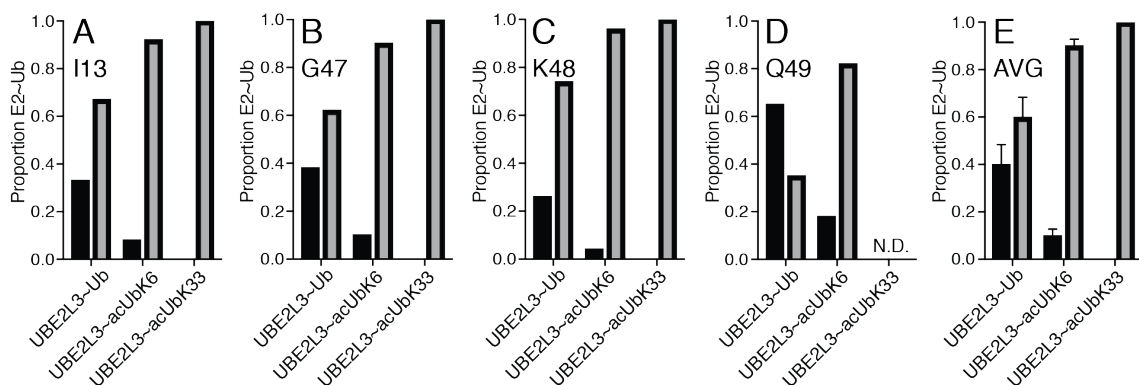
Figure 4.19. Ub acetylation at K6 or K33 influences the conformation of the UBE2L3~Ub conjugate.
The signal intensities were obtained from the non-black spectra in Figures 4.16, 4.17, and 4.18 using NMRViewJ for the reporter residues (A) I13, (B) G47, (C) K48, and (D) Q49. The proportion of UBE2L3~Ub that populates the closed state (grey bars) was calculated using the equation $f_{closed} = V_{closed}/(V_{closed} + V_{open})$, where V_{closed} and V_{open} represent the volume of the closed and open signals, respectively. The proportion occupying the open state (black bars) was then calculated using $f_{open} = 1 - f_{closed}$. N.D. represents no data due to signals not being in their expected location. (E) The data from panels A-D were averaged and are shown with error bars representing the standard error of the mean (SEM).

Of all acUb proteins, UBE2L3 conjugates containing acUbK48 showed ^{1}H^{15}N-HSQC spectra that were nearly identical to that of unconjugated ^{15}N-acUbK48. As expected, the

signal for acK48 is NMR invisible and therefore, cannot be used as a reporter residue for UBE2L3~acUbK48 conjugate conformation. However, the signals for G47 and Q49 have both shifted in the direction of the expected signals for the closed conformation (Fig. 4.20). The G47 signal also exhibits a weak signal for the open conformation, and the only signal for I13 represents the open conformation. Since these reporter residues (aside from I13) lie on either side of the acetylated residue at K48, it is possible that the inconsistent signals correlate to variations due to the acetylation directly. This possibility seems unlikely due to the presence of the signals for G47 and Q49 in their expected positions in the unconjugated ^{15}N-acUbK48 spectrum when compared to unconjugated ^{15}N-Ub spectrum. Interestingly, out of all the acUb proteins, the signal for Q49 in the acUbK48-containing UBE2L3 conjugate is the closest to its position in the open conformation, indicating that acetylation at K48 might not influence UBE2L3~Ub conformation to the same extent as other acetylation sites. Due to the missing signal for the K48 reporter (due to acetylation in the acUbK48 protein) and the inconsistent changes in the I13, G47, and Q49 signals, more experiments would be required to confirm exact proportions in the closed vs. open state. Together, these results indicate that each acetylation site in Ub has different influences on the conformation of the UBE2L3~Ub conjugate.
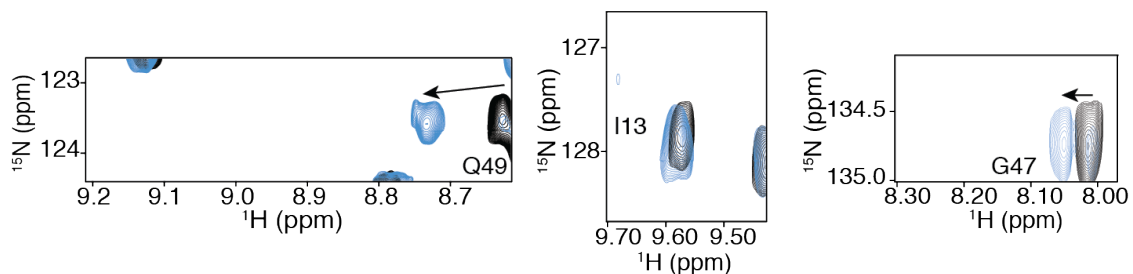
Figure 4.20. Acetylation at K48 has minor influences on the UBE2L3~Ub conjugate conformation.
^{1}H^{15}N-HSQC spectra were collected as described in the Materials and methods. The reporter residues I13, G47, and Q49 are shown for ^{15}N-acUbK48 (black) and UBE2L3~^{15}N-acUbK48 (blue). Arrows represent direction of shift for signals in the UBE2L3~^{15}N-acUbK48 spectrum.

4.3.10 Formation of a stable UBE2L3–Ub isopeptide conjugate for NMR assignments

In studying E2~Ub conjugates, many groups use the isopeptide linkage as a surrogate for the thioester due to its increased stability permitting longer experiments [50,54,152]. An assumption made is that the type of linkage has no impact on the relationship between the E2 and Ub in the conjugate. We used the isopeptide linkage to create stable UBE2L3–^{15}N-Ub and UBE2L3–^{15}N-acUb species to be able to assign signals in the ^{1}H^{15}N-HSQC spectra of various UBE2L3~^{15}N-acUb conjugates. Here, the em dash (–) is used to denote the isopeptide linkage. In these conjugates, the catalytic cysteine of UBE2L3 (C86) is substituted for a lysine residue (C86K), and Ub can be covalently attached using the UBA1 protein and ATP. This modified version of the E2~Ub conjugate is required to prevent hydrolysis of the E2~Ub bond during the longer 3D NMR experiments required to assign signals. While we attempted these experiments for all acUb proteins, the reaction produced a limited quantity of UBE2L3–Ub for many of the acUb proteins. We attributed this to two factors: 1) the initial yield of many acUb proteins as described in section 2.3.3 was significantly less than that of Ub, and 2) many of the acUb proteins showed impaired UBE2L3~Ub conjugate formation as noted in section 3.3.3. Despite this, we were able to make NMR-quality samples of UBE2L3–Ub, UBE2L3–acUbK6, and UBE2L3–acUbK33 to provide insight as to how acetylation, in addition to the modified linkage, might alter conjugate conformation. Figure 4.21 shows SDS-PAGE throughout the formation and purification of the UBE2L3–^{13}C^{15}N-acUbK33 conjugate. Since Ub and acUb are small proteins, measuring the concentration using conventional methods can be challenging. Instead, SDS-PAGE with Coomassie staining was used to determine the relative concentrations of UBE2L3 C86K and ^{13}C^{15}N-His-acUbK33 (Fig. 4.21A). Aiming for a slight excess of the UBE2L3 C86K protein, we chose to use 50% ^{13}C^{15}N-His-acUbK33 protein, and 25% UBE2L3 C86K (In a final volume of 1 mL, the acUbK33 protein was 500 μL and the UBE2L3 protein was 250 μL). We used 50 μM UBA1 in this reaction, but knowing the exact concentration was not required for the preparative formation of UBE2L3–^{13}C^{15}N-acUbK33. Prior to conjugation, individual protein samples were prepared as indicated in section 4.2.6.1. Briefly, all proteins were dialyzed into 50 mM Ches, 150 mM NaCl, 10 mM MgATP pH 9.5 for 2 hours at room temperature. The proteins
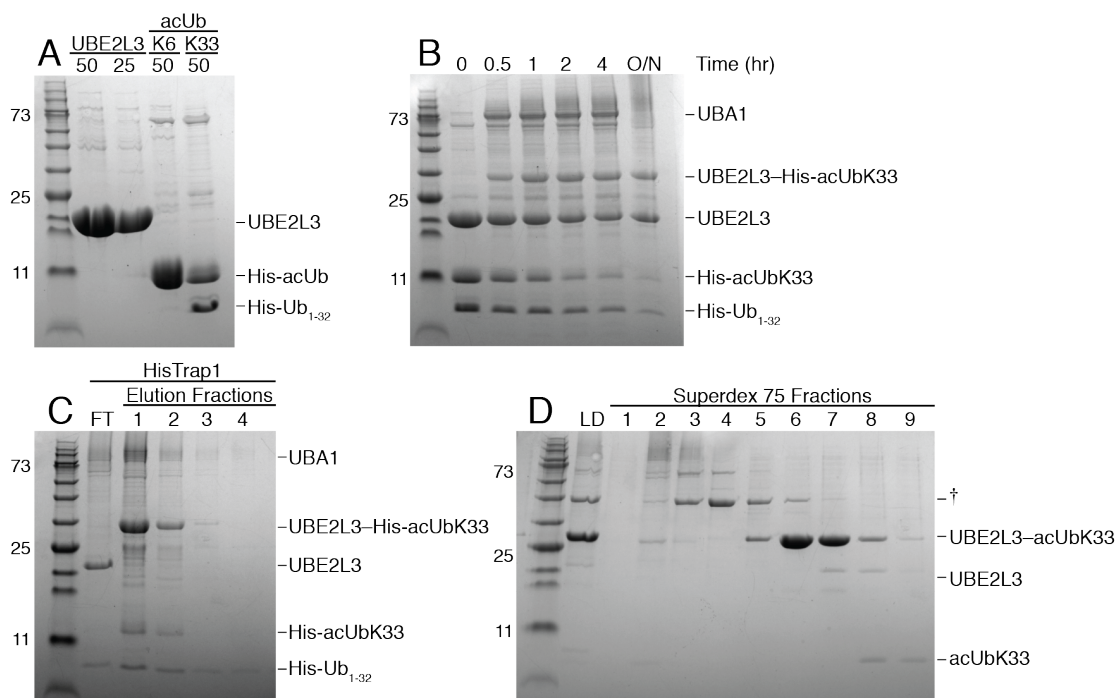
Figure 4.21. Formation of a stable UBE2L3–^{13}C^{15}N-acUbK33 conjugate.
Individual UBE2L3 C86K, ^{13}C^{15}N-His-acUbK33, and UBA1 proteins were expressed and purified as indicated. (A) SDS-PAGE was used to determine the relative starting concentrations of UBE2L3 C86K and the specified ^{13}C^{15}N-acUb proteins. Numbers along the top of the gel correlate to the proportions of protein used (ie. 50 corresponds to 50% or a 1:2 dilution of the stock). The stock concentration of UBE2L3 C86K was 550 μM. Unlabeled bands correspond to impurities from the initial purifications of reaction components. (B) Time course for the formation of UBE2L3–^{13}C^{15}N-His-acUbK33 with time points along the top of the gel. Reaction components were pre-equilibrated in conjugation buffer containing 50 mM Ches, 150 mM NaCl, 10 mM MgATP pH 9.5. Components were mixed using a 1:2 ratio of UBE2L3:acUbK33 based on the gel from (A). (C) Purification of the UBE2L3–^{13}C^{15}N-His-acUbK33 conjugate was accomplished as described in section 4.2.6.2. Fractions were collected as indicated at the top of the gel where FT corresponds to the flowthrough collected after batch binding. (D) The appropriate fractions from (C) were pooled and cleaved with TEV protease, and the solution was again passed through the Ni^{2+}-NTA resin. The flowthrough was collected, concentrated and injected onto a Superdex75 column sizing column pre-equilibrated in NMR buffer. Fractions from the sizing column are provided along the top of the gel, and LD refers to the concentrated, loaded sample. The band marked † appeared after TEV cleavage and is a contaminant from the TEV aliquot. In all panels, 16.5% Tris-tricine gels were used to resolve protein species, and the protein species are labeled to the right of each gel.

were then mixed in a dialysis bag at the appropriate proportions and left overnight shaking

slowly at 37°C. Timepoints were taken throughout the reaction and protein components

were resolved on SDS-PAGE (Fig. 4.21B). We found there was fast turnover of the UBE2L3 C86K protein, and the UBE2L3–^{13}C^{15}N-His-acUbK33 species began to accumulate after 30 minutes. For some other reactions, we noticed that the reaction progression was slower, requiring between 2-4 hours to make the same amount shown at 30 minutes for acUbK33 (data not shown). Interestingly, in the reactions that produced the highest yield of UBE2L3–acUb, we observed heavy precipitation in the solution after overnight conjugation. Most often this precipitation was the UBA1 protein in addition to some unconjugated UBE2L3 or acUb protein. In all cases, the precipitate was removed, and the protein solution was applied to Ni^{2+}-NTA resin to separate the UBE2L3–^{13}C^{15}N-His-acUbK33 from remaining UBE2L3 C86K. The purification was done using UbW2 and UbE buffers described in section 4.2.6.2. As expected, all UBE2L3–^{13}C^{15}N-His-acUbK33 came off in the elution, and only a small amount of Ub$_{1-32}$ did not bind to the column, evidenced by the weak band present in the flow through lane (Fig. 4.21C). For this reaction, fractions 1-3 were pooled and incubated with 2.5 mg of TEV protease to cleave the His-tag from the acUbK33 protein. Overnight dialysis into UbW2 was used to remove imidazole from the solution prior to re-application to the Ni^{2+}-NTA resin. This time, the flowthrough was collected, concentrated, and injected onto a preparatory Superdex75 gel filtration column pre-equilibrated in NMR buffer. The Superdex75 column gave good resolution between the UBE2L3–^{13}C^{15}N-acUbK33 and unconjugated ^{13}C^{15}N-acUbK33 proteins (Fig. 4.21D). Despite the minor amount of contamination in fractions 6 and 7, they were pooled and concentrated to make an NMR sample. Therefore, UBE2L3 C86K and ^{13}C^{15}N-acUb proteins can be conjugated to form a stable UBE2L3–acUb conjugate required for longer NMR experiments.

4.3.11   The UBE2L3–Ub conjugate has different properties than the UBE2L3~Ub conjugate

We used the stable UBE2L3–Ub or UBE2L3–acUb conjugates to assign ^{1}H, ^{15}N signals for Ub or acUb in their respective two-dimensional ^{1}H^{15}N-HSQC spectra. This was accomplished by collecting HNCA experiments for UBE2L3–Ub, UBE2L3–acUbK6, and UBE2L3–acUbK33 to specifically assign the reporter resonances as described in section 4.2.7.2.

As expected, most of the Ub signals in the UBE2L3–Ub ^{1}H^{15}N-HSQC spectrum overlapped with those found in the Ub and UBE2L3~Ub spectra, indicating that the formation of the isopeptide linkage did not drastically alter the conformations of the E2~Ub conjugates. Interestingly however, we found that the reporter residues I13, K48, and Q49 did not shift as far as the expected signals for the closed UBE2L3~Ub conjugate (Fig. 4.22).
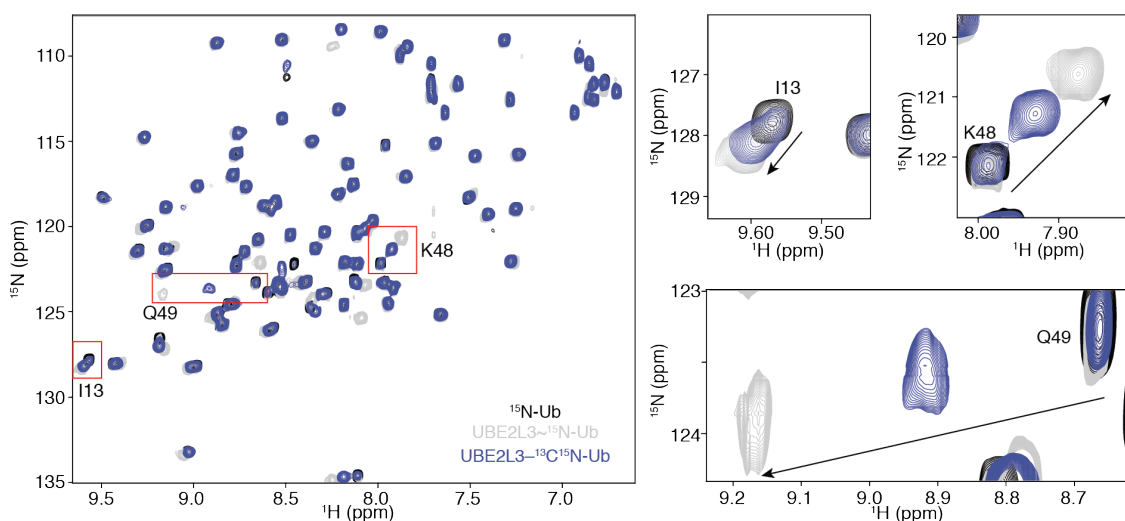
Figure 4.22. The stable UBE2L3–Ub conjugate displays a ^{1}H^{15}N-HSQC spectrum unique from the UBE2L3~Ub spectrum.
The ^{1}H^{15}N-HSQC spectra are shown for the unconjugated Ub protein, the thioester UBE2L3~Ub conjugate, and the isopeptide UBE2L3–Ub conjugate for Ub. The black spectrum corresponds to the unconjugated ^{15}N-Ub, and the dark purple spectrum corresponds to the isopeptide-linked UBE2L3–^{13}C^{15}N-Ub. The grey spectrum represents the UBE2L3~^{15}N-Ub spectrum from Figures 4.15 and 4.16 and is shown here again for clarity. Expanded regions around reporter residues I13, K48, and Q49 are highlighted on the right side of the figure and correspond to the red boxes in the full spectrum.

Instead, we observed signals somewhere in the middle of the open and expected closed states detected in the thioester-linked conjugate. For the I13 signal in the UBE2L3–Ub spectrum, we detected a wider signal with a peak approximately 57% closed, based on location between the open and closed signals in the UBE2L3~Ub spectrum. For the K48 and Q49 signals, we again noticed two signals; one corresponding to the open conformation and the other approximately 50% closed. For both residues, the two signals were not the

same intensity, providing evidence that the UBE2L3–Ub conjugate populates two distinct conformations.

A similar observation was noted for the UBE2L3–acUbK6 spectrum: Most signals overlapped with the unconjugated acUbK6 and UBE2L3~acUbK6 conjugate spectra, and the I13 signal was approximately 59% of the way to the closed signal (Fig. 4.23). In the UBE2L3–acUbK6 spectrum, however, the signals for K48 and Q49 no longer have two locations. Instead, the single peak for each residue lies approximately 51% of the way between the open and expected closed signals observed in the UBE2L3~acUbK6 spectrum.
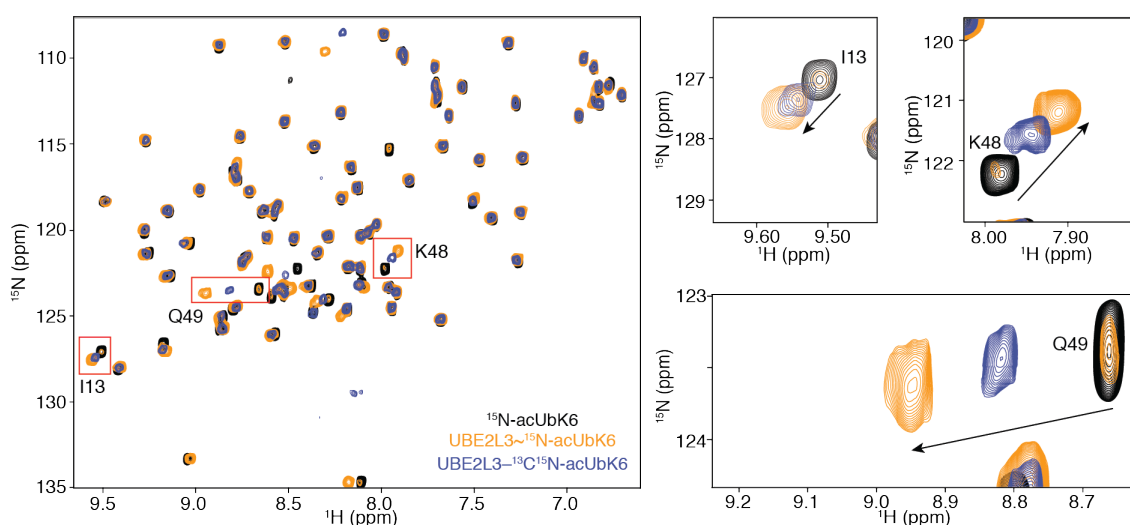
Figure 4.23. The UBE2L3–acUbK6 conjugate spectrum differs from the UBE2L3~acUbK6 spectrum.
[1]H[15]N-HSQC experiments were collected and are shown for ^{15}N-acUbK6 (black), UBE2L3~[15]N-acUbK6 (orange), and UBE2L3–[13]C[15]N-acUbK6 (dark purple). The UBE2L3~[15]N-acUbK6 spectrum is identical to the one shown in Figures 4.15 and 4.17 and is shown here for clarity. Regions around the reporter residues I13, K48, and Q49 are boxed in red and are expanded.

The presence of the single peaks for K48 and Q49 could indicate that the combination of isopeptide linkage and acetylation at K6 promotes flexibility in the UBE2L3–Ub conjugate to enable the transition from slow exchange (observed in the UBE2L3~acUbK6 conjugate) to fast exchange in terms of conjugate conformation. The fact that the single peaks for I13, K48, and Q49 do not overlap with the positions observed in the free acUbK6 spectrum

provides further evidence that Ub acetylation at K6 favours the closed conformation of UBE2L3~Ub conjugate.

For the UBE2L3–acUbK33 conjugate, we observed more variation throughout the spectrum (Fig. 4.24). As observed for the other two isopeptide conjugates, the I13 resonance occupies a position that is more closed than open (66%). For the K48 and Q49 residues, we again only observed a single signal. Using the signal for the open conformation and that of the expected closed conformation, the signal for K48 was located 55% of the way to the closed position. Unfortunately, we were unable to observe a signal
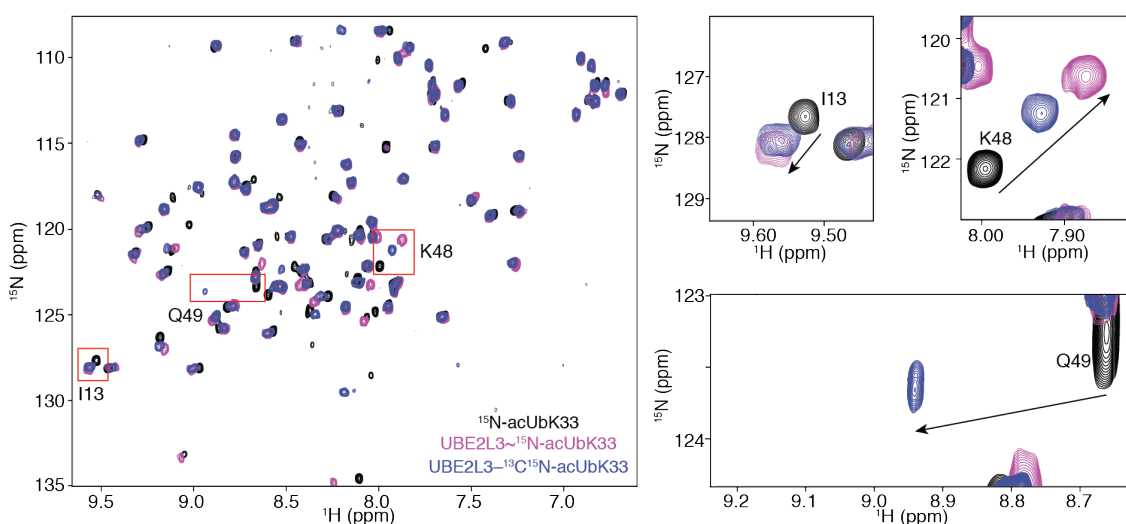
Figure 4.24. The UBE2L3–acUbK33 spectrum is dissimilar to the UBE2L3~acUbK33 spectrum.
Two-dimensional ^{1}H^{15}N-HSQC experiments for ^{15}N-acUbK33 (black), UBE2L3~^{15}N-acUbK33 (pink), and UBE2L3~^{13}C^{15}N-acUbK33 (dark purple) are shown. The reporter residues I13, K48, and Q49 are shown in red boxes in the full spectrum and are expanded to the side. The thioester-bound UBE2L3~15N-acUbK33 spectrum is identical to that shown in Figure 4.18 and is shown here for clarity.

that would obviously correspond to Q49 in the closed conformation in the UBE2L3~acUbK33 spectrum. However, in the UBE2L3–acUbK33 spectrum, we observed a signal much weaker than the others in the spectrum that was quite close to the position observed for the Q49 signal in the UBE2L3–Ub spectrum. These results further confirm that the isopeptide linkage influences the dynamics of the UBE2L3–Ub conjugate,

resulting in a species that is in faster exchange than the UBE2L3~Ub conjugates. The appearance of single resonances for I13, K48, and Q49 that do not occupy the position observed in unconjugated acUbK33 supports the idea that acetylation at K33 promotes a closed conformation of UBE2L3~Ub conjugate.

4.4 Discussion

Here, we used Ub proteins site-specifically modified with acetyl-lysine to create a library of seven uniquely acetylated Ub (acUb) molecules. We have previously shown that acetylation alters the rate of E2~Ub conjugate formation with the E2 proteins UBE2D1 [165] and UBE2L3. We used similar methodology to study the next step in ubiquitination: discharge of the E2~Ub conjugate. Our experiments provided evidence that cysteine-mediated reactions are more influenced by Ub acetylation than their lysine-mediated counterparts. For this reason, we examined HECT-mediated unloading of the UBE2D1~Ub and UBE2L3~Ub conjugates with acUb. We found that of the two E3 proteins used, neither of them was affected identically by the same acUb protein; in other words, there was no single acUb molecule that impaired E3-mediated turnover for both ligases tested. These findings provide insight on how Ub acetylation at a given site might influence only a small set of E3 ligases.

Invasion plasmid antigen H3 (IPAH3) is a bacterial E3 ligase characterized as forming K48-linked chains and hijacking host ubiquitination machinery to degrade host proteins [127]. It was expected that acetylation at K48 might impair this reaction by preventing the formation of polyUb chains at K48. We found that less than 20% of the total UBE2D1~acUbK48 was able to discharge in the presence of IPAH3 in the timeframe studied, supporting this expectation. Interestingly however, we also noted impaired turnover with acUbK11 and acUbK27, though not to the same extent as acUbK48. K11 and K27 in Ub are involved in two intermolecular salt bridges (with E34 and D52, respectively) observed in structures of Ub [153]. It could be that a modified Ub fold due to acetylation of K11 or K27 impairs the transthiolation between UBE2D1 and IPAH3.

Acetylation of K27 in Ub also moderately impaired the transthiolation between UBE2D1 and HUWE1, a mitochondrial E3 ligase involved in mitophagy through the formation of K6-linked polyubiquitin, though other cellular involvements and linkage types are prevalent [166–168]. Since HUWE1 builds K6-linked polyUb chains, acetylation at K6 severely impaired turnover of the UBE2D1~Ub conjugate in the presence of HUWE1. Acetylation of K11 impaired catalysis to almost the same extent as K6. This could be a result of the loss of the K11-E34 salt bridge, or it could reflect more localized changes in the β1-β2 part of Ub that houses both K6 and K11.

Similar results were obtained for acUbK6 and acUbK11 in the UBE2L3:HUWE1 system where both proteins severely impaired turnover (maximum 25% discharge). This similarity suggests that the influence that acUbK6 and acUbK11 have on these systems is HUWE1 dependent and less reflects roles by either UBE2D1 or UBE2L3. Interestingly, in the UBE2L3:HUWE1 system, there appeared to be better turnover of the E2~Ub with acUbK27, acUbK29, and acUbK33 where all proteins reached near complete turnover compared to Ub. Acetylation at K63 impaired UBE2L3~Ub discharge with HUWE1 to the same extent as K11 but did not alter UBE2D1:HUWE1 to the same extent. These findings suggest that acUbK63 might have more of a role in altering interactions specifically within the UBE2L3:HUWE1 complex that might not be conserved with UBE2D1:HUWE1. Acetylation at K48 in Ub did not appear to impair HUWE1 mediated discharge of either UBE2D1 or UBE2L3, despite the enzyme being known to synthesize K48-linked polyUb. It is possible that K48-linkages are not the preferred linkage type for HUWE1 autoubiquitination and would mean acetylation at K48 would not block catalysis in our experiments. Also surprising was the finding that E2 unloading experiments with HUWE1 could not be fit with a one-phase decay, but instead fit a sigmoidal curve. Experiments conducted by others frequently only monitor a single time point to determine functionality [68,88,163,169] and do not show faster time points in the reaction. Therefore, by not collecting these fast timepoints, it would be possible that a similar lag is masked in these experiments. The lag we observe in the initial stages of the unloading of UBE2D1~Ub or UBE2L3~Ub conjugates with HUWE1 could be attributed to the multiple products formed as a result of this reaction. In other words, the initial unloading by some E2~Ub could auto-

ubiquitinate HUWE1 in monoUb or polyUb forms that might be altered due to an acetylated Ub protein. Additionally, allosteric regulation of HUWE1 function through its auto-ubiquitination could account for the lag observed, where the first round of unloaded Ub positively modulates HUWE1 catalysis. Finally, the initial lag time observed in our studies could be due to the presence of residues in our construct that would be contained in the canonical helix α1 of the HUWE1 HECT domain (E4006-D4009). This helix has been established to alter stability and impair catalysis by the HECT domain of HUWE1 [170]. Other HECT E3 ligases like ITCH [171] and E6AP [172,173] undergo allosteric modulation of activity either directly through the HECT domain or through other regions of the protein. Further experiments would need to confirm the possible allosteric modulation of HUWE1 through ubiquitination.

In addition to impairing E2~Ub turnover due to the innate preference in polyUb linkage type by the E3 ligase, acetylation of Ub could impair unloading by promoting conformations of the E2~Ub conjugate that are less competent in certain ubiquitination pathways. Various works have described the necessity for closed conformations of E2~Ub in RING pathways [50,59,60], while HECT and RBR pathways require an open conformation of E2~Ub [53–56]. Our NMR experiments suggest that certain acUb proteins like K6 or K33 promote the UBE2L3~Ub conjugate to populate more closed states compared to Ub. In various E2~Ub conjugate structures, the sidechain of K33 extends into solution, distal to the E2:Ub non-covalent interface [52,57,151,152]; yet, our NMR data indicate that acUbK33 favours the closed conformation of UBE2L3~Ub more than Ub. This is evident by the two signals for the reporter residue K48 in the UBE2L3~Ub spectrum, but one signal in the UBE2L3~acUbK33 spectrum. Here, the spectra likely reflect slow exchange between open and closed states as the lone signal for K48 in the UBE2L3~acUbK33 spectrum has a similar position to that of the closed state in the UBE2L3~Ub spectrum. The presence of the single signal for K48 via slow exchange in the UBE2L3~acUbK33 spectrum indicates the conformation is 100% closed. This structural insight could explain why the discharge of UBE2L3~acUbK33 with HUWE1 was slow initially but ultimately reached a faster rate of discharge than the UBE2L3~Ub conjugate. It would be expected that the slow start might reflect the need for the UBE2L3~acUbK33

conjugate to open in the presence of HUWE1, where a complex with the closed UBE2L3~acUbK33 conjugate would limit catalysis.

Interestingly, in the UBE2L3~acUbK6 conjugate, acK6 lies in proximity to crossover helix α2 of UBE2L3 that is involved in non-covalent coordination of the Ub fold through the hydrophobic I44 patch of Ub. Our NMR data suggest that acetylation of K6 promotes a closed conformation of UBE2L3~Ub. Compared to the UBE2L3~Ub spectrum that has two signals relatively equal in intensity for K48 and Q49, the UBE2L3~acUbK6 spectrum shows two signals of largely different intensities for both reporters. Again, this likely reflects slow exchange between open and closed states, where the closed state accounts for more than 90% of the conformation. The posterior side of helix α2 in UBE2L3 packs against β1-β3 forming an extensive hydrophobic core with helix α1. To stabilize the closed conformation of UBE2L3~Ub, it would be expected that the longer, more non-polar sidechain of acetyl lysine at position 6 could extend past crossover helix α2 into the predominantly hydrophobic core of UBE2L3. The preference for the closed conformation displayed by the UBE2L3~acUbK6 conjugate could also explain why discharge of this conjugate with HUWE1 was impaired.

Our results also provide evidence that use of a stable, isopeptide-linked UBE2L3–Ub species does not accurately reflect what happens in the innate UBE2L3~Ub conjugate. In each of the UBE2L3–Ub, UBE2L3–acUbK6, and UBE2L3–acUbK33 spectra, the signal corresponding to the closed conformation of the reporter residues occupies a position that is approximately 50% of the way between the open and closed signals in the respective thioester spectra. This difference likely reflects the shift from slow exchange to fast exchange that would be possible with the longer, more flexible isopeptide bond between the C-terminus of Ub and the catalytic site (residue 86) of UBE2L3.

Overall, our data indicate that the influence of acUb on HECT-mediated ubiquitination systems is binary: 1) Ub acetylation at the preferred polyUb chain building site of the E3 ligase results in worse turnover of the E2~Ub conjugate, and 2) some acetylation sites appear to favour a more closed E2~Ub conformation that would impair HECT-type cascades. For some systems like acUbK6/UBE2L3:HUWE1 described here, there would

likely be influences from both directions. The outcome of these impaired reactions would be expected to alter the various processes regulated by Ub. For acUbK6/UBE2L3:HUWE1, the impaired ability to form the K6-linked polyUb with an acUbK6 molecule could be a useful signal in the termination of mitophagy. Further experiments would be required to examine the fullest extent of Ub acetylation on various Ub processes and the cooperativity of acUb and Ub together, but our data provides evidence that the conformation of the UBE2L3~Ub conjugate and transfer from an E2 protein to a HECT ligase is altered by Ub acetylation.

5
Perspectives and Significance

5.1 Ub modifications

The various modifications to Ub detected in mass spectrometry experiments provide evidence that ubiquitination is even more tightly regulated than previously thought. In recent years, there have been several studies showing how phosphorylation at S65 is crucial for the activity of E3 ligase parkin, where the regulation of parkin activity through pUbS65 arises from allosteric binding and domain rearrangement of parkin. Further, phosphorylation at Thr12 (pUbT12) has been shown to be important in mediating the DNA damage response [105], and phosphorylation at Ser57 (pUbS57) might play roles in the oxidative stress response [174]. In terms of roles for Ub acetylation, acUbK6 and acUbK48 were observed to inhibit the extension of various polyUb linkages in vitro [119]. However, experiments involving the acUb proteins in vivo are still difficult and pose significant challenges to fully understanding Ub acetylation.

Acetylation competes with ubiquitination: These two PTMs at a given site on Ub are mutually exclusive. One might expect that E2:E3 systems that have preference for a certain chain topology might be unable to pass a specific acUb molecule through the Ub cascade. Through our work, we did observe impairment in certain cascades that prefer distinct chain topologies (UBE2D1:IPAH3/acUbK48, UBE2L3 or UBE2D1:HUWE1/acUbK6). In the event of *Shigella flexneri* infection, the effector protein IPAH3 hijacks host ubiquitination

and synthesizes K48-linked chains to degrade host proteins [127]. Intuitively, we observed that acetylation of Ub at K48 prevents the function of IPAH3. This finding would likely correlate to impaired degradation of host protein and limited *S. flexneri* infection, but these expectations would need to be examined. We also observed that although acUbK6 behaves the most like Ub throughout the E1 and E2 steps in ubiquitination, when it comes to HUWE1-mediated ubiquitination, acUbK6 severely impairs this process. The impairment likely stems from the preference for K6-linkages by HUWE1, whereby acetylation at K6 in Ub blocks the formation of K6-polyUb. Interestingly, we also observed that at least one specific system (UBE2N:UBE2V2:RNF8/acUbK63) can accommodate for the acetylation site and synthesize polyUb elsewhere in Ub. The synthesis of K63-linked chains has been observed in immune signaling events as well as in the nucleus at DNA. Perhaps acetylation at K63 in these systems promotes a less abundant chain topology involved in these processes, without being completely detrimental to the system.

5.2 Modifications to E2 and E3 proteins

In addition to Ub, the other proteins involved in ubiquitination are post-translationally modified to regulate their function. Many of these include E2 conjugating enzymes and E3 ligases. One of the better studied E3 proteins that is post-translationally modified is parkin, where S65 phosphorylation by PINK1 is crucial for activation [99,100]. However, other sites in parkin including S9 and Y143 have been observed to be phosphorylated and have pS65-independent regulatory roles [175,176]. Further, other E3 ligases such as ITCH or BRCA1 require phosphorylation to promote their nuclear localization and roles in chromatin regulation [64,177].

Unfortunately, the matching of acetyltransferases to acetylation sites on proteins remains largely uncharacterized. The mass spectrometry experiments evaluated for Ub peptides demonstrate that various E2 conjugating enzymes and E3 ligases are also acetylated during periods of cell stress [111,112]. Some of these include the E2 proteins UBE2L3, UBE2K, and UBE2N and the E3 ligases HUWE1, TRIM33, and NEDD4. Other datasets collected with deacetylase inhibition or knockout detect a larger number of acetylation sites, emphasizing the tight regulation of acetylation throughout the natural lifecycle of the cell

[107,108]. These experiments show acetylation sites in the UBE2D family of E2 proteins and additional sites not detected in cell stress experiments in other proteins such as UBE2L3 and HUWE1.

The acetylation sites detected in E2 conjugating enzymes frequently occur in the conserved UBC domain responsible for conjugating a Ub protein and forming non-covalent interactions with UBA1 and E3 ligases to facilitate various steps in ubiquitination [45]. Conversely, the E3 ligases are generally larger enzymes with multiple accessory domains that have roles outside of ubiquitination, and acetylation has frequently been observed outside of the ubiquitination-active domain (ie. RING or HECT domain). It would therefore be expected that acetylation of E2 enzymes might regulate ubiquitination more directly than acetylation of their ligase counterparts, possibly providing specificity along the way.

5.3 Possible roles for Ub acetylation

There has yet to be described a localized cellular event that increases the concentration of acUb in the cell. Regardless, the likelihood of cells containing only a given acUb protein is very low. It would be expected that a localized pool of acUb forms due to some external stimulus, but even then, the acUb protein would not be at 100% total available Ub. Additionally, it is still unclear when in the ubiquitination cascade the Ub molecule is acetylated: 1) Does the acetyltransferase modify the free pool of mono-Ub, 2) Are the various covalent E1~Ub, E2~Ub, or E3~Ub molecules the target, or 3) Does Ub acetylation occur once the Ub has been incorporated into a chain? Although our work here mainly assumes question 1 by using 100% acUb, we also provide some insight into question 3 being true as well. Conversely, question 2 is likely not true: The instability or transient nature of the various E1~Ub, E2~Ub, or E3~Ub conjugates would be expected to dissuade for PTMs at these points in the Ub cascade. We observed that certain acUb proteins are less competent in E3-mediated steps in ubiquitination. As the termination of the function of the E3 ligase would likely cause other problems in the cells, it seems unlikely that cells would need to rely completely on a pool of pre-acetylated ubiquitin. Rather, a single acetylation in a pre-established polyUb chain or passage of a mono-acUb through the

ubiquitination machinery might be enough of a signal for the E3 ligase to terminate or modify its activity. Our experiments show that the E1 protein UBA1 is still able to activate a pool of acUb at each of the seven sites, and these pools of acUb are competent with two common E2 proteins UBE2D1 and UBE2L3.

It is tempting to speculate on the roles of Ub acetylation in a broader context in cells. Although our experiments show that certain acUb proteins hinder the activity of E3 ligases in vitro, the cellular relevance of this finding is difficult to identify. Primarily, multiple E2:E3 pairs build the same topologies of polyUb chains: Would a specific acUb protein impair these pathways to the same extent? Second, the formation of branched or mixed chains of polyUb are becoming more prevalent in the literature: Does acetylation have a role in guiding the formation of these chains? Finally, many E3 proteins have a distinct hierarchy in their preference for polyUb chain building sites: Can acetylation at their preferred site induce the formation of lesser preferred topologies? Of course, these experiments would need to be done, but with the current limits that cannot pin acetylation sites to specific compartments or topologies in cells, these questions remain difficult to address.

5.4 Chemical biology tools for studying ubiquitination

The use of chemical biology tools has rapidly expanded the study of various steps in ubiquitination. From using crosslinkers to capture transient structural intermediates [39], to the development of activity-based probes [178,179] to study the covalent E3~Ub or Deubiquitinase~Ub intermediates, to the use of fluorescent molecules to study conformation and function, the development of new techniques is astounding. Other recent advancements include the use of proteolysis targeting chimeras (PROTACs) to specifically target and degrade a protein of interest through crosslinking [180]. PROTACs have generated much interest and are being extensively studied for therapeutic uses like cancer treatments [181].

Further, genetic code expansion using an orthogonal tRNA and tRNA synthetase derived from species of methanoarchaea has been widely used to incorporate post-translationally modified amino acids into proteins during bacterial translation. In this work, we used genetic code expansion to site specifically incorporate acetyl-lysine at the position of interest in Ub [136]. This method has also been used to incorporate phosphoserine into Ub [182], and the optimization of other tRNA synthetases that allow for other PTMs such as phospho-tyrosine or phospho-threonine will advance the study of E3 ligases harboring these PTMs. Additionally, use of an orthogonal system can be used to incorporate amino acids harboring photo-crosslinking reagents to provide insight on protein conformations [183,184]. In recent years, similar chemical biology tools have been used to permit the addition of full Ub molecules at various positions in substrate proteins [185], and to chemically form specific topologies of polyUb chains [186,187].

Finally, the replacement of autoradiography approaches to studying ubiquitination are becoming more and more prevalent [145,188,189]. Various techniques such as western blotting or the use of small fluorescently labeled Ub or ubiquitination enzymes have replaced this older methodology. In addition to visualizing proteins on gels or blots, fluorescent molecules can be used with a plate-reader to optimize and mass examine different reactions. These experiments include Förster Resonance Energy Transfer (FRET) experiments and fluorescence polarization assays. In our work, we used fluorescently tagged Ub and E2 proteins to study the kinetics of E2~Ub formation using FRET [165], but there are many other applications and combinations of fluorescent molecules [133,134,190,191].

The list of chemical biology tools used in ubiquitination is continually growing. The rapid and ongoing advancements of these tools will aid tremendously in the study of ubiquitination proteins with the hope of understanding the full molecular mechanism of autoimmune diseases, neurodegenerative diseases, and cancers.

5.5 Significance

The Ub system is heavily implicated in many human diseases that remain difficult to treat. Determining the underlying molecular mechanisms and how ubiquitin pathways are

implicated in such mechanisms will provide new avenues for therapeutic targeting. In several disease states, post-translational modifications such as ubiquitination, acetylation, or phosphorylation of proteins hold the key to the underlying pathogeneses [3,10,13,15]. Recently discovered Ub peptides that have been modified themselves provide an additional complication to understanding disease pathogenesis. Prior to this thesis, there were a handful of studies on Ub phosphorylation, but only one publication that showed how acetylation at K6 or K48 impairs certain types of ubiquitination [119]. A comprehensive study on the various acetylation sites was lacking. This thesis provides a robust analysis of the different acUb proteins (acUbK6, acUbK11, acUbK27, acUbK29, acUbK33, acUbK48, and acUbK63) and their interactions with a subset of the E2 conjugating enzymes and functional E3 counterparts. While the work done in this thesis will not directly cure cancer, autoimmune disorders, or Parkinson's disease, it provides substantial information about how Ub acetylation influences the different steps in ubiquitination, and it would be expected to promote the study of other acetylated proteins in ubiquitination.

6

References

[1]   T. Frogne, A.-V. Laenkholm, M.B. Lyng, K.L. Henriksen, A.E. Lykkesfeldt, Determination of HER2 phosphorylation at tyrosine 1221/1222 improves prediction of poor survival for breast cancer patients with hormone receptor-positive tumors, Breast Cancer Res. 11 (2009) R11. https://doi.org/10.1186/bcr2230.

[2]   M. Gijsen, P. King, T. Perera, P.J. Parker, A.L. Harris, B. Larijani, A. Kong, HER2 Phosphorylation Is Maintained by a PKB Negative Feedback Loop in Response to Anti-HER2 Herceptin in Breast Cancer, PLoS Biol. 8 (2010) 16. https://doi.org/10.1371/journal.pbio.1000563.

[3]   Y. Miyoshi, K. Murase, M. Saito, M. Imamura, K. Oh, Mechanisms of estrogen receptor-α upregulation in breast cancers, Med Mol Morphol. 43 (2010) 193–196. https://doi.org/10.1007/s00795-010-0514-3.

[4]   M. Colom-Cadena, J. Pegueroles, A.G. Herrmann, C.M. Henstridge, L. Muñoz, M. Querol-Vilaseca, C.S. Martín-Paniello, J. Luque-Cabecerans, J. Clarimon, O. Belbin, R. Núñez-Llaves, R. Blesa, C. Smith, C.-A. McKenzie, M.P. Frosch, A. Roe, J. Fortea, J. Andilla, P. Loza-Alvarez, E. Gelpi, B.T. Hyman, T.L. Spires-Jones, A. Lleó, Synaptic phosphorylated α-synuclein in dementia with Lewy bodies, Brain. 140 (2017) 3204–3214. https://doi.org/10.1093/brain/awx275.

[5]   H. Fujiwara, M. Hasegawa, N. Dohmae, A. Kawashima, E. Masliah, M.S. Goldberg, J. Shen, K. Takio, T. Iwatsubo, α-Synuclein is phosphorylated in synucleinopathy lesions, Nat Cell Biol. 4 (2002) 160–164. https://doi.org/10.1038/ncb748.

[6]   L.C. Cork, N.H. Sternberger, L.A. Sternberger, M.F. Casanova, R.G. Struble, D.L. Price, Phosphorylated Neurofilament Antigens in Neurofibrillary Tangles in Alzheimer's Disease, J Neuropathol Exp Neurol. 45 (1986) 56–64.

[7]   N.H. Sternberger, L.A. Sternberger, J. ULRICHt, Aberrant neurofilament phosphorylation in Alzheimer disease, PNAS. 82 (1985) 4274–4276.

[8]   I. Grundke-Iqbal, H.M. Wisniewski, L.I. BINDERt, Abnormal phosphorylation of the microtubule-associated protein X (tau) in Alzheimer cytoskeletal pathology, PNAS. 83 (1986) 4913–4917.

[9]   K. Halkidou, L. Gaughan, S. Cook, H.Y. Leung, D.E. Neal, C.N. Robson, Upregulation and Nuclear Recruitment of HDAC1 in Hormone Refractory Prostate Cancer, Prostate. 59 (2004) 177–189. https://doi.org/10.1002/pros.20022.

[10]   H. Osada, Y. Tatematsu, H. Saito, Y. Yatabe, T. Mitsudomi, T. Takahashi, Reduced expression of class II histone deacetylase genes is associated with poor prognosis in lung cancer patients, Int J Cancer. 112 (2004) 26–32. https://doi.org/10.1002/ijc.20395.

[11]   S.-W. Min, S.-H. Cho, Y. Zhou, S. Schroeder, V. Haroutunian, W.W. Seeley, E.J. Huang, Y. Shen, E. Masliah, C. Mukherjee, D. Meyers, P.A. Cole, M. Ott, L. Gan, Acetylation of Tau Inhibits Its Degradation and Contributes to Tauopathy, Neuron. 67 (2010) 953–966. https://doi.org/10.1016/j.neuron.2010.08.044.

[12]   T.J. Cohen, J.L. Guo, D.E. Hurtado, L.K. Kwong, I.P. Mills, J.Q. Trojanowski, V.M.Y. Lee, The acetylation of tau inhibits its function and promotes pathological tau aggregation, Nat Commun. 2 (2011) 9. https://doi.org/10.1038/ncomms1255.

[13]   L.H. Gallo, J. Ko, D.J. Donoghue, The importance of regulatory ubiquitination in cancer and metastasis, Cell Cycle. 16 (2017) 634–648. https://doi.org/10.1080/15384101.2017.1288326.

[14]   D. Pascovici, J.X. Wu, M.J. McKay, C. Joseph, Z. Noor, K. Kamath, Y. Wu, S. Ranganathan, V. Gupta, M. Mirzaei, Clinically Relevant Post-Translational Modification Analyses—Maturing Workflows and Bioinformatics Tools, Int J Mol Sci. 20 (2018) 16. https://doi.org/10.3390/ijms20010016.

[15]   J. Zinngrebe, A. Montinaro, N. Peltzer, H. Walczak, Ubiquitin in the immune system, EMBO Rep. 15 (2014) 28–45. https://doi.org/10.1002/embr.201338025.

[16]   M.A. Basar, D.B. Beck, A. Werner, Deubiquitylases in developmental ubiquitin signaling and congenital diseases, Cell Death Differ. 28 (2021) 538–556. https://doi.org/10.1038/s41418-020-00697-5.

[17]   Q. Zheng, T. Huang, L. Zhang, Y. Zhou, H. Luo, H. Xu, X. Wang, Dysregulation of Ubiquitin-Proteasome System in Neurodegenerative Diseases, Front Aging Neurosci. 8 (2016) 10. https://doi.org/10.3389/fnagi.2016.00303.

[18]   A.J. George, Y.C. Hoffiz, A.J. Charles, Y. Zhu, A.M. Mabb, A Comprehensive Atlas of E3 Ubiquitin Ligase Mutations in Neurological Disorders, Front Genet. 9 (2018) 17. https://doi.org/10.3389/fgene.2018.00029.

[19] V.G. Allfrey, R. Faulkner, A.E. Mirsky, Acetylation and methylation of histones and their possible role in the regulation of RNA synthesis, PNAS. 51 (1964) 786–794.

[20] H. Masumoto, D. Hawke, R. Kobayashi, A. Verreault, A role for cell-cycle-regulated histone H3 lysine 56 acetylation in the DNA damage response, Nature. 436 (2005) 294–298. https://doi.org/10.1038/nature03714.

[21] A. Ozdemir, S. Spicuglia, E. Lasonder, M. Vermeulen, C. Campsteijn, H.G. Stunnenberg, C. Logie, Characterization of Lysine 56 of Histone H3 as an Acetylation Site in Saccharomyces cerevisiae, J Biol Chem. 280 (2005) 25949–25952. https://doi.org/10.1074/jbc.C500181200.

[22] M. Shogren-Knaak, Histone H4-K16 Acetylation Controls Chromatin Structure and Protein Interactions, Science. 311 (2006) 844–847. https://doi.org/10.1126/science.1124000.

[23] C.D. Allis, S.L. Berger, J. Cote, S. Dent, T. Jenuwien, T. Kouzarides, L. Pillus, D. Reinberg, Y. Shi, R. Shiekhattar, A. Shilatifard, J. Workman, Y. Zhang, New Nomenclature for Chromatin-Modifying Enzymes, Cell. 131 (2007) 633–636. https://doi.org/10.1016/j.cell.2007.10.039.

[24] M.K. Shanmugam, A. Dharmarajan, S. Warrier, A. Bishayee, A.P. Kumar, G. Sethi, K.S. Ahn, Role of histone acetyltransferase inhibitors in cancer therapy, in: Advances in Protein Chemistry and Structural Biology, Elsevier, 2021: pp. 149–191. https://doi.org/10.1016/bs.apcsb.2020.08.002.

[25] S.-Y. Park, J.-S. Kim, A short guide to histone deacetylases including recent progress on class II enzymes, Exp Mol Med. 52 (2020) 204–212. https://doi.org/10.1038/s12276-020-0382-4.

[26] E. Pajarillo, A. Rizor, J. Lee, M. Aschner, E. Lee, The role of posttranslational modifications of α-synuclein and LRRK2 in Parkinson's disease: Potential contributions of environmental factors, Biochim Biophys Acta Mol Basis Dis. 1865 (2019) 1992–2000. https://doi.org/10.1016/j.bbadis.2018.11.017.

[27] T. Sun, X. Li, P. Zhang, W.-D. Chen, H. Zhang, D.-D. Li, R. Deng, X.-J. Qian, L. Jiao, J. Ji, Y.-T. Li, R.-Y. Wu, Y. Yu, G.-K. Feng, X.-F. Zhu, Acetylation of Beclin 1 inhibits autophagosome maturation and promotes tumour growth, Nat Commun. 6 (2015) 12. https://doi.org/10.1038/ncomms8215.

[28] X.-J. Yang, E. Seto, HATs and HDACs: from structure, function and regulation to novel strategies for therapy and prevention, Oncogene. 26 (2007) 5310–5318. https://doi.org/10.1038/sj.onc.1210599.

[29] M.B. Metzger, J.N. Pruneda, R.E. Klevit, A.M. Weissman, RING-type E3 ligases: Master manipulators of E2 ubiquitin-conjugating enzymes and ubiquitination,

Biochim Biophys Acta Mol Cell Res. 1843 (2014) 47–60.
https://doi.org/10.1016/j.bbamcr.2013.05.026.

[30] J. Sluimer, B. Distel, Regulating the human HECT E3 ligases, Cellular and Molecular Life Sciences. 75 (2018) 3121–3141. https://doi.org/10.1007/s00018-018-2848-2.

[31] D.E. Spratt, H. Walden, G.S. Shaw, RBR E3 ubiquitin ligases: new structures, new insights, new questions, Biochem J. 458 (2014) 421–437. https://doi.org/10.1042/BJ20140006.

[32] K.-C. Pao, N.T. Wood, A. Knebel, K. Rafie, M. Stanley, P.D. Mabbitt, R. Sundaramoorthy, K. Hofmann, D.M.F. van Aalten, S. Virdee, Activity-based E3 ligase profiling uncovers an E3 ligase with esterification activity, Nature. 556 (2018) 381–385. https://doi.org/10.1038/s41586-018-0026-1.

[33] S. Vijay-Kumar, C.E. Bugg, K.D. Wilkinson, R.D. Vierstra, P.M. Hatfield, W.J. Cook, Comparison of the three-dimensional structures of human, yeast, and oat ubiquitin., J Biol Chem. 262 (1987) 6396–6399. https://doi.org/10.1016/S0021-9258(18)45583-4.

[34] D. Komander, M. Rape, The Ubiquitin Code, Annu Rev Biochem. 81 (2012) 203–229. https://doi.org/10.1146/annurev-biochem-060310-170328.

[35] L. Jin, A. Williamson, S. Banerjee, I. Philipp, M. Rape, Mechanism of Ubiquitin-Chain Formation by the Human Anaphase-Promoting Complex, Cell. 133 (2008) 653–665. https://doi.org/10.1016/j.cell.2008.04.012.

[36] P. Liu, W. Gan, S. Su, A.V. Hauenstein, T. Fu, B. Brasher, C. Schwerdtfeger, A.C. Liang, M. Xu, W. Wei, K63-linked polyubiquitin chains bind to DNA to facilitate DNA damage repair, Sci Signal. 11 (2018) 12. https://doi.org/10.1126/scisignal.aar8133.

[37] I. Lee, H. Schindelin, Structural Insights into E1-Catalyzed Ubiquitin Activation and Transfer to Conjugating Enzymes, Cell. 134 (2008) 268–278. https://doi.org/10.1016/j.cell.2008.05.046.

[38] S.K. Olsen, C.D. Lima, Structure of a Ubiquitin E1-E2 Complex: Insights to E1-E2 Thioester Transfer, Mol Cell. 49 (2013) 884–896. https://doi.org/10.1016/j.molcel.2013.01.013.

[39] Z.S. Hann, C. Ji, S.K. Olsen, X. Lu, M.C. Lux, D.S. Tan, C.D. Lima, Structural basis for adenylation and thioester bond formation in the ubiquitin E1, Proc Natl Acad Sci USA. 116 (2019) 15475–15484. https://doi.org/10.1073/pnas.1905488116.

[40] Z. Lv, L. Yuan, J.H. Atkison, G. Aldana-Masangkay, Y. Chen, S.K. Olsen, Domain alternation and active site remodeling are conserved structural features of

ubiquitin E1, J Biol Chem. 292 (2017) 12089–12099.
https://doi.org/10.1074/jbc.M117.787622.

[41] A. Schäfer, M. Kuhn, H. Schindelin, Structure of the ubiquitin-activating enzyme
      loaded with two ubiquitin molecules, Acta Crystallogr D. 70 (2014) 1311–1320.
      https://doi.org/10.1107/S1399004714002910.

[42] B.W. Cook, R.E. Lacoursiere, G.S. Shaw, Recruitment of Ubiquitin within an E2
      Chain Elongation Complex, Biophysical Journal. 118 (2020) 1679–1689.
      https://doi.org/10.1016/j.bpj.2020.02.012.

[43] A.J. Middleton, C.L. Day, The molecular basis of lysine 48 ubiquitin chain
      synthesis by Ube2K, Scientific Reports. 5 (2015) 16793.
      https://doi.org/10.1038/srep16793.

[44] Y. Ye, M. Rape, Building ubiquitin chains: E2 enzymes at work, Nat Rev Mol Cell
      Biol. 10 (2009) 755–764. https://doi.org/10.1038/nrm2780.

[45] M.D. Stewart, T. Ritterhoff, R.E. Klevit, P.S. Brzovic, E2 enzymes: more than just
      middle men, Cell Res. 26 (2016) 423–440. https://doi.org/10.1038/cr.2016.35.

[46] Z. Lv, K.M. Williams, L. Yuan, J.H. Atkison, S.K. Olsen, Crystal structure of a
      human ubiquitin E1–ubiquitin complex reveals conserved functional elements
      essential for activity, J Biol Chem. 293 (2018) 18337–18352.
      https://doi.org/10.1074/jbc.RA118.003975.

[47] K.M. Williams, S. Qie, J.H. Atkison, S. Salazar-Arango, J. Alan Diehl, S.K. Olsen,
      Structural insights into E1 recognition and the ubiquitin-conjugating activity of the
      E2 enzyme Cdc34, Nat Commun. 10 (2019). https://doi.org/10.1038/s41467-019-
      11061-8.

[48] T.J. Siepmann, R.N. Bohnsack, Z. Tokgöz, O.V. Baboshina, A.L. Haas, Protein
      Interactions within the N-end Rule Ubiquitin Ligation Pathway, J Biol Chem. 278
      (2003) 9448–9457. https://doi.org/10.1074/jbc.M211240200.

[49] L. Buetow, M. Gabrielsen, N.G. Anthony, H. Dou, A. Patel, H. Aitkenhead, G.J.
      Sibbet, B.O. Smith, D.T. Huang, Activation of a Primed RING E3-E2–Ubiquitin
      Complex by Non-Covalent Ubiquitin, Mol Cell. 58 (2015) 297–310.
      https://doi.org/10.1016/j.molcel.2015.02.017.

[50] A.J. Middleton, J. Zhu, C.L. Day, The RING Domain of RING Finger 12
      Efficiently Builds Degradative Ubiquitin Chains, J Mol Biol. 432 (2020) 3790–
      3801. https://doi.org/10.1016/j.jmb.2020.05.001.

[51] L. Kiss, J. Zeng, C.F. Dickson, D.L. Mallery, J.-C. Yang, S.H. McLaughlin, A.
      Boland, D. Neuhaus, L.C. James, A tri-ionic anchor mechanism drives Ube2N-
      specific recruitment and K63-chain ubiquitination in TRIM ligases, Nat Commun.
      10 (2019) 4502. https://doi.org/10.1038/s41467-019-12388-y.

[52] K.S. Hamilton, M.J. Ellison, K.R. Barber, R.S. Williams, J.T. Huzil, S. McKenna, C. Ptak, M. Glover, G.S. Shaw, Structure of a Conjugating Enzyme-Ubiquitin Thiolester Intermediate Reveals a Novel Role for the Ubiquitin Tail, Structure. 9 (2001) 897–904. https://doi.org/10.1016/S0969-2126(01)00657-8.

[53] K.K. Dove, B. Stieglitz, E.D. Duncan, K. Rittinger, R.E. Klevit, Molecular insights into RBR E3 ligase ubiquitin transfer mechanisms, EMBO Rep. 17 (2016) 1221–1235. https://doi.org/10.15252/embr.201642641.

[54] B.C. Lechtenberg, A. Rajput, R. Sanishvili, M.K. Dobaczewska, C.F. Ware, P.D. Mace, S.J. Riedl, Structure of a HOIP/E2~ubiquitin complex reveals RBR E3 ligase mechanism and regulation, Nature. 529 (2016) 546–550. https://doi.org/10.1038/nature16511.

[55] L. Yuan, Z. Lv, J.H. Atkison, S.K. Olsen, Structural insights into the mechanism and E2 specificity of the RBR E3 ubiquitin ligase HHARI, Nat Commun. 8 (2017) 14. https://doi.org/10.1038/s41467-017-00272-6.

[56] H.B. Kamadurai, J. Souphron, D.C. Scott, D.M. Duda, D.J. Miller, D. Stringer, R.C. Piper, B.A. Schulman, Insights into Ubiquitin Transfer Cascades from a Structure of a UbcH5B~Ubiquitin-HECTNEDD4L Complex, Mol Cell. 36 (2009) 1095–1102. https://doi.org/10.1016/j.molcel.2009.11.010.

[57] R.C. Page, J.N. Pruneda, J. Amick, R.E. Klevit, S. Misra, Structural Insights into the Conformation and Oligomerization of E2~Ubiquitin Conjugates, Biochemistry. 51 (2012) 4175–4187. https://doi.org/10.1021/bi300058m.

[58] J.N. Pruneda, K.E. Stoll, L.J. Bolton, P.S. Brzovic, R.E. Klevit, Ubiquitin in Motion: Structural Studies of the Ubiquitin-Conjugating Enzyme~Ubiquitin Conjugate, Biochemistry. 50 (2011) 1624–1633. https://doi.org/10.1021/bi101913m.

[59] A. Plechanovová, E.G. Jaffray, M.H. Tatham, J.H. Naismith, R.T. Hay, Structure of a RING E3 ligase and ubiquitin-loaded E2 primed for catalysis, Nature. 489 (2012) 115–120. https://doi.org/10.1038/nature11376.

[60] E. Branigan, J. Carlos Penedo, R.T. Hay, Ubiquitin transfer by a RING E3 ligase occurs from a closed E2~ubiquitin conformation, Nat Commun. 11 (2020) 11. https://doi.org/10.1038/s41467-020-16666-y.

[61] N.A.S. Ismail, D.L. Baines, S.M. Wilson, The phosphorylation of endogenous Nedd4-2 In Na+—absorbing human airway epithelial cells, Eur J Pharmacol. 732 (2014) 32–42. https://doi.org/10.1016/j.ejphar.2014.03.005.

[62] J.P. Arroyo, D. Lagnaz, C. Ronzaud, N. Vázquez, B.S. Ko, L. Moddes, D. Ruffieux-Daidié, P. Hausel, R. Koesters, B. Yang, J.B. Stokes, R.S. Hoover, G. Gamba, O. Staub, Nedd4-2 Modulates Renal Na$^+$-Cl$^-$ Cotransporter via the

Aldosterone-SGK1-Nedd4-2 Pathway, JASN. 22 (2011) 1707–1719. https://doi.org/10.1681/ASN.2011020132.

[63]   I.-H. Lee, A. Dinudom, A. Sanchez-Perez, S. Kumar, D.I. Cook, Akt Mediates the Effect of Insulin on Epithelial Sodium Channels by Inhibiting Nedd4-2*, J Biol Chem. 282 (2007) 29866–29873.

[64]   L. Chang, L. Shen, H. Zhou, J. Gao, H. Pan, L. Zheng, B. Armstrong, Y. Peng, G. Peng, B.P. Zhou, S.T. Rosen, B. Shen, ITCH nuclear translocation and H1.2 polyubiquitination negatively regulate the DNA damage response, Nucleic Acids Res. 47 (2019) 824–842. https://doi.org/10.1093/nar/gky1199.

[65]   S. Bekker-Jensen, J.R. Danielsen, K. Fugger, I. Gromova, A. Nerstedt, C. Lukas, J. Bartek, J. Lukas, N. Mailand, HERC2 coordinates ubiquitin-dependent assembly of DNA repair factors on damaged chromosomes, Nat Cell Biol. 12 (2010) 80–86. https://doi.org/10.1038/ncb2008.

[66]   J.M. Perez, S.M. Chirieleison, D.W. Abbott, An IκB Kinase-Regulated Feedforward Circuit Prolongs Inflammation, Cell Rep. 12 (2015) 537–544. https://doi.org/10.1016/j.celrep.2015.06.050.

[67]   M.S. Anglesio, V. Evdokimova, N. Melnyk, L. Zhang, C.V. Fernandez, P.E. Grundy, S. Leach, M.A. Marra, A.R. Brooks-Wilson, J. Penninger, P.H.B. Sorensen, Differential expression of a novel ankyrin containing E3 ubiquitin-protein ligase, Hace1, in sporadic Wilms' tumor versus normal kidney, Hum Mol Genet. 13 (2004) 2061–2074. https://doi.org/10.1093/hmg/ddh215.

[68]   J.L. Parsons, P.S. Tait, D. Finch, I.I. Dianova, M.J. Edelmann, S.V. Khoronenkova, B.M. Kessler, R.A. Sharma, W.G. McKenna, G.L. Dianov, Ubiquitin ligase ARF-BP1/Mule modulates base excision repair, EMBO J. 28 (2009) 3207–3215. https://doi.org/10.1038/emboj.2009.243.

[69]   V.P. Ronchi, J.M. Klein, D.J. Edwards, A.L. Haas, The Active Form of E6-associated protein (E6AP)/UBE3A Ubiquitin Ligase Is an Oligomer, J Biol Chem. 289 (2014) 1033–1048. https://doi.org/10.1074/jbc.M113.517805.

[70]   M. Wang, D. Cheng, J. Peng, C.M. Pickart, Molecular determinants of polyubiquitin linkage selection by an HECT ubiquitin ligase, EMBO J. 25 (2006) 1710–1719. https://doi.org/10.1038/sj.emboj.7601061.

[71]   H. Ashida, C. Sasakawa, Bacterial E3 ligase effectors exploit host ubiquitin systems, Curr Opin Microbiol. 35 (2017) 16–22. https://doi.org/10.1016/j.mib.2016.11.001.

[72]   P.D. Mabbitt, A. Loreto, M.-A. Déry, A.J. Fletcher, M. Stanley, K.-C. Pao, N.T. Wood, M.P. Coleman, S. Virdee, Structural basis for RING-Cys-Relay E3 ligase activity and its role in axon integrity, Nat Chem Biol. 16 (2020) 1227–1236. https://doi.org/10.1038/s41589-020-0598-6.

[73] R.J. Deshaies, C.A.P. Joazeiro, RING Domain E3 Ubiquitin Ligases, Annual Review of Biochemistry. 78 (2009) 399–434. https://doi.org/10.1146/annurev.biochem.78.101807.093809.

[74] H.C. Nguyen, W. Wang, Y. Xiong, Cullin-RING E3 Ubiquitin Ligases: Bridges to Destruction, in: J.R. Harris, J. Marles-Wright (Eds.), Macromolecular Protein Complexes, Springer International Publishing, Cham, 2017: pp. 323–347. https://doi.org/10.1007/978-3-319-46503-6_12.

[75] A. Das, A.J. Middleton, P. Padala, E.C. Ledgerwood, P.D. Mace, C.L. Day, The Structure and Ubiquitin Binding Properties of TRAF RING Heterodimers, J Mol Biol. 433 (2021) 15. https://doi.org/10.1016/j.jmb.2021.166844.

[76] K. Nomura, M. Klejnot, D. Kowalczyk, A.K. Hock, G.J. Sibbet, K.H. Vousden, D.T. Huang, Structural analysis of MDM2 RING separates degradation from regulation of p53 transcription activity, Nat Struct Mol Biol. 24 (2017) 578–587. https://doi.org/10.1038/nsmb.3414.

[77] S. Nowsheen, M. Deng, Z. Lou, Ubiquitin and the DNA double-strand break repair pathway, Genome Instab Dis. (2019). https://doi.org/10.1007/s42764-019-00007-5.

[78] M. Sadowski, R. Suryadinata, A.R. Tan, S.N.A. Roesley, B. Sarcevic, Protein monoubiquitination and polyubiquitination generate structural diversity to control distinct biological processes, IUBMB Life. 64 (2012) 136–142. https://doi.org/10.1002/iub.589.

[79] K.N. Swatek, D. Komander, Ubiquitin modifications, Cell Res. 26 (2016) 399–422. https://doi.org/10.1038/cr.2016.39.

[80] Z. Chen, C.M. Pickart, Carrier Protein (E2) Catalyzes Multi- via Lysine 48 of Ubiquitin, J Biol Chem. 265 (1990) 21835–21842.

[81] B.L. Lee, A. Singh, J.N. Mark Glover, M.J. Hendzel, L. Spyracopoulos, Molecular Basis for K63-Linked Ubiquitination Processes in Double-Strand DNA Break Repair: A Focus on Kinetics and Dynamics, J Mol Biol. 429 (2017) 3409–3429. https://doi.org/10.1016/j.jmb.2017.05.029.

[82] M. Tracz, W. Bialek, Beyond K48 and K63: non-canonical protein ubiquitination, Cell Mol Biol Lett. 26 (2021) 17. https://doi.org/10.1186/s11658-020-00245-6.

[83] A. Rohaim, M. Kawasaki, R. Kato, I. Dikic, S. Wakatsuki, Structure of a compact conformation of linear diubiquitin, Acta Crystallogr D Biol Crystallogr. 68 (2012) 102–108. https://doi.org/10.1107/S0907444911051195.

[84] S. Virdee, Y. Ye, D.P. Nguyen, D. Komander, J.W. Chin, Engineered diubiquitin synthesis reveals Lys29-isopeptide specificity of an OTU deubiquitinase, Nat Chem Biol. 6 (2010) 750–757. https://doi.org/10.1038/nchembio.426.

[85] C.A. Castañeda, T.R. Kashyap, M.A. Nakasone, S. Krueger, D. Fushman, Unique Structural, Dynamical, and Functional Properties of K11-Linked Polyubiquitin Chains, Structure. 21 (2013) 1168–1181. https://doi.org/10.1016/j.str.2013.04.029.

[86] M. Pan, Q. Zheng, S. Ding, L. Zhang, Q. Qu, T. Wang, D. Hong, Y. Ren, L. Liang, C. Chen, Z. Mei, L. Liu, Chemical Protein Synthesis Enabled Mechanistic Studies on the Molecular Recognition of K27-linked Ubiquitin Chains, Angew. Chem. Int. Ed. 58 (2019) 2627–2631. https://doi.org/10.1002/anie.201810814.

[87] Y.A. Kristariyanto, S.A. Abdul Rehman, D.G. Campbell, N.A. Morrice, C. Johnson, R. Toth, Y. Kulathu, K29-Selective Ubiquitin Binding Domain Reveals Structural Basis of Specificity and Heterotypic Nature of K29 Polyubiquitin, Molecular Cell. 58 (2015) 83–94. https://doi.org/10.1016/j.molcel.2015.01.041.

[88] Y.A. Kristariyanto, S.-Y. Choi, S.A.A. Rehman, M.S. Ritorto, D.G. Campbell, N.A. Morrice, R. Toth, Y. Kulathu, Assembly and structure of Lys33-linked polyubiquitin reveals distinct conformations, Biochem J. 467 (2015) 345–352. https://doi.org/10.1042/BJ20141502.

[89] J.-F. Trempe, N.R. Brown, M.E.M. Noble, J.A. Endicott, A new crystal form of Lys48-linked diubiquitin, Acta Crystallogr F Struct Biol Cryst Commun. 66 (2010) 994–998. https://doi.org/10.1107/S1744309110027600.

[90] D. Komander, F. Reyes-Turcu, J.D.F. Licchesi, P. Odenwaelder, K.D. Wilkinson, D. Barford, Molecular discrimination of structurally equivalent Lys 63-linked and linear polyubiquitin chains, EMBO Reports. 10 (2009) 466–473. https://doi.org/10.1038/embor.2009.55.

[91] A.L. Haas, I.A. Rose, The mechanism of ubiquitin activating enzyme. A kinetic and equilibrium analysis., J Biol Chem. 257 (1982) 10329–10337. https://doi.org/10.1016/S0021-9258(18)34024-9.

[92] T.J. Burch, A.L. Haas, Site-directed mutagenesis of ubiquitin. Differential roles for arginine in the interaction with ubiquitin-activating enzyme., Biochemistry. 33 (1994) 7300–7308.

[93] N.W. Pierce, G. Kleiger, S. Shan, R.J. Deshaies, Detection of sequential polyubiquitylation on a millisecond timescale, Nature. 462 (2009) 615–619. https://doi.org/10.1038/nature08595.

[94] T. Wu, Y. Merbl, Y. Huo, J.L. Gallop, A. Tzur, M.W. Kirschner, UBE2S drives elongation of K11-linked ubiquitin chains by the anaphase-promoting complex, PNAS. 107 (2010) 1355–1360. https://doi.org/10.1073/pnas.0912802107.

[95] B. Soufi, N.C. Soares, V. Ravikumar, B. Macek, Proteomics reveals evidence of cross-talk between protein modifications in bacteria: focus on acetylation and phosphorylation, Curr Opin Microbiol. 15 (2012) 357–363. https://doi.org/10.1016/j.mib.2012.05.003.

[96] A. Vancura, S. Nagar, P. Kaur, P. Bu, M. Bhagwat, I. Vancurova, Reciprocal Regulation of AMPK/SNF1 and Protein Acetylation, Int J Mol Sci. 19 (2018) 3314. https://doi.org/10.3390/ijms19113314.

[97] A.E. Raposo, S.C. Piller, Protein arginine methylation: an emerging regulator of the cell cycle, Cell Div. 13 (2018) 3. https://doi.org/10.1186/s13008-018-0036-2.

[98] R.J. Separovich, C.N.I. Pang, M.R. Wilkins, Controlling the Controllers: Regulation of Histone Methylation by Phosphosignalling, Trends Biochem Sci. 45 (2020) 1035–1048. https://doi.org/10.1016/j.tibs.2020.08.004.

[99] C. Kondapalli, A. Kazlauskaite, N. Zhang, H.I. Woodroof, D.G. Campbell, R. Gourlay, L. Burchell, H. Walden, T.J. Macartney, M. Deak, A. Knebel, D.R. Alessi, M.M.K. Muqit, PINK1 is activated by mitochondrial membrane potential depolarization and stimulates Parkin E3 ligase activity by phosphorylating Serine 65, Open Biology. 2 (2012) 120080. https://doi.org/10.1098/rsob.120080.

[100] K. Shiba-Fukushima, Y. Imai, S. Yoshida, Y. Ishihama, T. Kanao, S. Sato, N. Hattori, PINK1-mediated phosphorylation of the Parkin ubiquitin-like domain primes mitochondrial translocation of Parkin and regulates mitophagy, Scientific Reports. 2 (2012). https://doi.org/10.1038/srep01002.

[101] T. Hori, F. Osaka, T. Chiba, C. Miyamoto, K. Okabayashi, N. Shimbara, S. Kato, K. Tanaka, Covalent modification of all members of human cullin family proteins by NEDD8, Oncogene. 18 (1999) 6829–6834.

[102] D.L. Swaney, R.A. Rodriguez-Mias, J. Villen, Phosphorylation of ubiquitin at Ser65 affects its polymerization, targets, and proteome-wide turnover, EMBO Rep. 16 (2015) 1131–1144. https://doi.org/10.15252/embr.201540298.

[103] X. Dong, Z. Gong, Y.-B. Lu, K. Liu, L.-Y. Qin, M.-L. Ran, C.-L. Zhang, Z. Liu, W.-P. Zhang, C. Tang, Ubiquitin S65 phosphorylation engenders a pH-sensitive conformational switch, PNAS. (2017) 6770–6775. https://doi.org/10.1073/pnas.1705718114.

[104] F. Koyano, K. Okatsu, H. Kosako, Y. Tamura, E. Go, M. Kimura, Y. Kimura, H. Tsuchiya, H. Yoshihara, T. Hirokawa, T. Endo, E.A. Fon, J.-F. Trempe, Y. Saeki, K. Tanaka, N. Matsuda, Ubiquitin is phosphorylated by PINK1 to activate parkin, Nature. 510 (2014) 162–166. https://doi.org/10.1038/nature13392.

[105] F. Walser, M.P.C. Mulder, B. Bragantini, S. Burger, T. Gubser, M. Gatti, M.V. Botuyan, A. Villa, M. Altmeyer, D. Neri, H. Ovaa, G. Mer, L. Penengo, Ubiquitin Phosphorylation at Thr12 Modulates the DNA Damage Response, Mol Cell. 80 (2020) 423–436. https://doi.org/10.1016/j.molcel.2020.09.017.

[106] S. George, S.M. Wang, Y. Bi, M. Treidlinger, K.R. Barber, G.S. Shaw, P. O'Donoghue, Ubiquitin phosphorylated at Ser57 hyper-activates parkin,

Biochimica et Biophysica Acta (BBA) - General Subjects. 1861 (2017) 3038–3046. https://doi.org/10.1016/j.bbagen.2017.06.023.

[107] C. Schölz, B.T. Weinert, S.A. Wagner, P. Beli, Y. Miyake, J. Qi, L.J. Jensen, W. Streicher, A.R. McCarthy, N.J. Westwood, S. Lain, J. Cox, P. Matthias, M. Mann, J.E. Bradner, C. Choudhary, Acetylation site specificities of lysine deacetylase inhibitors in human cells, Nat Biotechnol. 33 (2015) 415–423. https://doi.org/10.1038/nbt.3130.

[108] Y. Chen, W. Zhao, J.S. Yang, Z. Cheng, H. Luo, Z. Lu, M. Tan, W. Gu, Y. Zhao, Quantitative Acetylome Analysis Reveals the Roles of SIRT1 in Regulating Diverse Substrates and Cellular Pathways, Mol Cell Proteomics. 11 (2012) 1048–1062. https://doi.org/10.1074/mcp.M112.019547.

[109] C. Choudhary, C. Kumar, F. Gnad, M.L. Nielsen, M. Rehman, T.C. Walther, J.V. Olsen, M. Mann, Lysine Acetylation Targets Protein Complexes and Co-Regulates Major Cellular Functions, Science. 325 (2009) 834–840. https://doi.org/10.1126/science.1175371.

[110] B.K. Hansen, R. Gupta, L. Baldus, D. Lyon, T. Narita, M. Lammers, C. Choudhary, B.T. Weinert, Analysis of human acetylation stoichiometry defines mechanistic constraints on protein regulation, Nat Commun. 10 (2019). https://doi.org/10.1038/s41467-019-09024-0.

[111] Z. Zhou, Y. Chen, M. Jin, J. He, A. Guli, C. Yan, S. Ding, Comprehensive Analysis of Lysine Acetylome Reveals a Site-Specific Pattern in Rapamycin-Induced Autophagy, J Proteome Res. 18 (2019) 865–877. https://doi.org/10.1021/acs.jproteome.8b00533.

[112] A.E.H. Elia, A.P. Boardman, D.C. Wang, E.L. Huttlin, R.A. Everley, N. Dephoure, C. Zhou, I. Koren, S.P. Gygi, S.J. Elledge, Quantitative Proteomic Atlas of Ubiquitination and Acetylation in the DNA Damage Response, Mol Cell. 59 (2015) 867–881. https://doi.org/10.1016/j.molcel.2015.05.006.

[113] J.R. Jabusch, H.F. Deutsch, Localization of lysines acetylated in ubiquitin reacted with p-nitrophenyl acetate, Arch Biochem Biophys. 238 (1985) 170–177. https://doi.org/10.1016/0003-9861(85)90153-5.

[114] D.-X. Zhu, A. Zhang, N.-C. Zhu, L.-X. Xu, H.F. Deutsch, K.-K. Han, Investigations of primary and secondary structure of porcine ubiquitin. Its Ne-acetylated lysine derivative, Int J Biochem. 18 (1986) 473–476.

[115] J.S. Rane, A. Kumari, D. Panda, An acetylation mimicking mutation, K274Q, in tau imparts neurotoxicity by enhancing tau aggregation and inhibiting tubulin polymerization, Biochem J. 476 (2019) 1401–1417. https://doi.org/10.1042/BCJ20190042.

[116] A. Gärtner, K. Wagner, S. Hölper, K. Kunz, M.S. Rodriguez, S. Müller, Acetylation of SUMO2 at lysine 11 favors the formation of non-canonical SUMO chains, EMBO Rep. 19 (2018) 13. https://doi.org/10.15252/embr.201846117.

[117] H. Neumann, S.Y. Peak-Chew, J.W. Chin, Genetically encoding Nε-acetyllysine in recombinant proteins, Nat Chem Biol. 4 (2008) 232–234. https://doi.org/10.1038/nchembio.73.

[118] D.E. Wright, Z. Altaany, Y. Bi, Z. Alperstein, P. O'Donoghue, Acetylation Regulates Thioredoxin Reductase Oligomerization and Activity, Antioxid Redox Signal. 29 (2018) 377–388. https://doi.org/10.1089/ars.2017.7082.

[119] F. Ohtake, Y. Saeki, K. Sakamoto, K. Ohtake, H. Nishikawa, H. Tsuchiya, T. Ohta, K. Tanaka, J. Kanno, Ubiquitin acetylation inhibits polyubiquitin chain elongation, EMBO Rep. 16 (2015) 192–201. https://doi.org/10.15252/embr.201439152.

[120] M. Oppikofer, S. Kueng, F. Martino, S. Soeroes, S.M. Hancock, J.W. Chin, W. Fischle, S.M. Gasser, A dual role of H4K16 acetylation in the establishment of yeast silent chromatin: Dual role of H4K16ac in yeast silencing, EMBO J. 30 (2011) 2610–2621. https://doi.org/10.1038/emboj.2011.170.

[121] M. Lammers, H. Neumann, J.W. Chin, L.C. James, Acetylation regulates Cyclophilin A catalysis, immunosuppression and HIV isomerization, Nat Chem Biol. 6 (2010) 331–337. https://doi.org/10.1038/nchembio.342.

[122] R. Ullmann, C.D. Chien, M.L. Avantaggiati, S. Muller, An Acetylation Switch Regulates SUMO-Dependent Protein Interaction Networks, Molecular Cell. 46 (2012) 759–770. https://doi.org/10.1016/j.molcel.2012.04.006.

[123] T.E. Condos, K.M. Dunkerley, E.A. Freeman, K.R. Barber, J.D. Aguirre, V.K. Chaugule, Y. Xiao, L. Konermann, H. Walden, G.S. Shaw, Synergistic recruitment of UbcH7~Ub and phosphorylated Ubl domain triggers parkin activation, EMBO J. 37 (2018) 16. https://doi.org/10.15252/embj.2018100014.

[124] A. Fradet-Turcotte, M.D. Canny, C. Escribano-Díaz, A. Orthwein, C.C.Y. Leung, H. Huang, M.-C. Landry, J. Kitevski-LeBlanc, S.M. Noordermeer, F. Sicheri, D. Durocher, 53BP1 is a reader of the DNA-damage-induced H2A Lys 15 ubiquitin mark, Nature. 499 (2013) 50–54. https://doi.org/10.1038/nature12318.

[125] S.J. Campbell, R.A. Edwards, C.C.Y. Leung, D. Neculai, C.D. Hodge, S. Dhe-Paganon, J.N.M. Glover, Molecular Insights into the Function of RING Finger (RNF)-containing Proteins hRNF8 and hRNF168 in Ubc13/Mms2-dependent Ubiquitylation, J Biol Chem. 287 (2012) 23900–23910. https://doi.org/10.1074/jbc.M112.359653.

[126] A.M. Grishin, K.R. Barber, R.-X. Gu, D.P. Tieleman, G.S. Shaw, M. Cygler, Regulation of Shigella Effector Kinase OspG through Modulation of Its Dynamic

Properties, J Mol Biol. 430 (2018) 2096–2112.
https://doi.org/10.1016/j.jmb.2018.05.015.

[127] Y. Zhu, H. Li, L. Hu, J. Wang, Y. Zhou, Z. Pang, L. Liu, F. Shao, Structure of a Shigella effector reveals a new class of ubiquitin ligases, Nat Struct Mol Biol. 15 (2008) 1302–1308. https://doi.org/10.1038/nsmb.1517.

[128] Y. Perez-Riverol, A. Csordas, J. Bai, M. Bernal-Llinares, S. Hewapathirana, D.J. Kundu, A. Inuganti, J. Griss, G. Mayer, M. Eisenacher, E. Pérez, J. Uszkoreit, J. Pfeuffer, T. Sachsenberg, Ş. Yılmaz, S. Tiwary, J. Cox, E. Audain, M. Walzer, A.F. Jarnuczak, T. Ternent, A. Brazma, J.A. Vizcaíno, The PRIDE database and related tools and resources in 2019: improving support for quantification data, Nucleic Acids Res. 47 (2019) D442–D450. https://doi.org/10.1093/nar/gky1106.

[129] L.-J. Liang, Y. Si, S. Tang, D. Huang, Z.A. Wang, C. Tian, J.-S. Zheng, Biochemical properties of K 11,48 -branched ubiquitin chains, Chin Chem Lett. 29 (2018) 1155–1159. https://doi.org/10.1016/j.cclet.2018.03.022.

[130] L.A. Kane, M. Lazarou, A.I. Fogel, Y. Li, K. Yamano, S.A. Sarraf, S. Banerjee, R.J. Youle, PINK1 phosphorylates ubiquitin to activate Parkin E3 ubiquitin ligase activity, The Journal of Cell Biology. 205 (2014) 143–153. https://doi.org/10.1083/jcb.201402104.

[131] A. Kazlauskaite, C. Kondapalli, R. Gourlay, D.G. Campbell, M.S. Ritorto, K. Hofmann, D.R. Alessi, A. Knebel, M. Trost, M.M.K. Muqit, Parkin is activated by PINK1-dependent phosphorylation of ubiquitin at Ser65, Biochemical Journal. 460 (2014) 127–141. https://doi.org/10.1042/BJ20140334.

[132] T. Wauer, M. Simicek, A. Schubert, D. Komander, Mechanism of phospho-ubiquitin-induced PARKIN activation, Nature. 524 (2015) 370–374. https://doi.org/10.1038/nature14879.

[133] L. Jiang, A.N. Saavedra, G. Way, J. Alanis, R. Kung, J. Li, W. Xiang, J. Liao, Specific substrate recognition and thioester intermediate determinations in ubiquitin and SUMO conjugation cascades revealed by a high-sensitive FRET assay, Mol Biosyst. 10 (2014) 778–786. https://doi.org/10.1039/c3mb70155g.

[134] H. Wiryawan, K. Dan, M. Etuale, Y. Shen, J. Liao, Determination of SUMO1 and ATP affinity for the SUMO E1 by quantitative FRET technology: Determination of SUMO1 and ATP Affinity, Biotechnol Bioeng. 112 (2015) 652–658. https://doi.org/10.1002/bit.25480.

[135] B.P. Kleinstiver, A.D. Fernandes, G.B. Gloor, D.R. Edgell, A unified genetic, computational and experimental framework identifies functionally relevant residues of the homing endonuclease I-BmoI, Nucleic Acids Res. 38 (2010) 2411–2427. https://doi.org/10.1093/nar/gkp1223.

[136] R.E. Lacoursiere, P. O'Donoghue, G.S. Shaw, Programmed ubiquitin acetylation using genetic code expansion reveals altered ubiquitination patterns, FEBS Lett. 594 (2020) 1226–1234.

[137] M.O. Palmier, S.R. Van Doren, Rapid determination of enzyme kinetics from fluorescence: Overcoming the inner filter effect, Anal Biochem. 371 (2007) 43–51. https://doi.org/10.1016/j.ab.2007.07.008.

[138] M. Windheim, M. Peggie, P. Cohen, Two different classes of E2 ubiquitin-conjugating enzymes are required for the mono-ubiquitination of proteins and elongation by polyubiquitin chains with a specific topology, Biochem J. 409 (2008) 723–729. https://doi.org/10.1042/BJ20071338.

[139] D.M. Wenzel, A. Lissounov, P.S. Brzovic, R.E. Klevit, UBCH7 reactivity profile reveals parkin and HHARI to be RING/HECT hybrids, Nature. 474 (2011) 105–108. https://doi.org/10.1038/nature09966.

[140] C. Purbeck, Z.M. Eletr, B. Kuhlman, Kinetics of the Transfer of Ubiquitin from UbcH7 to E6AP, Biochemistry. 49 (2010) 1361–1363. https://doi.org/10.1021/bi9014693.

[141] Y. Sheng, J.H. Hong, R. Doherty, T. Srikumar, J. Shloush, G.V. Avvakumov, J.R. Walker, S. Xue, D. Neculai, J.W. Wan, S.K. Kim, C.H. Arrowsmith, B. Raught, S. Dhe-Paganon, A Human Ubiquitin Conjugating Enzyme (E2)-HECT E3 Ligase Structure-function Screen, Molecular & Cellular Proteomics. 11 (2012) 329–341. https://doi.org/10.1074/mcp.O111.013706.

[142] T. Ohashi, S.D. Galiacy, G. Briscoe, H.P. Erickson, An experimental study of GFP-based FRET, with application to intrinsically unstructured proteins, Protein Sci. 16 (2007) 1429–1438. https://doi.org/10.1110/ps.072845607.

[143] K.S. Hamilton, M.J. Ellison, G.S. Shaw, Identification of the ubiquitin interfacial residues in a ubiquitin-E2 covalent complex, J Biomol NMR. 18 (2000) 319–327. https://doi.org/10.1023/A:1026773008237.

[144] M.K. Rout, C.D. Hodge, C.J. Markin, X. Xu, J.N.M. Glover, W. Xiao, L. Spyracopoulos, Stochastic Gate Dynamics Regulate the Catalytic Activity of Ubiquitination Enzymes, J Am Chem Soc. 136 (2014) 17446–17458. https://doi.org/10.1021/ja505440b.

[145] Z. Tokgöz, R.N. Bohnsack, A.L. Haas, Pleiotropic Effects of ATP·Mg2+ Binding in the Catalytic Cycle of Ubiquitin-activating Enzyme, J Biol Chem. 281 (2006) 14729–14737. https://doi.org/10.1074/jbc.M513562200.

[146] Z. Tokgöz, T.J. Siepmann, F. Streich, B. Kumar, J.M. Klein, A.L. Haas, E1-E2 Interactions in Ubiquitin and Nedd8 Ligation Pathways*, J Biol Chem. 287 (2012) 311–321. https://doi.org/10.1074/jbc.M111.294975.

[147] S.K. Olsen, A.D. Capili, X. Lu, D.S. Tan, C.D. Lima, Active site remodelling accompanies thioester bond formation in the SUMO E1, Nature. 463 (2010) 906–912. https://doi.org/10.1038/nature08765.

[148] D.T. Huang, H.W. Hunt, M. Zhuang, M.D. Ohi, J.M. Holton, B.A. Schulman, Basis for a ubiquitin-like protein thioester switch toggling E1–E2 affinity, Nature. 445 (2007) 394–398. https://doi.org/10.1038/nature05490.

[149] Z. Lv, K.A. Rickman, L. Yuan, K. Williams, S.P. Selvam, A.N. Woosley, P.H. Howe, B. Ogretmen, A. Smogorzewska, S.K. Olsen, S. pombe Uba1-Ubc15 Structure Reveals a Novel Regulatory Mechanism of Ubiquitin E2 Activity, Mol Cell. 65 (2017) 699–714. https://doi.org/10.1016/j.molcel.2017.01.008.

[150] K.E. Wee, Z. Lai, K.R. Auger, J. Ma, K.Y. Horiuchi, R.L. Dowling, C.S. Dougherty, J.I. Corman, R. Wynn, R.A. Copeland, Steady-State Kinetic Analysis of Human Ubiquitin-Activating Enzyme (E1) Using a Fluorescently Labeled Ubiquitin Substrate, J Protein Sci. 19 (2000) 489–498.

[151] S.A. Serniwka, G.S. Shaw, The structure of the UbcH8-ubiquitin complex shows a unique ubiquitin interaction site, Biochem. 48 (2009) 12169–12179. https://doi.org/10.1021/bi901686j.

[152] K.K. Dove, J.L. Olszewski, L. Martino, D.M. Duda, X.S. Wu, D.J. Miller, K.H. Reiter, K. Rittinger, B.A. Schulman, R.E. Klevit, Structural Studies of HHARI/UbcH7~Ub Reveal Unique E2~Ub Conformational Restriction by RBR RING1, Structure. 25 (2017) 890–900. https://doi.org/10.1016/j.str.2017.04.013.

[153] S. Vijay-Kumar, C.E. Bugg, W.J. Cook, Structure of ubiquitin refined at 1.8 Å resolution, J Mol Biol. 194 (1987) 531–544. https://doi.org/10.1016/0022-2836(87)90679-6.

[154] K.E. Wickliffe, A. Williamson, H.J. Meyer, A. Kelly, M. Rape, K11-linked ubiquitin chains as novel regulators of cell division, Trends Cell Biol. 21 (2011) 656–663. https://doi.org/10.1016/j.tcb.2011.08.008.

[155] C.M. Pickart, I.A. Rose, Functional heterogeneity of ubiquitin carrier proteins., J Biol Chem. 260 (1985) 1573–1581. https://doi.org/10.1016/S0021-9258(18)89632-6.

[156] L.E. Kay, M. Ikura, R. Tschudin, Three-Dimensional Triple-Resonance NMR Spectroscopy of Isotopically Enriched Proteins, J Magn Reson. 89 (1990) 496–514.

[157] F. Delaglio, S. Grzesiek, GeertenW. Vuister, G. Zhu, J. Pfeifer, A. Bax, NMRPipe: A multidimensional spectral processing system based on UNIX pipes, J Biomol NMR. 6 (1995) 277–293. https://doi.org/10.1007/BF00197809.

[158] B.A. Johnson, R.A. Blevins, NMR View: A computer program for the visualization and analysis of NMR data, J Biomol NMR. 4 (1994) 603–614. https://doi.org/10.1007/BF00404272.

[159] P. Schuck, Size-Distribution Analysis of Macromolecules by Sedimentation Velocity Ultracentrifugation and Lamm Equation Modeling, Biophys J. 78 (2000) 1606–1619. https://doi.org/10.1016/S0006-3495(00)76713-0.

[160] M.L. Johnson, J.J. Correia, D.A. Yphantis, H.R. Halvorson, Analysis of data from the analytical ultracentrifuge by nonlinear least-squares techniques, Biophys J. 36 (1981) 575–588. https://doi.org/10.1016/S0006-3495(81)84753-4.

[161] P.D. Adams, P.V. Afonine, G. Bunkóczi, V.B. Chen, N. Echols, J.J. Headd, L.-W. Hung, S. Jain, G.J. Kapral, R.W. Grosse Kunstleve, A.J. McCoy, N.W. Moriarty, R.D. Oeffner, R.J. Read, D.C. Richardson, J.S. Richardson, T.C. Terwilliger, P.H. Zwart, The Phenix software for automated determination of macromolecular structures, Methods. 55 (2011) 94–106. https://doi.org/10.1016/j.ymeth.2011.07.005.

[162] P. Emsley, K. Cowtan, *Coot* : model-building tools for molecular graphics, Acta Crystallogr D Biol Crystallogr. 60 (2004) 2126–2132. https://doi.org/10.1107/S0907444904019158.

[163] S.E. Schwarz, J.L. Rosa, M. Scheffner, Characterization of Human hect Domain Family Members and Their Interaction with UbcH5 and UbcH7, J Biol Chem. 273 (1998) 12148–12154. https://doi.org/10.1074/jbc.273.20.12148.

[164] T. Hirano, O. Serve, M. Yagi-Utsumi, E. Takemoto, T. Hiromoto, T. Satoh, T. Mizushima, K. Kato, Conformational Dynamics of Wild-type Lys-48-linked Diubiquitin in Solution, J Biol Chem. 286 (2011) 37496–37502. https://doi.org/10.1074/jbc.M111.256354.

[165] R.E. Lacoursiere, G.S. Shaw, Acetylated Ubiquitin Modulates the Catalytic Activity of the E1 Enzyme Uba1, Biochemistry. 60 (2021) 1276–1285. https://doi.org/10.1021/acs.biochem.1c00145.

[166] E.R. Jang, P. Shi, J. Bryant, J. Chen, V. Dukhande, M.S. Gentry, H. Jang, M. Jeoung, E. Galperin, HUWE1 Is a Molecular Link Controlling RAF-1 Activity Supported by the Shoc2 Scaffold, Mol Cell Biol. 34 (2014) 3579–3593. https://doi.org/10.1128/MCB.00811-14.

[167] M.A. Michel, K.N. Swatek, M.K. Hospenthal, D. Komander, Ubiquitin Linkage-Specific Affimers Reveal Insights into K6-Linked Ubiquitin Signaling, Mol Cell. 68 (2017) 233–246. https://doi.org/10.1016/j.molcel.2017.08.020.

[168] S.-H. Kao, H.-T. Wu, K.-J. Wu, Ubiquitination by HUWE1 in tumorigenesis and beyond, J Biomed Sci. 25 (2018) 15. https://doi.org/10.1186/s12929-018-0470-0.

[169] M. Jäckl, C. Stollmaier, T. Strohäker, K. Hyz, E. Maspero, S. Polo, S. Wiesner, β-Sheet Augmentation Is a Conserved Mechanism of Priming HECT E3 Ligases for Ubiquitin Ligation, J Mol Biol. 430 (2018) 3218–3233. https://doi.org/10.1016/j.jmb.2018.06.044.

[170] R.K. Pandya, J.R. Partridge, K.R. Love, T.U. Schwartz, H.L. Ploegh, A Structural Element within the HUWE1 HECT Domain Modulates Self-ubiquitination and Substrate Ubiquitination Activities, Journal of Biological Chemistry. 285 (2010) 5664–5673. https://doi.org/10.1074/jbc.M109.051805.

[171] K. Zhu, Z. Shan, X. Chen, Y. Cai, L. Cui, W. Yao, Z. Wang, P. Shi, C. Tian, J. Lou, Y. Xie, W. Wen, Allosteric auto-inhibition and activation of the Nedd4 family E3 ligase Itch, EMBO Rep. 18 (2017) 1618–1630. https://doi.org/10.15252/embr.201744454.

[172] S. Kühnle, U. Kogel, S. Glockzin, A. Marquardt, A. Ciechanover, K. Matentzoglu, M. Scheffner, Physical and Functional Interaction of the HECT Ubiquitin-protein Ligases E6AP and HERC2, J Biol Chem. 286 (2011) 19410–19416. https://doi.org/10.1074/jbc.M110.205211.

[173] F. Mortensen, D. Schneider, T. Barbic, A. Sladewska-Marquardt, S. Kühnle, A. Marx, M. Scheffner, Role of ubiquitin and the HPV E6 oncoprotein in E6AP-mediated ubiquitination, PNAS. 112 (2015) 9872–9877. https://doi.org/10.1073/pnas.1505923112.

[174] N.L. Hepowit, K.N. Pereira, J.M. Tumolo, W.J. Chazin, J.A. MacGurn, Identification of ubiquitin Ser57 kinases regulating the oxidative stress response in yeast, ELife. 9 (2020) 19. https://doi.org/10.7554/eLife.58155.

[175] S.B. Lee, J.J. Kim, S.-A. Han, Y. Fan, L.-S. Guo, K. Aziz, S. Nowsheen, S.S. Kim, S.-Y. Park, Q. Luo, J.O. Chung, S.I. Choi, A. Aziz, P. Yin, S.-Y. Tong, F.C. Fiesel, W. Springer, J.-S. Zhang, Z. Lou, The AMPK–Parkin axis negatively regulates necroptosis and tumorigenesis by inhibiting the necrosome, Nat Cell Biol. 21 (2019) 940–951. https://doi.org/10.1038/s41556-019-0356-8.

[176] H.S. Ko, Y. Lee, J.-H. Shin, S.S. Karuppagounder, B.S. Gadad, A.J. Koleske, O. Pletnikova, J.C. Troncoso, V.L. Dawson, T.M. Dawson, Phosphorylation by the c-Abl protein tyrosine kinase inhibits parkin's ubiquitination and protective function, PNAS. 107 (2010) 16691–16696. https://doi.org/10.1073/pnas.1006083107.

[177] C.V. Hinton, L.D. Fitzgerald, M.E. Thompson, Phosphatidylinositol 3-kinase/Akt signaling enhances nuclear localization and transcriptional activity of BRCA1, Exp Cell Res. 313 (2007) 1735–1744. https://doi.org/10.1016/j.yexcr.2007.03.008.

[178] D.S. Hewings, J.A. Flygare, M. Bogyo, I.E. Wertz, Activity-based probes for the ubiquitin conjugation-deconjugation machinery: new chemistries, new tools, and new insights, FEBS J. 284 (2017) 1555–1576. https://doi.org/10.1111/febs.14039.

[179] N.C. Taylor, J.F. McGouran, Strategies to Target Specific Components of the Ubiquitin Conjugation/Deconjugation Machinery, Front Chem. 7 (2020) 9. https://doi.org/10.3389/fchem.2019.00914.

[180] X. Sun, H. Gao, Y. Yang, M. He, Y. Wu, Y. Song, Y. Tong, Y. Rao, PROTACs: great opportunities for academia and industry, Sig Transduct Target Ther. 4 (2019) 33. https://doi.org/10.1038/s41392-019-0101-6.

[181] S.-M. Qi, J. Dong, Z.-Y. Xu, X.-D. Cheng, W.-D. Zhang, J.-J. Qin, PROTAC: An Effective Targeted Protein Degradation Strategy for Cancer Therapy, Front Pharmacol. 12 (2021) 13. https://doi.org/10.3389/fphar.2021.692574.

[182] S. George, J.D. Aguirre, D.E. Spratt, Y. Bi, M. Jeffery, G.S. Shaw, P. O'Donoghue, Generation of phospho-ubiquitin variants by orthogonal translation reveals codon skipping, FEBS Letters. 590 (2016) 1530–1542. https://doi.org/10.1002/1873-3468.12182.

[183] C.N. Braxton, E. Quartner, W. Pawloski, D. Fushman, T.A. Cropp, Ubiquitin Chains Bearing Genetically Encoded Photo-Cross-Linkers Enable Efficient Covalent Capture of (Poly)ubiquitin-Binding Domains, Biochemistry. 58 (2019) 883–886. https://doi.org/10.1021/acs.biochem.8b01089.

[184] S. Mathur, A.J. Fletcher, E. Branigan, R.T. Hay, S. Virdee, Photocrosslinking Activity-Based Probes for Ubiquitin RING E3 Ligases, Cell Chem Biol. 27 (2020) 74–86. https://doi.org/10.1016/j.chembiol.2019.11.013.

[185] W. Gui, G.A. Davidson, Z. Zhuang, Chemical methods for protein site-specific ubiquitination, RSC Chem Biol. 2 (2021) 450–467. https://doi.org/10.1039/D0CB00215A.

[186] M. Fottner, M. Weyh, S. Gaussmann, D. Schwarz, M. Sattler, K. Lang, A modular toolbox to generate complex polymeric ubiquitin architectures using orthogonal sortase enzymes, Nat Commun. 12 (2021) 15. https://doi.org/10.1038/s41467-021-26812-9.

[187] G.M. Burslem, The chemical biology of ubiquitin, Biochim Biophys Acta Gen Subj. 1866 (2022) 6. https://doi.org/10.1016/j.bbagen.2021.130079.

[188] Y. David, T. Ziv, A. Admon, A. Navon, The E2 Ubiquitin-conjugating Enzymes Direct Polyubiquitination to Preferred Lysines, Journal of Biological Chemistry. 285 (2010) 8595–8604. https://doi.org/10.1074/jbc.M109.089003.

[189] J.D. Aguirre, K.M. Dunkerley, R. Lam, M. Rusal, G.S. Shaw, Impact of altered phosphorylation on loss of function of juvenile Parkinsonism–associated genetic variants of the E3 ligase parkin, J Biol Chem. 293 (2018) 6337–6348. https://doi.org/10.1074/jbc.RA117.000605.

[190] D.T. Krist, S. Park, G.H. Boneh, S.E. Rice, A.V. Statsyuk, UbFluor: a mechanism-based probe for HECT E3 ligases, Chem Sci. 7 (2016) 5587–5595. https://doi.org/10.1039/C6SC01167E.

[191] A.F. Schubert, J.V. Nguyen, T.G. Franklin, P.P. Geurink, C.G. Roberts, D.J. Sanderson, L.N. Miller, H. Ovaa, K. Hofmann, J.N. Pruneda, D. Komander, Identification and characterization of diverse OTU deubiquitinases in bacteria, EMBO J. 39 (2020) 16. https://doi.org/10.15252/embj.2020105127.
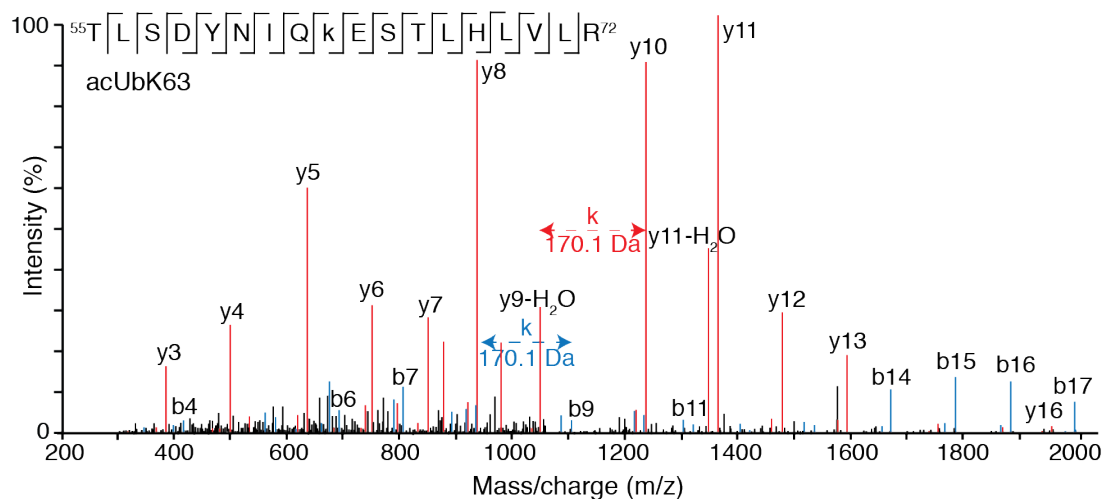
Appendix A

MS/MS data for acUb peptides
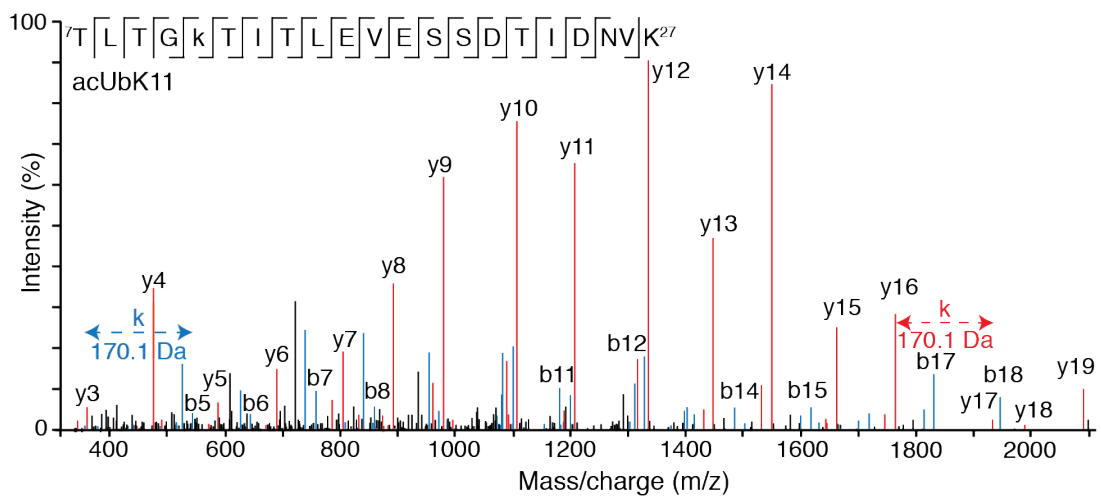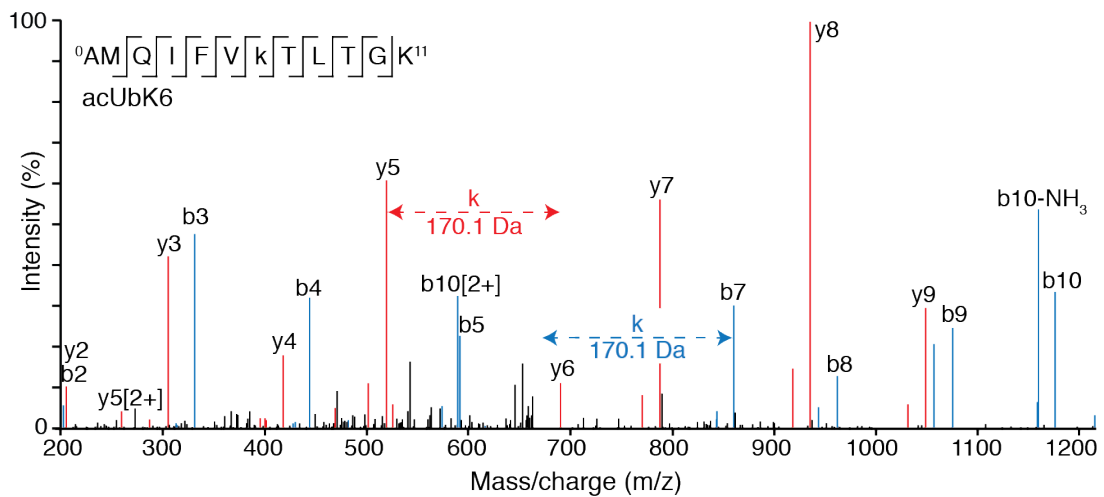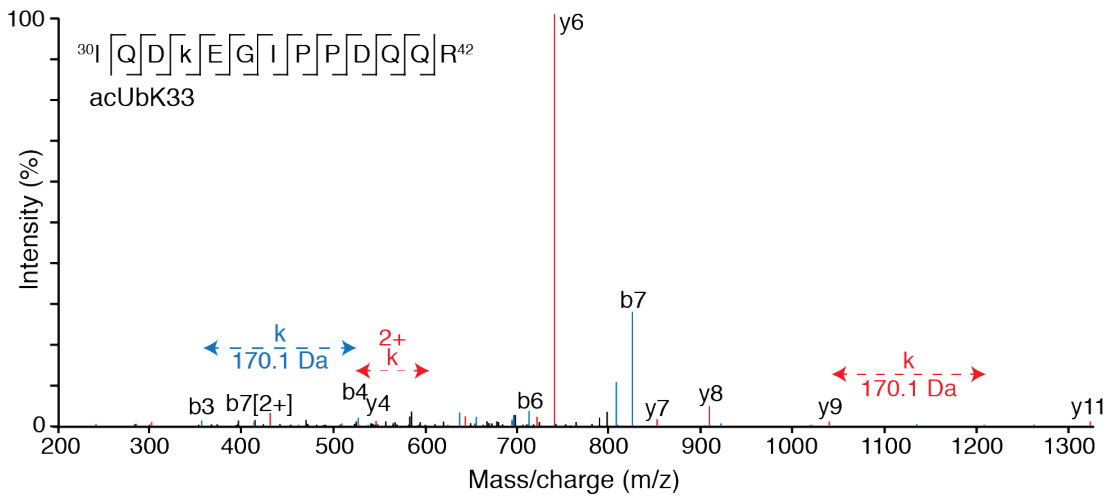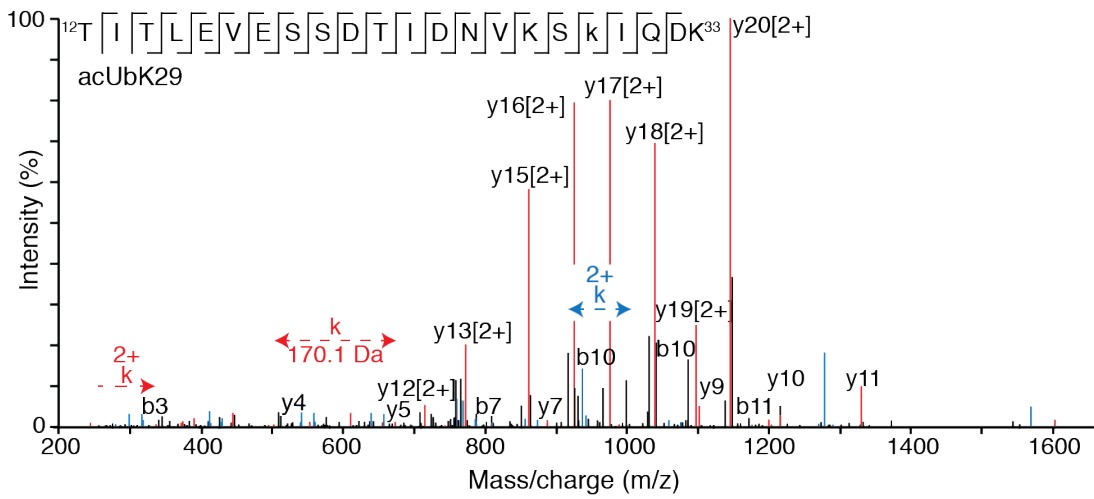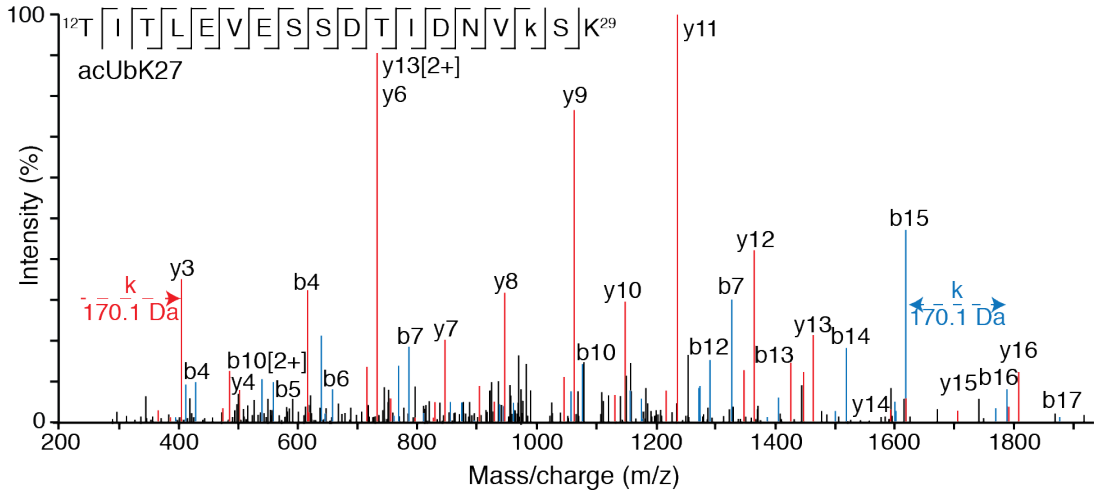
Figure A.1. MS/MS spectra for Ub peptides containing position specific acetyl-lysine. Singly acetylated Ub variants were purified as described in section 2.2.2.3 and tryptic digested. Peptides were analyzed using LC-ESI-MS/MS to confirm site-specific incorporation of acetyl-lysine. Shown are peptides that correspond to each of the remaining 6 lysine constructs (acUbK6, acUbK11, acUbK27, acUbK29, acUbK33, and acUbK63). In each case, lowercase 'k' indicates modified lysine; here, the monoisotopic mass of 170.1 Da indicates acetyl-lysine. Data were analyzed using PEAKS X software.

Rachel E Lacoursiere

Department of Biochemistry, The University of Western Ontario
London, Ontario, Canada, N6A 5C1

EDUCATION

University of Western Ontario | Doctor of Philosophy in Biochemistry   2017-2022
- London, Ontario, Canada

University of Windsor | Bachelor of Forensic Science (Molecular Biology/Biochemistry Specialization)   2013-2017
- Windsor, Ontario, Canada
- First in Class with Distinction and a Mathematics Minor
- *Recipient*, Board of Governors Medal; Dean's List

Keele University | International Exchange Year   2015-2016
- Keele, Staffordshire, United Kingdom

RESEARCH EXPERIENCE

Research Assistant   2017 - 2022
Laboratory of Dr. Gary Shaw, University of Western Ontario | London, ON, Canada
- Thesis: Kinetic and structural influences of acetylation on ubiquitin processing

Undergraduate Research Assistant   2014 - 2017
Laboratories of Dr. Michael Boffa and Dr. Sherah VanLaerhoven, University of Windsor | Windsor, ON, Canada
- Outstanding Scholar's Project: Biochemical approaches to forensic entomology
- Thesis: Oviposition of *L. sericata* as a result of size of medium and relative humidity

AWARDS

Ontario Graduate Scholarship (OGS) Queen Elizabeth II Award 2021-2022
Ontario Graduate Scholarship (OGS) 2020-2021
Western Graduate Research Scholarship 2017-2021
John Hughes Memorial Scholarship- University of Windsor 2014-2017
Outstanding Scholars Award- University of Windsor 2014-2017
Renewable Entrance Scholarship- University of Windsor 2013-2017
Outstanding Scholars Candidate Year Award- University of Windsor 2013-2014

SCIENTIFIC CONTRIBUTIONS

Publications:
- **Lacoursiere, R.E.**, and Shaw, G.S. (2021). Acetylated Ubiquitin Modulates the Catalytic Activity of the E1 Enzyme Uba1. Biochemistry. 60(16): 1276-85.
- Cook, B.W., **Lacoursiere, R.E.**, and Shaw, G.S. (2020). Recruitment of ubiquitin within an E2 chain elongation complex. Biophysical Journal. 118(7): 1679-89.
- **Lacoursiere, R.E.**, O'Donoghue, P., and Shaw, G.S. (2020). Programmed ubiquitin acetylation using genetic code expansion reveals altered ubiquitination patterns. FEBS Letters. 594(7): 1226-34.

Presentations:
- **Lacoursiere, R.E.**, and Shaw, G.S. (2021). Impact of programmed acetylation on the ubiquitination pathway. Pacifichem International Congress of Pacific Basin Societies.

International Conference, <u>invited oral presentation.</u> Virtual.

- **Lacoursiere, R.E.**, Madlol, G., O'Donoghue, P., and Shaw, G.S. (2019). Don't FRET! Acetylation modifies Ub loading by an E2 enzyme. EMBO Ubiquitin workshop. International Conference, <u>poster presentation.</u> Cavtat, Croatia.
- **Lacoursiere, R.E.**, Madlol, G., and Shaw, G.S. (2019). Acetylation: a method of regulating ubiquitination. London Health Research Day. Institutional Conference, <u>poster presentation.</u> London, Canada.
- **Lacoursiere, R.E.**, and VanLaerhoven, S. (2017). Oviposition of *Lucilia sericata* as a result of changes to size of medium and relative humidity. Trends in Forensic Science (TIFS). Collaborative international conference (Wayne State University, MI and University of Windsor, ON), <u>poster presentation.</u> Windsor, Canada.
- **Lacoursiere, R.E.** (2015). Outstanding Scholars in Forensic Science at UWindsor. Trends in Forensic Science (TIFS). Collaborative international conference (Wayne State University, MI and University of Windsor, ON), <u>oral presentation.</u> Windsor, Canada.

TEACHING EXPERIENCE

Teaching Assistant   2017 - 2021
Department of Biochemistry, University of Western Ontario | London, ON, Canada
<u>Biochemistry 3381A- Biological Macromolecules (Fall 2021):</u>

- Course supervisor: Dr. Murray Junop
- Hosted tutorial sessions for > 200 students and delivered content both live and virtually, emphasis on proper figure making and enzyme kinetics
- Facilitated the inquiry project for 7 groups of students by providing feedback and evaluating progress
- Marked reports and assignments for > 200 students

<u>Biochemistry 3380G- Biochemistry Laboratory (Winter 2019, 2020, 2021):</u>

- Course supervisor: Dr. Derek McLachlin
- Fostered small group relationships with 8-10 students yearly, and served as a primary contact for course-related queries
- Reviewed biochemical concepts and theory, and supervised technical skills in the laboratory
- Nurtured individual thinking by proposing questions to guide students to answer their own
- Assisted students with literature review and scientific writing, and evaluated student progress through lab reports and assignments
- **Key contributions (Winter 2021)**
  - Developed and revised course material including laboratory protocols and assignments prior to student engagement
  - Streamlined student experiments by preparing biological materials in advance of the laboratory session
  - Promoted the use of Microsoft Teams to engage and communicate with students during the SARS-CoV-2 pandemic
  - Regularly posted updates to my Team to encourage students and to provide group and individual feedback

<u>Biochemistry 2280A- Biochemistry and Molecular Biology (Fall 2017):</u>

- Course supervisor: Dr. Christopher Brandl
- Marked reports and assignments for > 300 students
- Supervised midterm examination review
- Chief proctored midterm (70 students) and final exam (400 students)

Summer Student Supervisor   Summers 2018, 2019, and 2021
Department of Biochemistry, University of Western Ontario | London, ON, Canada
- Lab supervisor: Dr. Gary Shaw
- Trained undergraduate research assistants in common laboratory methods including plasmid mutagenesis, protein expression and purification, enzyme assays, and various lab upkeep tasks
- Encouraged the development of skills such as problem solving, scientific communication, and literature review
- Modeled excellent notetaking and laboratory notebook keeping